Dynamics of rainwater lenses on upward seeping saline groundwater

Sara Eeman

Dynamics of rainwater lenses on upward seeping saline groundwater

Sara Eeman

Thesis committee

Promotor
Prof. Dr S.E.A.T.M van der Zee
Personal chair Ecohydrology
Wageningen University

Co-promotor
Prof. Dr A. Leijnse
External staff member, Soil Physics and Land Management Group
Wageningen University

Other members
Prof . Dr R. Uijlenhoet, Wageningen University
Prof. Dr M. Th. Van Genuchten, Federal University of Rio de Janeiro, Brazil
Prof. Dr L. Lebbe, Ghent University, Belgium
Dr D.G. Cirkel, KWR Water Cycle Research Institute, Nieuwegein

This research was conducted under the auspices of the Graduate School for Socio-Economic and Natural Sciences of the environment (SENSE).

Dynamics of rainwater lenses on upward seeping saline groundwater

Sara Eeman

Thesis

submitted in fulfilment of the requirements for the degree of doctor
at Wageningen University
by the authority of the Rector Magnificus
Prof. Dr A.P.J. Mol,
in the presence of the
Thesis Committee appointed by the Academic Board
to be defended in public
on Wednesday 25 January 2017
at 4 p.m. in the Aula.

Sara Eeman
Dynamics of rainwater lenses on upward seeping saline groundwater,
158 pages.
PhD thesis, Wageningen University, Wageningen, NL (2017)
With references, with summaries in English and Dutch
ISBN: 978-94-6257-933-0
DOI: http://dx.doi.org/10.18174/390156

CONTENTS

NOMENCLATURE

a	shape parameter for step- and impulse-response function [-]
f	frequency of recharge sinus [T^{-1}]
g	acceleration of gravity [$L\,T^{-2}$]
h	thickness of rainwater lens [L]
h_p	soil water pressure head [L]
i, j	empiricial shape parameters [-]
k, k_0	unsaturated resp. saturated soil hydraulic conductivity [LT^{-1}]
l_r	root length density [L^{-3}]
m_{sb}	total salt mass flux across the ditch boundary [$L^{-2}T^{-1}$]
n	porosity [-]
p, p_0, p_b	pressure of fluid, hydrostat. fresh water and fluid in ditch [$M\,L^{-1}\,T^{-2}$]
$\boldsymbol{q}$	specific discharge of the fluid [$L\,T^{-1}$]
r_{agg}	spherical aggregate radius [L]
r_d, r_s, r_w	transpiration reduction factors for drought, salt and oxygen stress [-]
$s(t)$	step response function
$s_{//}, s_{\perp}$	local coordinate axes parallel and perpendicular to the interface [L]
t	time [T]
v	fluid velocity [$L\,T^{-1}$]
$\langle\lvert v\rvert\rangle$	average abs. velocity of center of mixing zone in middle of field [LT^{-1}]
x, z	horizontal and vertical spatial coordinates [L]
$\bar{z}$	normalized first moment of the vertical center of salt mass change [L]
A	amplitude of sinusoidal recharge curve [L]
$A_{\bar{z}}$	amplitude of center of the mixing zone in the middle of the field [L]
C_s	concentration of the seepage water [M/L^3]
D_m	apparent mlc. diffusion coefficient, incl. the effect of tortuosity [$L^2\,T^{-1}$]
$\boldsymbol{D}$	hydrodynamic dispersion tensor, incl. apparent mlc.diffusion [$L^2\,T^{-1}$]
D_{eff}	dispersion tensor, including $\boldsymbol{D}, D_m$ and the exchange between mobile/immobile water regions [$L^2\,T^{-1}$]
D_{agg}	diffusion coefficient of a spherical aggregate [L^2T^{-1}]
D_r	root layer thickness [L]

E_p	potential evaporation [LT^{-1}]
ΔF_r	change of fresh water volume [L^3/L^2]
H	depth of system [L]
$I(t)$	impulse response function
$\boldsymbol{J}$	diffusive/dispersive salt mass flux [M L^{-2}T^{-1}]
L, L_{in}	half field width and width of the fresh water inflow region [L]
$P, P_s, \langle P \rangle$	net precipitation, resp. constant, sinusoidal and average [L T$^-$]
S	salt water seepage flux [L T^{-1}]
S_a,S_p	actual resp. potential root water uptake [L/T]
S_r	relative saturation [-]
T_p,T_a,T_r	potential, actual and relative transpiration [LT^{-1}, LT^{-1},-]
$V_n, V_m, \langle V \rangle$	resp. normalized, maximum and average volumes of fresh water [L^2]
Z	max. thickness of the rainwater lens in the middle of the field [L]
$\alpha_l, \alpha_t, \alpha_{eff}$	longitudinal and transversal dispersivity [L]
β	slope of the lens deviation [-]
γ	constant in the equation of state for the fluid density [-]
$\theta, \theta_s, \theta_r$	soil water content, resp. actual, saturated and residual [L^{3}L^{-3}]
κ	intrinsic permeability of the porous medium [L^2]
λ	shape parameter dependent on $\delta k / \delta h_p$ [-]
μ	fluid viscosity [M L^{-1} T^{-1}]
ξ	conductance of the boundary between porous medium and ditch [L]
ρ, ρ_0, ρ_{max}	fluid density, fresh water density and max. salt water density [M L^{-3}]
ΔSal	change in dissolved salts [M]
Δz	ultimate change of lens thickness for step/impulse response func. [L]
$\Delta\rho = \rho - \rho_0$	fresh water-salt water density difference [M L^{-3}]
σ_S	standard deviation of center of the mixing zone, middle of the field [L]
τ	integration variable in the convolution integral [T]
ϕ_m	fraction of water in the mobile phase [-]
χ, χ_S, χ_n	traveled distance per period of the center of the mixing zone in the middle of the field, resp. for a sinusoidal recharge function and actual weather data [LT^{-1}]
$\omega, \omega_i, \omega_{\max}$	salt mass fraction, and resp. initial and maximum fractions [-]

1 INTRODUCTION

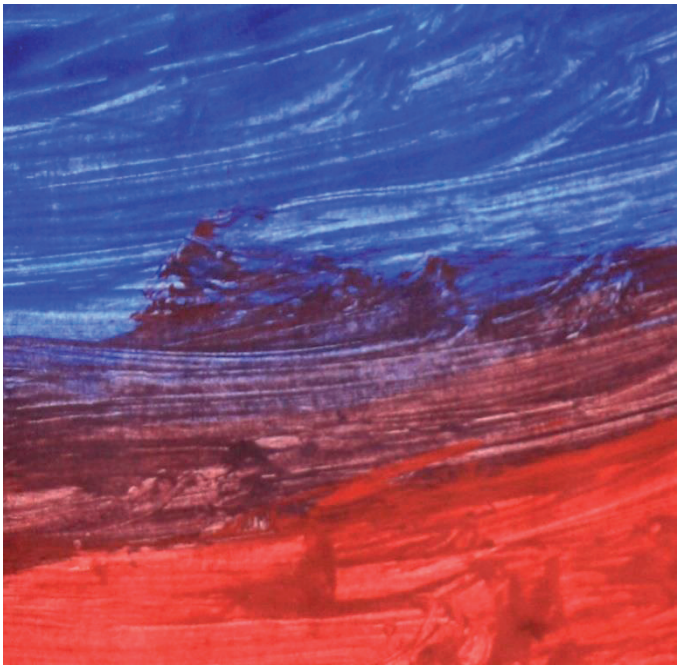

1.1 Dynamic rainwater lenses

In densely populated deltaic areas, resources of fresh water needed for industrial, domestic and agricultural purposes are often limited. In most of these coastal zones, groundwater at some depth is brackish or saline. In the case of a precipitation surplus, an important resource of fresh water for vegetation is formed by thin lenses that develop on top of the saline ground water, creating an environment suitable for salt intolerant plants and crops. Understanding the dynamics of such lenses is vital for sustainable food production and development of natural vegetation and biodiversity under changing conditions like sea level rise and climate change. Where the coast is somewhat elevated and the groundwater level is above mean sea level, the thickness of freshwater lenses that float on top of saline water can be very large. This is caused by the difference in density between fresh (1000 kg/m^3) and saline (±1025 kg/m^3) water according to the Badon Ghyben-Herzberg relation, or even more basic, Archimedes law. The dynamics of such lenses, illustrated in Figure 1.1, are very limited, and they have been studied already in the 19th century, because of their importance for drinking water supply. Several analytical solutions describe relations between recharge, seepage, soil hydraulic conductivity and the thickness of such lenses. They all assume a sharp interface between fresh and saline water and differ in their conditions for outflow at the edge of the lens and movement of the saline water (Badon Ghijben, 1988; Herzberg, 1901; Van der Veer, 1977; Maas, 2007, Raats, 2015).

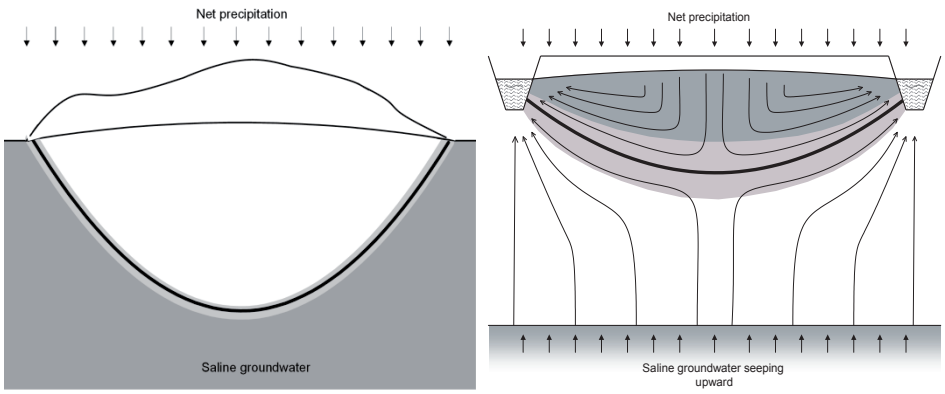

Figure 1.1: a (left) Badon Ghijben-Herzberg lens. b (right) Thin, dynamic, rainwaterlens.

1.1.1 Small but important systems

In situations where the coast is flat and low lying, as occurring often in deltas, the rainwater lens is thin and dynamic. In the prediction of the effects of climate change and sea level rise, the sustainability of these small but important sources of fresh water becomes questionable, and careful water management is of utmost importance. Up to 2007, many studies focused on situations with a relatively thin mixing zone between fresh and saline water relative to the lens thickness, justifying the

assumption of a sharp interface, for example Vos and Souza (1987), and Oude Essink (2001). The validity of assuming a sharp interface between fresh and saline water for coastal aquifers was discussed by Sakr (1999), who concluded that it is limited to cases with either a small dispersion to convection ratio or a large seepage factor (flux to conductivity ratio). However, the mixing zone in thin lenses is generally found to have a thickness of more than one meter according to De Louw et al. (2013, Chapter 4 of this thesis), based on field measurements. In that study, the measurements of rainwater lenses and mixing zones between the lens and the underlying saline seepage water illustrate that the mixing zone forms a substantial part of the total amount of fresh water in the lens. The term fresh water lens was shown to be incorrect in some cases, since even the top of a lens is in some cases brackish. Therefore, I will use the term rainwater lens in this thesis, implying that rainfall surplus is the source of the relatively fresh water on top of the saline groundwater.

Since 2007, the thin lenses and associated topics like fresh water recharge in lowland catchments and upscaling of local systems have been investigated in several ways. De Louw (2013) focused on sand boils and the geohydrology and measurement of thin lenses. Pauw (2015) started upscaling of the local system to a regional model and investigated the possibilities for recharging creek ridges and associated pumping. Delsman (2015) modelled the origin of the saline water during the Holocene and the role of local and regional groundwater quality on drain water quality. Field work has been conducted on point-, field-, and regional scale, using monitoring networks varying from piezometers to helicopter borne electromagnetic surveys. Together with chemical sampling to derive quality and possible origin of the water, this has enabled the development of models that improve the capacity to upscale the functioning of rainwater lenses. Other studies that concern mixing between fresh and saline water in coastal areas (e.g. Vandenbohede et al., 2014; Mollema et al. 2011) and other topics mentioned above, show that the necessity of maintaining the fresh water resources in coastal zones is widely recognized. Steps towards applying the theoretical and experimental knowledge obtained over the last decade are starting to be put into practice by the Province and Waterboard* in the Southwest of The Netherlands (e.g. GO-FRESH project, 2016).

This thesis also focusses on thin lenses in low lying areas with saline groundwater. Figure 1.2 schematically illustrates the main research topics investigated in this thesis (rectangles) and their relation to previously investigated topics (ellipses) and new research topics related to this thesis (circles).

* Dutch Water boards are regional government bodies charged with managing water barriers, waterways, water levels, water quality and sewage treatment in their respective regions. These regional water authorities are among the oldest forms of local government in the Netherlands, some of them having been founded in the 13th century.

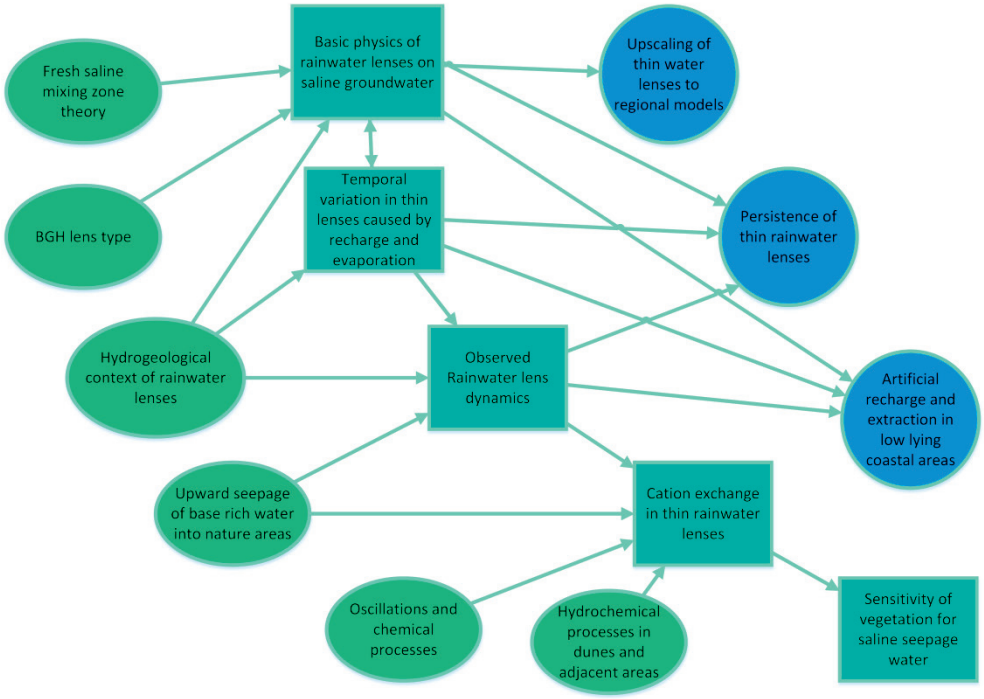

Figure 1.2: Schematic research context, Green ellipses: previous research, basis for thin lenses on saline seepage water. Aqua rectangles: this thesis. Blue circles: recent research linked to work presented in this thesis.

1.1.2 Basic physics of rainwater lenses on saline groundwater

Based on the findings of Maas (2007) and the field observations by De Louw et al. (2011), the need of understanding the relations between seepage, net precipitation, density difference, field geometry and soil hydraulic parameters is evident. Mixing zones have been investigated for theoretical problems by e.g. Henry (1964), Abarca et al. (2007) and De Josselin de Jong and Van Duijn (1986). Their findings together with those of Maas (2007) were used in this thesis to develop a two dimensional model for a field with a precipitation surplus and upward seeping saline water between two drains or ditches (Figure 1.1b). A physical analysis showing their relative influence on the thickness of the lens as well as the mixing zone, both near and away from drains, forms the basis (Chapter 2) of this thesis. To obtain insight in the basic relations in the system, steady state lenses, developed from initially saline conditions have been studied. This analysis of basic relations has been used by Pauw et al. (2014) to upscale the behavior of thin lenses in a system of densely distributed drainage networks in polders. An investigation on the persistence of thin lenses in dry periods was also linked to this study.

1.1.3 Temporal variation in lenses caused by recharge and evaporation

Changes on the long term, like sea level rise and climate change can be well described using steady state analysis. However, development of crops or natural vegetation may well be influenced by short-term events, especially when these events influence the availability of rainwater in a thin lens, increasing stress caused by drought with stress caused by saline water in the root zone. The change of flow direction in the lens, caused by alternating precipitation and evaporation requires analysis of the effect of these oscillations on the thickness of lens and mixing zone. Cirkel et al. (2015) already showed the influence of the travelled distance of the middle of the mixing zone on its width in a vertical column. I used this concept to establish relations between weather events of different duration on mixing zone thickness. Cartwright (2004) looked into response functions of fresh-saline interfaces at the beach caused by storm events. This was a good starting point for investigating response of thin lenses in terms of damping and delay of the impulse, being a precipitation event or period of drought, with a certain intensity and duration.

1.1.4 Observed rainwater lens dynamics

The physical mechanisms of the small lenses are largely influenced by heterogeneity caused by geological and biological features. The theory on variations therefore needs to be put in perspective of a field study on dynamics. A large set of field observations of rainwater lenses has been obtained between 2006 and 2011 by De Louw and Eeman et al. They first studied the different methods that may be used to map rainwater lenses on different scales and with different resolution. Based on this experience, two study sites in Zeeland, in the south west of The Netherlands, were monitored for two years. The mixing zones at different distances from drains, and with different seepage rates provided information on the fast dynamics caused by weather conditions, and the more stable conditions towards the bottom of the lens. This data has added important information on the dynamics of thin lenses, such as the importance of soil layering and heterogeneity that needs to be taken into account when analysing the future possibilities of the lenses. Pauw et al. (2015a, b) continued the studies on thickness variation to man-induced variation, aimed at optimizing sustainable use of fresh water by means of infiltration in elevated creek ridges and the impact of pumping on rainwater lenses.

1.1.5 Cation exchange in thin rainwater lenses

Delsman et al. (2014a) established a model that shows the origin and development of saline groundwater water during the Holocene in the Dutch Coastal zone, providing the hydrogeological context on a regional scale. The differences between local and regional scale (saline) ground water systems and their influence on the salt water load in a polder field were investigated by them as well (2014b). Another important effect of the composition of the saline seepage water is its influence on the composition of

the pore water and soil complex near or in the root zone. As a rainwater lens develops from initially saline conditions, two very different water types start interacting. The influence of the mixing of seepage water and rainwater on water and soil quality has been recognized and investigated by amongst others Stuyfzand (1993) for regional coastal systems. The influence of cation exchange on soil complex and pore water on field scale, including the influence of drainage provides insight into the major hydrogeochemical processes. The influence of regular oscillations of the fresh-saline interface on pore water and complex composition were recently investigated by Cirkel et al. (2015) for one dimensional calcium-sodium exchange. In many field situations with saline seepage, magnesium and potassium may be present in significant concentrations. In a field situation, the regular artificial oscillations are replaced by a natural, irregular alternation of precipitation and evaporation. The often present tile drains cause an important horizontal flow component complicating the vertical oscillation pattern compared to a one dimensional situation.

1.1.6 Sensitivity of vegetation for saline groundwater

As saline water reaches the root zone, it is expected to start influencing crop yield and growth of natural vegetation. This situation occurs as the rainwater has evaporated, and brackish or saline water reaches the root zone. The lens has then (temporarily) disappeared. The occurrence of such situations was lately investigated by Stofberg et al. (2016). Therefore, apart from the characteristics of the lens, the situations in which the effect of saline seepage on vegetation is significant need to be characterized. This depends not only on hydrogeological and meteorological parameters, but could also depend on vegetation characteristics like rooting depth and sensitivity to saline water. The actual effects of saline water on vegetation have proven hard to characterize, and are subject of current research programs such as the STW/Ministry I&M funded WaterNexus. Using a range of relevant plant- ,soil-, water- and atmospheric parameters in a standard crop growth model, a first order assessment of the influence of these parameters on salinity induced vegetation stress can be given. Using such a tool for situations in which saline seepage water can reach the root zone, priorities may be set on where changes in water management are most effective and urgent.

1.2 Aim and research questions

The aim of this thesis is to contribute to the understanding of the mechanisms, characteristics and processes that influence the functioning of thin rainwater lenses on saline seepage water as source of fresh water for crops or natural vegetation.

The specific research questions focused on in this thesis are:

- How is the thickness of a thin rainwater lens and its mixing zone related to hydrological and geometrical parameters?
- What is the influence of intrinsic variability on the thickness of a lens and its mixing zone?
- In which way does cation exchange due to mixing of saline seepage and infiltrating rainwater in a lens influence the quality of water and soil?
- Which parameters dominate the influence of saline seepage water on plant growth?

1.3 Thesis outline

Chapter 2 defines relations between fluxes, soil parameters, field geometry, salinity and the thickness of lens and mixing zone. A dimensionless set of parameter groups is established to enable an efficient comparison of the influence of different parameters and their sensitivity on the thickness of both lens and mixing zone and the effect of convergence near drains. In Chapter 3, the influence of variations in the average, amplitude and frequency of recharge is quantified for the thickness of lens and mixing zone. Using convolution theory, the damping and delay of lens response to weather or climate changes is studied. Chapter 4 shows the results of 2 years of monitoring two thin rainwater lenses in the southwest of The Netherlands. Temporal and spatial variations of the lenses are analyzed using a calibrated transport model for one of the sites. Differences in dynamics between the top and bottom of a rainwater lens are illustrated and explained. In Chapter 5, the dynamics of a lens with respect to cation exchange are investigated. I start with a one-dimensional analysis of the effect of alternating flow directions on cation exchange at the fresh-saline interface. From there, I work towards a conceptual two dimensional model of the study site based on the transport model from the previous chapter and compare this with geochemical data. Chapter 6 contains the analysis of one dimensional simulations relating hydrology, geology and meteorology to yield response. Systems with different soils, water levels and salinity, weather data and vegetation characteristics are compared with respect to salinity induced vegetation stress. I provide a first order approximation of the relative importance of the different variables that influence vulnerability of a system with respect to salinity, compared with stress induced by drought or lack of oxygen. Chapter 7, the synthesis of this research, combines the previous chapters to answer the research questions. Possible implications for water management in areas with saline seepage are identified, and recommendations for future research are provided.

2 BASIC RELATIONS AND DEVELOPMENT OF RAINWATER LENSES

ABSTRACT

In regions with saline groundwater, rainwater lenses may develop due to precipitation infiltration. The amount of fresh water that is available for e.g. agricultural crops depends on the thickness of the lens and the extent of mixing between fresh and saline water. In this paper, we consider the mixing of fresh water and upward moving saline ground water in low-lying deltaic areas. The parameters that dominate the flow and transport problem are investigated using dimensionless groups and scaled sensitivities. We characterize the numerically simulated thicknesses of the lens and of the mixing zone by spatial moments. Rayleigh number and mass flux ratio, i.e. the ratio of the salt water seepage and the precipitation, determine the thickness of the rainwater lens. The thickness of the mixing zone is mainly influenced by the dispersive/diffusive groups and the mass flux ratio. Analytical and numerical steady-state solutions for lens thickness are compared, taking into account upward seepage, for the two cases with and without a density difference between lens and underlying groundwater. Agreement between the numerical and analytical cases for the lens thickness is good except when the mass flux ratio becomes small. For zero mass flux ratio, it is implicitly assumed in the analytical solution that salt water is stagnant, and that is unrealistic. As expected, the steady state situation is independent of the different initial salt distributions that we considered. Relative contributions of longitudinal and transversal hydrodynamic dispersion and diffusion to the thickness of the mixing zone are quantified numerically for different phases of lens formation. Longitudinal dispersion dominates in the early stages of lens formation, while diffusion and transversal dispersion dominate at steady state. In addition, convergence of streamlines towards an outflow boundary affects the thickness of the mixing zone.

This chapter is based on: S. Eeman, A. Leijnse, P.A.C. Raats, and S.E.A.T.M. van der Zee. 2011. The transition zone between a fresh water lens and underlying saline groundwater. Advances in Water Resources (34): p. 291–302.

2.1 Introduction

One of the classical problems in hydrology is the so-called 'dune problem' that considers the flow of fresh water on top of saline groundwater in coastal dunes. It has been studied by Badon Ghyben and Herzberg (Badon-Ghyben, 1888, Herzberg, 1901) and many others, e.g. Bear (1972), Van der Veer (1977), Bruggeman (1999), Collins et al. (1999), Fiori et al. (2000), Maas (2007) and Kacimov (2008), and can be regarded as an extension of studies of laterally confined, 2-D groundwater flow to a drain or ditch in the absence of density differences (Childs, 1969). Both cases without and with density differences in the flow domain have received considerable attention (Hooghoudt, 1937, Childs, 1969 and Fetter,1972). This interest may originate from the need to dimension drainage systems, and because sustainable use of fresh water reserves for drinking water supply or irrigated agriculture require that we understand the dynamics of these water resources. The dune problem has relevance for other geographical situations, such as barrier islands (Collins et al., 1999) and atoll islands (Underwood et al., 1992). Of interest also may be the similarity with immiscible flow of oil spills at the phreatic water surface, as affected by capillarity (Van Dijke et al., 1998a).

Of particular interest is the dune problem with upward flowing saline water that was considered by Maas (2007). He mentions similarities with much smaller scale flow in agricultural fields in lowland areas behind the dunes. These often deltaic or lacustrine sedimentary deposits are usually characterized by complexes with alternating fine and coarse textured layers (Dagan, 1989, Oude Essink, 2001a, Ruppel et al. 2000, Vandenbohede et al, 2008). In such areas, upward seeping brackish or saline water flows through confining layers and meets infiltrating fresh rainwater, upon which both discharge into the drains or ditches.

A common assumption in addressing the dune problem is to consider the transition from fresh to saline water to be sharp. Making this assumption, analytical solutions for the shape of the interface can be found for some steady-state, two-dimensional problems (Van der Veer, 1977, Bruggeman, 1999, Bakker, 2000 and Maas 2007). These problems represent islands or coastal dune areas, either in the presence or in the absence of confining layers. Those solutions differ with regard to whether the saline water is considered to flow or to be stagnant. The validity of assuming a sharp interface for coastal aquifers was discussed by Sakr (1999) for confined aquifers, assuming a constant diffusion coefficient. He concluded that the sharp interface assumption only holds for a relatively small diffusion coefficient, which is disputable for the cases we consider here.

The fresh water reserves in dune areas depend on both the mean position and the thickness of the mixing zone between fresh and salt water. Analytical solutions assuming a sharp interface provide an estimate for the mean position of this mixing

zone. For the thickness of the fresh-saline mixing zone, however, very limited generic understanding is available. This is due to the mathematical complexity of the dispersion process, even for relatively simple cases. The mechanical dispersion depends on the water flow pattern and velocity field that is affected significantly by the density difference between the fresh and salt water (De Josselin de Jong et al.,1986, Van Duijn et al., 1998). Taking into account the impact of such density variations on the flow field, Paster and Dagan (2008) analyzed the mixing zone for the three dimensional case, extending their earlier work. Regarding dispersion, they assumed a small value of the transversal dispersivity and therefore limited transversal mixing that justified their boundary layer approach. Other generic mathematical analyses of the density affected mixing process also emphasized the importance of transversal dispersion for the water flow parallel to the fresh-salt water mixing zone (De Josselin de Jong et al.,1986, Van Duijn et al., 1998).

To describe the mixing zone between fresh water and salt water as caused by dispersion and diffusion, accounting for density affected flow, numerical codes such as MOCDENS3D (Oude Essink, 1998), SEAWAT (Langevin et al., 2003) and SUTRA (Voss et al., 1987 and 2003) can be used. Numerical studies that consider the density affected mixing zone for the dune problem (Oude Essink et al., 2000, Vaeret, 2008 and Vandenbohede et al., 2008) or for other cases of fresh-salt shear flow (Abarca et al., 2007, Henry, 1964 and Kaleris et al. 2002) are quite site specific.

In this chapter, we use SUTRA to numerically determine the mean position and the thickness of the mixing zone of a rainwater lens overlying upward seeping saline groundwater in a coastal lowland field, in order to quantify the fresh water reserve. Since physical conditions differ for different fields, we determine the sensitivities of parameters using dimensionless groups. In addition, we consider in detail the relative importance of longitudinal and transversal mixing in the mixing zone during the formation of the lenses.

2.2 Theory

2.2.1 Qualitative description of the problem

Consider the system shown in Figure 2.1. It is a vertical cross section of the flow domain between two ditches or drains, which we assume to be locations of vertical axes of symmetry. Other vertical axes of symmetry are located halfway between the ditches. Recharge of fresh water (colored grey) occurs at the upper boundary, while vertical upward saline seepage (uncolored) occurs at the lower boundary. All water entering the flow domain leaves through the ditches or drains. The geometry of the flow domain is similar to that of the dune problem as described by Underwood et al. (1992) (their Figure 13), and Maas (2007), whose analytical solution will be compared with our numerical results.

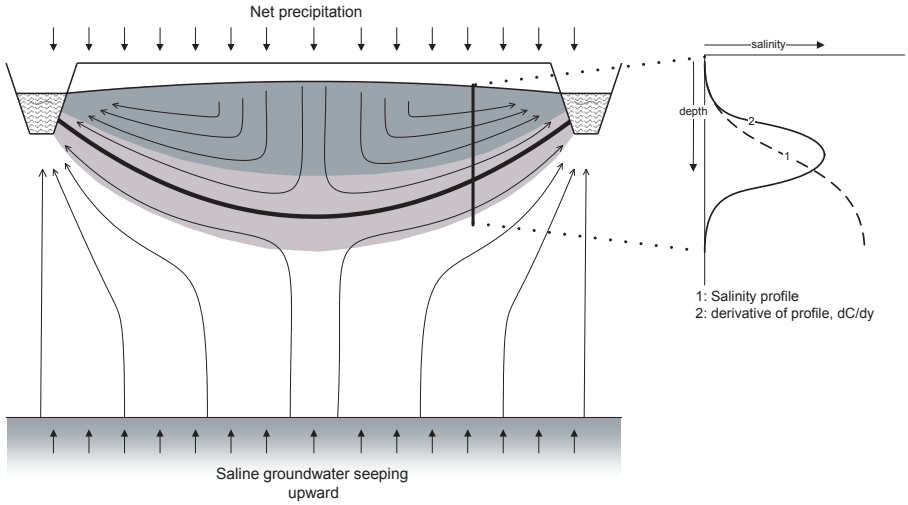

Figure 2.1: A steady rainwater lens (in grey) on top of saline upward flowing ground water (white) with arrows that illustrate flow lines. The mixing zone (light grey) lies in between. The thick black line indicates the "position of the interface". On the right hand side a visualization of the salt mass fraction profile and its first derivative.

In coastal lowlands, the upper, phreatic aquifer is often separated from the deeper aquifer by a confining layer that is significantly less permeable than the aquifers (Collins et al.,1999, De Louw et al., 2010, Ruppel et al., 2000 and Vandenbohede et al. 2008). If in such a case the land is drained at a level below mean sea level, the gradient of the driving force (pressure and gravitational forces) will be directed upward and the assumption of uniform upward saline seepage is justified.

The formation of the freshwater lens depends on different factors, such as water fluxes, potentials, and salt concentrations at the boundaries of the domain, properties of the aquifer (such as hydraulic conductivity, porosity, dispersivities), and geometry (such as aspect ratio of the domain). Whereas many of these factors can be measured, dispersivities remain difficult to quantify. The values of dispersivities proposed in the literature range from 0.1-1 mm (Fiori et al. 2000) to meters (Kaleris et al., 2002 and Kaleris, 2006) or even larger (Gelhar et al.,1992). This large range is caused by differences between pore scale dispersion and macro- or mega-dispersion. Proposed pore scale dispersivities (e.g. Dagan, 1989 and Fiori et al. 2000) are usually much smaller than macro- and mega-dispersivities, because the latter also account for mixing related with larger scale spatial variability of the hydraulic conductivity. In their work, Paster and Dagan (2008) assumed small pore scale transversal dispersivities, and that assumption justified their boundary layer approach. The dispersivities used by Kaleris et al. (2002) and Kaleris (2006) are intended to represent the combination of pore scale dispersion and macro dispersion. They are related to the length scale of the flow domain, in view of observations by Gelhar et al. (1992). As Kaleris et al. (2002) indicate, also their numerical discretization affected

their choice of the dispersivity, which was taken equal in the longitudinal and transversal directions. For the present purpose, we find it appropriate to consider macroscopic values for the dispersivities, since variability of the hydraulic conductivity in the domain at scales larger than the pore scale cannot be ignored. In order to avoid inaccuracies in the numerical simulations, we choose our discretization such that it is compatible with the smallest dispersivities we consider.

2.2.2 Model Equations

We briefly give the equations for the water-saturated domain. For symbols and units we refer to the Nomenclature on p. vii and viii.

The mass balances for the fluid and salt are, respectively, given by

$$\frac{\partial}{\partial t}(n\rho)+\frac{\partial}{\partial x}(\rho q_x)+\frac{\partial}{\partial z}(\rho q_z)=0 \tag{2.1}$$

$$\frac{\partial}{\partial t}(n\rho\omega)+\frac{\partial}{\partial x}(\rho\omega q_x)+\frac{\partial}{\partial z}(\rho\omega q_z)+\frac{\partial}{\partial x}(J_x)+\frac{\partial}{\partial z}(J_z)=0 \tag{2.2}$$

As used e.g. by Landman and Schotting (2007) where $\rho\omega$ is the mass density of the salt in the fluid phase and $\rho\omega q_x$ and $\rho\omega q_z$ are the convective components of the salt flux in the x- and z-direction, respectively. The porosity and the fluid density are both assumed independent of the pressure in the fluid phase. The equation of state is assumed to give the fluid density ρ as a linear function of the salt mass fraction ω (Weast, 1982)

$$\rho=\rho_0\left(1+\gamma\omega\right) \qquad \text{or} \qquad \Delta\rho=\rho-\rho_0=\rho_0\gamma\omega \tag{2.3}$$

Assuming that the porous medium is isotropic and taking the z-coordinate positive in the downward direction, the components q_x and q_z of the specific discharge $\boldsymbol{q}$ of the fluid are given by Darcy's law

$$q_x=-\frac{\kappa}{\mu}\frac{\partial p}{\partial x} \qquad\qquad q_z=-\frac{\kappa}{\mu}\left(\frac{\partial p}{\partial z}-\rho g\right) \tag{2.4}$$

where κ and μ are constant, i.e., we consider a homogeneous flow domain. A constant viscosity μ is justified as it changes less than 2% between fresh water and seawater (Weast, 1982).

For the hydrostatic fresh water pressure p_0 it is assumed that at reference level $z=0$ the pressure $p_0=0$. Therefore

$$p_0 = \rho_0 g z \tag{2.5}$$

In Eq. 2.4 the deviation $\Delta p = p - p_0 = p - \rho_0 g z$ is introduced to obtain

$$q_x = -\frac{\kappa}{\mu}\frac{\partial \Delta p}{\partial x} \qquad q_z = -\frac{\kappa}{\mu}\left(\frac{\partial \Delta p}{\partial z} - \Delta\rho g\right) = -\frac{\kappa}{\mu}\left(\frac{\partial \Delta p}{\partial z} - \rho_0 g \gamma\omega\right) \tag{2.6}$$

Later in our paper, we analyze the different components of the diffusive/dispersive salt mass flux $\boldsymbol{J}$ in the vicinity of the mixing zone. For this reason we give the components J_x and J_z of this mass flux

$$J_x = -n\rho\left(D_{xx}\frac{\partial\omega}{\partial x} + D_{xz}\frac{\partial\omega}{\partial z}\right) \qquad J_z = -n\rho\left(D_{zx}\frac{\partial\omega}{\partial x} + D_{zz}\frac{\partial\omega}{\partial z}\right) \tag{2.7}$$

and the well-known elements of the diffusion/dispersion tensor (Bear, 1972)

$$\begin{bmatrix} D_{xx} & D_{xz} \\ D_{zx} & D_{zz} \end{bmatrix} = \begin{bmatrix} = D_m + \alpha_l \frac{v_x^2}{|v|} + \alpha_t \frac{v_z^2}{|v|} & \left(\alpha_l - \alpha_t\right)\frac{v_x v_z}{|v|} \\ \left(\alpha_l - \alpha_t\right)\frac{v_x v_z}{|v|} & D_m + \alpha_l \frac{v_z^2}{|v|} + \alpha_t \frac{v_x^2}{|v|} \end{bmatrix} \tag{2.8}$$

The components v_x and v_z and the magnitude $|v|$ of the fluid velocity in Eq. 2.8 are given by

$$v_x = q_x / n \qquad v_z = q_z / n \qquad |v| = \sqrt{v_x^2 + v_z^2} \tag{2.9}$$

2.2.3 Initial and boundary conditions

Initially, the entire region is assumed to be occupied by fluid with salt mass fraction ω_i:

$$\omega = \omega_i \quad @ \quad t = 0 \quad \text{in the region} \quad 0 < x < L \quad \text{and} \quad 0 < z < H \tag{2.10}$$

At the upper boundary $z = 0$, the net precipitation of fresh water enters the domain at a rate P with salt mass fraction $\omega = 0$ and corresponding density $\rho = \rho_0$ and no salt enters or leaves the domain. This results in the following boundary conditions

$$\rho q_z = \rho_0 P \qquad \rho\omega q_z + J_z = 0 \qquad @ \qquad z = 0 \tag{2.11}$$

The left boundary underneath the ditch at $x = 0$ and the right boundary at $x = L$ act as no-flow boundaries for both the fluid and the salt

$$\rho q_x = 0 \qquad J_x = 0 \qquad @ \qquad x = 0 \quad \text{and} \quad x = L \qquad (2.12)$$

At the lower boundary $z = H$, the upward seepage of salt water has a rate S, a salt mass fraction $\omega = \omega_{max}$ and a corresponding density $\rho = \rho_{max}$. Assuming that the inflow reservoir outside the model domain is a well-mixed reservoir, gives

$$\rho q_z = -\rho_{max} S \qquad \rho\omega q_z + J_z = -\rho_{max}\omega_{max} S \qquad @ \qquad z = H \quad (2.13)$$

where the upward seepage S is defined positive.

At the boundary of the ditch, the component q_n of the fluid flux normal to that boundary is assumed to be linearly dependent on the difference between the fluid pressure in the porous medium and the fluid pressure in the ditch. In all cases studied here, fluid is flowing into the ditch (q_n>0), and the dispersive component of the salt mass flux normal to the boundary J_n is assumed to be zero. Boundary conditions are then given by

$$q_n = \frac{\xi}{\mu}(p - p_b) \qquad J_n = 0 \qquad \text{if} \qquad q_n > 0 \qquad (2.14)$$

2.2.4 Dimensionless and scaled reformulation of the problem

Using L as the reference length, P/n as the reference velocity, P as the reference specific discharge, the fresh water density ρ_0 as the reference density, and the maximum salt mass fraction ω_{max} as the reference salt mass fraction, we redefine the variables as dimensionless variables. Choosing the reference time $t_r = Ln/P$, i.e. as the ratio of the reference length and the reference velocity, the reference pressure $p_r = \mu LP/\kappa$, i.e. as the ratio of the reference specific discharge and the conductance for flow in the horizontal direction over the distance L, the reference diffusion/dispersion coefficient $D_r = LP/n$, i.e. as the product of the reference length and the reference velocity, and the reference diffusive/dispersive salt mass flux as $J_r = \rho_0 P \omega_{\max}$, all equations can be rewritten in scaled form, resulting in a set of nine dimensionless groups.

The model equations generate five dimensionless groups. Eq. 2.3 yields the dimensionless derivative $F = \gamma\omega_{\max}$ of the fluid density ρ with respect to the salt

mass fraction ω. Eq. 2.6 yields the Rayleigh number $R = \frac{\kappa g(\Delta\rho)_{\max}}{\mu P}$, which is the ratio of the gravitational force and the viscous force. In this case, it can be interpreted as the ratio of the gravitational flux of a vertical column of salt water with density ρ_{max} surrounded by fresh water with density ρ_0 and flux P. Eq. 2.8 yields the dimensionless molecular diffusion coefficient $D = \frac{D_m n}{LP}$; the dimensionless transversal dispersivity $A_t = \alpha_t / L$; and the difference between the dimensionless longitudinal and transversal dispersivities $A_r = (\alpha_l - \alpha_t)/L$.

The initial and boundary conditions (Eq. 2.10, 2.13, and 2.14) generate four additional dimensionless groups. Eq. 2.10 yields the ratio ω_i / ω_{max} of the initial and maximum values of ω. Since this group is kept constant in this study we do not consider it further. Eq. 2.10 and 2.13 generate the aspect ratio $G = H/L$. Eq. 2.13 yields the ratio $M = (\rho_{max} S)/(\rho_0 P)$ of the mass fluxes at the lower and upper boundaries of the domain. Finally, Eq. 2.14 yields the dimensionless conductance $C = \xi L/\kappa$ of the soil-ditch interface.

Overview of dimensionless groups

M	Mass flux ratio	$M = (\rho_{\max} S)/(\rho_0 P)$
R	Rayleigh number	$R = (\kappa g(\Delta\rho)_{\max})/(\mu P)$
D	Molecular diffusion coefficient	$D = D_m n / LP$
G	Aspect ratio	$G = H/L$
A_r	Dispersivity difference	$A_r = (\alpha_l - \alpha_t)/L$
A_t	Transversal dispersivity	$A_t = \alpha_t / L$
F	Fluid density derivative	$F = \gamma\omega_{\max}$
C	Permeance	$C = \xi L/\kappa$

2.2.5 Analytical solution

Assuming a sharp interface between the fresh and saline water, a geometry and boundary conditions that represent an infinitely long island of width $2L_{in}$ (L) surrounded by (saline) sea water, and an aquifer of infinite depth, Maas (2007) has derived the steady state solution for the interface position. The maximum depth Z (L) of this interface is given by (cf., Equation 20)

$$\frac{Z}{\left(L_{in}{}^{2}+Z^{2}\right)^{1/2}}=\frac{-S/P+\left(\left(S/P\right)^{2}+4\left(1+S/P+R\right)\right)^{1/2}}{2\left(1+S/P+R\right)} \tag{2.15}$$

and its elliptical shape is described by

$$\frac{x^{2}}{L_{in}{}^{2}+Z^{2}}+\frac{z^{2}}{Z^{2}}=1 \tag{2.16}$$

In the absence of a density difference (Rayleigh number $R=0$) Eq. 2.15 reduces to

$$\frac{Z}{\left(L_{in}{}^{2}+Z^{2}\right)^{1/2}}=\frac{1}{1+S/P} \tag{2.17}$$

whereas for zero saline seepage, Eq. 2.15 simplifies to the classical result:

$$\frac{Z}{\left(L_{in}{}^{2}+Z^{2}\right)^{1/2}}=\frac{1}{\left(1+R\right)^{1/2}} \tag{2.18}$$

(see Equations 17-21 of Bakker, 2000).

2.2.6 Numerical solution and parameter values

The equations for fluid flow and salt transport were solved using the numerical model SUTRA of Voss and Provost (2003). This finite element model has been verified extensively for density dependent flow situations (Voss and Souza, 1987 and Voss and Provost, 2003). Our model domain shown in Figure 2.2 describes the lens system in a field bordered by ditches, as in Figure 2.1. In view of symmetry, only half of the field needs to be considered.

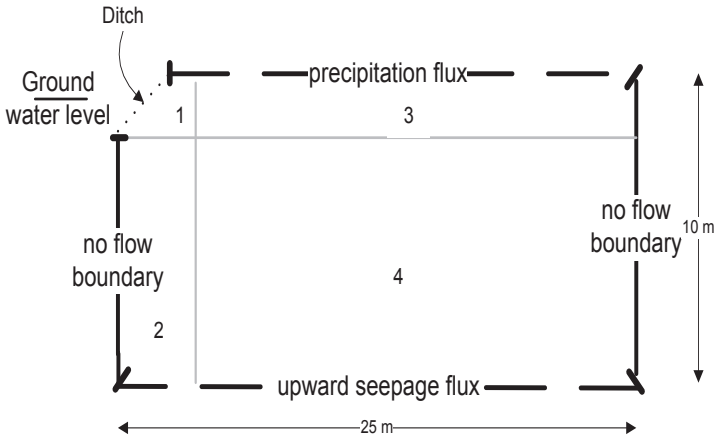

Figure 2.2: Sketch of the geometry and boundary conditions for a field draining in a ditch. Areas 1 to 4 represent different discretization zones. Indicated length and width correspond with the reference case, for which the ditch has a triangular cross section.

Initially, the entire flow region is assumed to be saline, i.e. $\omega_i = \omega_{\max}$. The upper boundary has constant recharge rate at zero salinity. At the lower boundary a constant upward seepage of salt water occurs. The vertical axes of symmetry below the ditch and halfway between ditches are no-flow boundaries. The ditch has a triangular cross section with a width of 3 m (half of this is within the domain, this is 0.06 L) and a depth of 1.5 m (this is 0.15 H). The water in the ditch has a hydrostatic pressure distribution that depends on the groundwater level. We compared calculated average fresh-saline interface positions and mixing zone thicknesses for different shapes of the ditch, to ascertain that the ditch shape does not affect our results. We found that interface positions at a distance of 0.2 L from the left boundary differed less than 10 % for different shapes of the ditch. The thickness of the mixing zone is influenced even less (less than 7% at distance 0.1 L from left boundary). For brevity we omit details of these exploratory calculations. Our further analysis is based on results farther than 0.2 L from the left boundary.

Temporal and spatial discretization of the quadrilateral elements were chosen such that the numerical dispersion was much smaller than the mechanical dispersion. The element size in the vertical direction was 0.1 m for the upper 1.5 m of the domain (Figure 2.2, zones 1 and 3) and 0.2 m for depths larger than 1.5 m (Figure 2.2, zones 2 and 4). The element size in the horizontal direction was 0.1 m in the outflow area near the ditch/ drainage (Figure 2.2, zones 1 and 2). In the infiltration area horizontal element sizes of 0.4 m were used (Figure 2.2, zones 3 and 4).

The accuracy of solutions was tested by repeating simulations with grids with twice the number of elements, both horizontally and vertically. The same results were obtained for the reference case and all other considered cases. Moreover, using a coarse grid with double spacing gave only minor differences in the results. This ascertained us that the used discretization is sufficient to obtain an accurate solution for the flow field and the salt mass fraction distribution.

The shape of rainwater lenses and the salinity distribution in the fresh-saline mixing zone were quantified using spatial moments. Those give compact information and have been widely used in other contexts (Acharya et al., 2005, Govindaraju et al.,2007, Janssen et al., 2006, Paster et al., 2008 and Van Dijke et al. 1998b). The spatial moments of the vertical derivative of the salt mass fraction (Figure 2.1, inset) provide information on the position, thickness, and shape of the mixing zone. Govindaraju and Das (2007) extensively discuss formulation and use of spatial moments. The used discretization was checked to be fine enough for determining the spatial moments. The first vertical spatial moment is approximately equal to the 50% iso-chlor for the studied cases.

Table 2.1: Parameter values. Minimum and maximum values are given where relevant for dimensionless groups

Parameter	ref. value	minimum	maximum
g	9.81 m s^{-2}	na	na
n	0.3	0.3	0.6
D_m	10^{-9} m^2s^{-1}	na	na
H	10 m	0.3 x L	1.00 x L
L	25 m	5	50
P	1.157 x 10^{-8} m s^{-1} (= 1 mm/d)	10^{-9}	6 x 10^{-8}
S	5.78 x 10^{-9} m s^{-1} (= 0.5 mm/d)	10^{-9}	6 x 10^{-8}
α_l	0.25 m	0.005 x L	5.0 % x L
α_t	0.025 m	0.0005 x L	0.5 % x L
γ	0.7	na	na
κ	10^{-12} m^2	10^{-14}	10^{-10}
μ	10^{-3} kg $m^{-1}s^{-1}$	na	na
ξ	10^{-10} m	10^{-11}	10^{-1}
ρ_0	1000 kg m^{-3}	na	na
ρ_s	1014 kg m^{-3}	1000.1	1025
$\Delta\rho_{\max} = \rho_s - \rho_0$	14 kg m^{-3}	0.1	25
$\omega_t, \omega_{\max}$	0.14%	0.001	0.25

For the reference case, we used parameter values that are typical for a situation in the Netherlands, shown in Table 2.1. Ranges of parameter values are estimated on the basis of typical geographical and geological situations in deltaic areas. These ranges are also shown in Table 2.1. The ranges in the parameter values lead to ranges in the values of the dimensionless groups, which are shown in Table 2.2. Sensitivity analysis is performed based on these ranges.

Table 2.2: Values of dimensionless groups under reference conditions and the minimum and maximum values.

Name	Group	Reference	Minimum	Maximum
Mass flux ratio	$M = (\rho_{max} S)/(\rho_0 P)$	5.07 x 10^{-1}	1.67 x 10^{-2}	6.15 x 10^{1}
Rayleigh number	$R = (\kappa g(\Delta\rho)_{\max})/(\mu P)$	1.19 x 10^{1}	1.64 x 10^{-4}	2.45 x 10^{4}
Mlc. diffusion coefficient	$D = D_m n / LP$	6.92 x 10^{-4}	5.00 x 10^{-5}	6.00 x 10^{-2}
Aspect ratio	$G = H/L$	4.00 x 10^{-1}	3.00 x 10^{-1}	1.00
Dispersivity difference	$A_r = (\alpha_l - \alpha_t)/L$	9.00 x 10^{-3}	5.00 x 10^{-3}	5.00 x 10^{-2}
Transversal dispersivity	$A_t = \alpha_t / L$	1.00 x 10^{-3}	5.00 x 10^{-4}	5.00 x 10^{-3}
Fluid density derivative	$F = \gamma\omega_{\max}$	1.00 x 10^{-3}	1.40 x 10^{-1}	2.50 x 10^{-1}
Permeance	$C = \xi L/\kappa$	2.55 x 10^{1}	5.10 x 10^{-1}	5.10E x 10^{3}

2.3 Results

2.3.1 Fresh and salt water flow patterns during rainwater lens development

In the numerical simulations, a steady state solution is obtained by simulating precipitation and salt water seepage for a long period, i.e. until the changes in salt mass fraction distribution become negligible. For these transient simulations, an initial condition for the salt mass fraction distribution is needed. No initial condition for the pressure distribution is required since we assume the system to be incompressible, i.e. both the fluid density and the porosity are independent of the pressure. Generally, we assumed that initially all water in the domain is saline (Figure 2.3a). In addition, simulations were carried out with different initial conditions for the fresh-salt water distribution such as that initially all water in the flow domain is fresh water or that a horizontal strip of fresh water is overlying saline water. As we expected, the resulting final steady state distribution is independent of the initial condition (results not shown). Obviously, for the transient phases that precede the steady state situation, the initial condition influences the development of the flow pattern. During this transient phase, streamlines originating from either the fresh or the saline domain may cross the mixing zone and this will affect its thickness. How these streamlines cross that zone depends on the exact initial conditions but here we consider this issue and its effect on the mixing zone thickness prior to steady state only for the reference case. For comparison with the sharp interface, we wish to define also an average interface position for the mixing zone. We call this average position ζ and we define its position by the normalized first moment $\bar{z}$ of the vertical derivative of the salt mass fraction at each horizontal position x.

Fig. 2.3 shows the development of the numerically calculated rainwater lens, starting from an initially salt water filled domain (Fig. 2.3a). We first describe the developing flow pattern by the positions of two streamlines ψ_{A} and ψ_B and the average mixing zone position ζ (Fig. 2.3b). The streamline ψ_{A} starts at point A on the right side boundary, and ends at the ditch in the left top corner. (In the transient phase (Fig. 2.3b), the region occupied by fresh water consists of two sub-regions separated by a streamline ψ_B that starts at point B. The sub-region left of point B is occupied by streamlines that are situated entirely in the rainwater lens. The sub-region on the right is occupied by streamlines that cross the moving average mixing zone position ζ at some non-orthogonal angle, except of course the streamline in the mid-plane between the ditches. Note that the separating streamlines ψ_{A} and ψ_B are not material lines: they will consist of different parcels of fluid in the course of time.

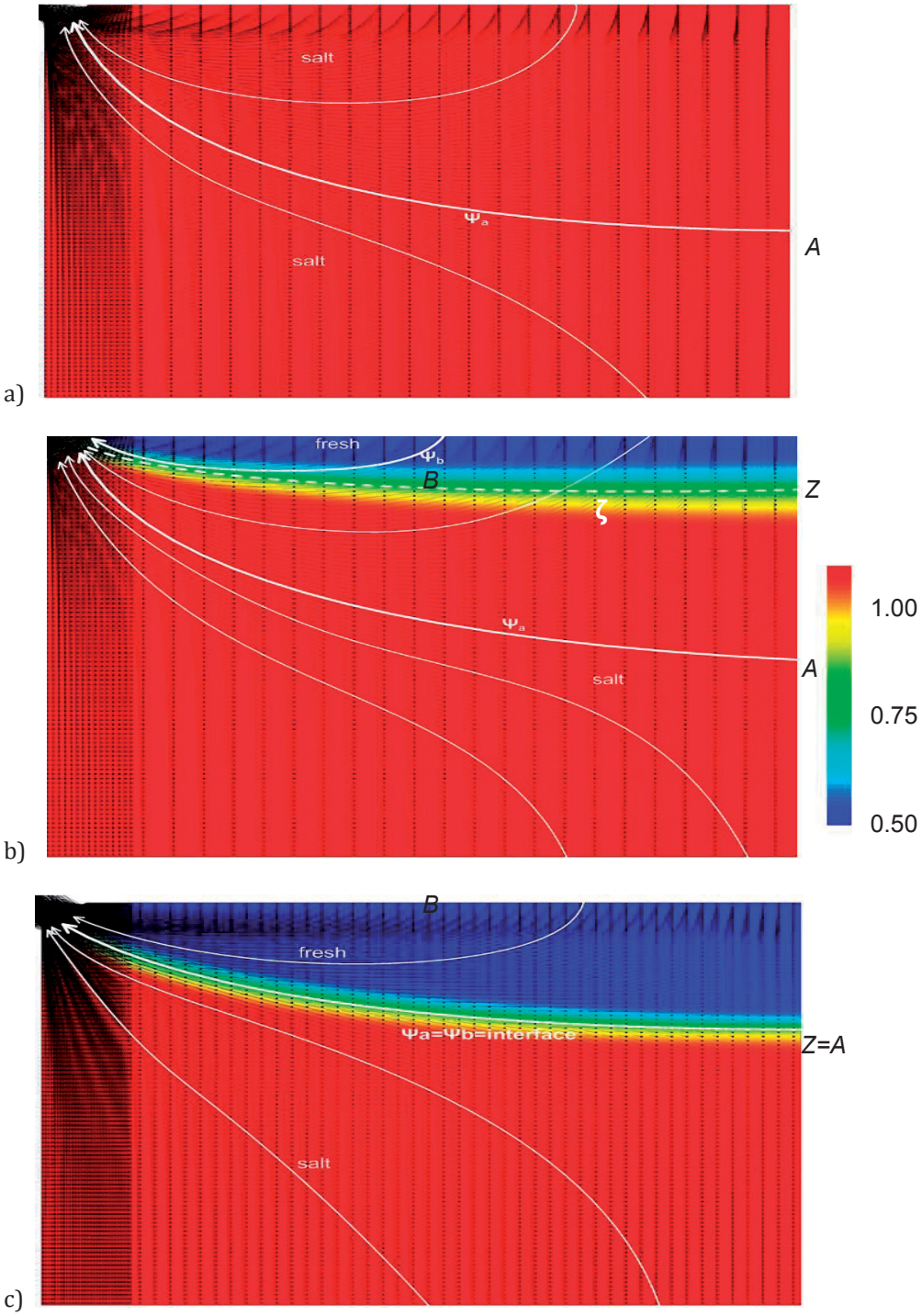

Figure 2.3: Numerically calculated flow pattern and spatial salinity distribution, a) initially, when all water is still saline, b) during formation of a rainwater lens from precipitation, c) well after a steady state lens has been reached. Streamlines are in white, including streamline ψa starting at the stagnation point A. The colour bar shows scaled salt mass fractions ranging from fresh to saline (0-1).

Figure 2.3a shows the flow pattern for very small times, when the amount of fresh water is still negligible. The flow pattern corresponds with a constant density ($\Delta\rho=0$) precipitation/seepage situation, and the position of the streamline ψ_A is approximately described by Eq. 2.17. Note that assuming all water to be either salt or fresh, will give the same initial flow pattern, since all parameters are unaffected by the salt mass fraction. The streamline ψ_B and the average mixing zone position ζ do not yet exist at this moment. This situation best illustrates that the streamlines originating at the groundwater surface, where an infinitely thin rainwater lens starts to develop, cross the fresh-saline mixing zone.

When fresh water starts to infiltrate, the flow gradually becomes affected by the density difference that develops between fresh precipitation and saline seepage water. Figure 2.3b shows the flow pattern in the transient phase when the fresh water body is still developing. For our initial conditions, the point A and the streamline ψ_A are moving upward. The flow pattern is continuously adjusting under the influence of the growing fresh-water lens that overlies the saline water. The average mixing zone position ζ, perpendicularly intersecting the right side axis of symmetry at point Z, is moving downward from the soil surface. Eventually, in the steady state situation as shown in Figure 2.3c, the upward moving point A approaches the fresh-saline interface at point Z and the separating streamline ψ_A and the average mixing zone position ζ will merge. Simultaneously, point B reaches the top right hand corner and the streamline ψ_B will meet the streamline ψ_A at the stagnation point Z = A.

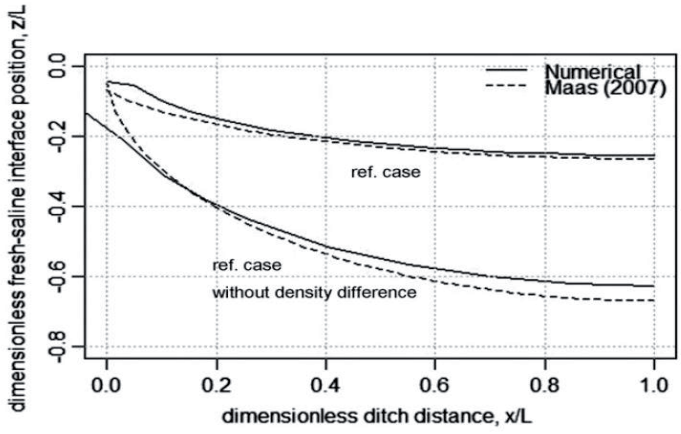

Figure 2.4: Comparison of the analytical approximation (Equation 2.16 combined with either 2.15 or 2.17) of the fresh-saline interface position (Maas, 2007) and the interface position estimated from the salt mass fraction distribution found numerically by calculating the normalized first vertical moment $\mathbf{d\omega/dz}$ at steady state conditions. The upper two lines show the reference case with density difference of 14 kg/m3 (Eq. 2.16 and 2.15), the lower two lines refer to zero density difference, (Eq. 2.16 and 2.17).

The already mentioned sharp interface solution by Maas (2007), for which our Eq. 2.17 gives the shape and Eq. 2.16 fixes the maximum depth of the interface at steady state, is for a slightly different situation than our numerically simulated case. One difference is that Maas considers an aquifer of infinite extent, both lateral and in depth. Additionally, the infiltrating fresh and saline water both leave the system through a horizontal seepage face with prescribed pressure defined by the seawater level, rather than through a ditch as in our case.

Increasing the density differences, the seepage face in the solution of Maas becomes smaller, and therefore better comparable with the ditch we modelled. In case density differences are absent, the seepage face has an extent that cannot be neglected. We have simulated that by extending the model in the lateral direction, and applying a pressure boundary condition along the horizontal upper boundary outside the area where fresh water infiltrates. As shown in Fig. 2.4, we find in both cases a good agreement for the average mixing zone position ζ between the solution given by Maas and the solution we obtain from the first spatial moment of the vertical derivative of the salt mass fraction. From these results it can also be seen that the average position of the mixing zone is significantly affected by the density gradients. For the present parameterization, the average mixing zone depths differ by more than a factor two.

Also of interest is the sensitivity of the depth of the interface to the assumption that the saline water is flowing upwards, since upward flow may not always be realistic. According to the solution by Maas (2007), zero upward saline water flow results in a stagnant salt water region (his Equation 16). Numerically, a zero upward salt water flux at the lower boundary is not easy to implement in our system. The reason is that for our boundary conditions, salt water cannot be replenished, whereas due to diffusion and dispersion, salt will continuously be removed through the ditch. In the limit $t \rightarrow \infty$ the salt mass fraction will approach zero in the entire flow domain. Such a salt depletion can be partly overcome by extending the flow domain to the left over a large distance and imposing hydrostatic (salt) water conditions at the left boundary. In that case, however, salt water will not be stagnant, but reveal a slow rotational, counter-clockwise flow below the interface (results not shown). In other words, the assumption of stagnant salt water in such a case is physically not realistic. In general, the solution as obtained by Maas allows for a jump in the velocity field across the interface, which will not occur in the diffusive/dispersive solution obtained numerically. Therefore we expect differences in the solutions when the mass flux ratio M is small, i.e. when the salt water seepage rate is much smaller than the precipitation rate. In those cases, both analytically and numerically, the general effect of decreasing upward seepage is a deeper infiltration of the fresh water. In the analytical case, where the salt water becomes stagnant, the interface will be located deeper than in the numerical case, where salt water rotational flow is directed upward below the interface, similar as in the case of Abarca et al. (2007). Hence, at small *M*-values, the discrepancy with numerical solutions will be large.

2.3.2 Sensitivity analysis

We tested the response of the lens and the mixing zone thicknesses to parameter variation by a sensitivity analysis based on the dimensionless groups. For each parameter in the dimensionless groups, we decided on a reference value and on a range that represents physically plausible variations (Table 2.1 & 2.2). The fresh water density ρ_0, the effective molecular diffusion coefficient D_m, the parameter γ in the equation of state for the fluid density, the acceleration of gravity g, and fluid viscosity μ, were not varied.

We simulated until the rainwater lens and mixing zone thicknesses were at steady state for the reference values and for the maximum and minimum value of each dimensionless group, keeping all other groups constant at their reference value. The resulting relative changes were determined for a profile at a distance of 0.8 L from the ditch, among others to avoid boundary effects, and are presented in Figure 2.5. The values of the dimensionless groups are normalized by division by the value for the reference case and this is also done for the average position and width of the mixing zone. Figure 2.5 shows that the mass flux ratio *M* is negatively correlated with both the thickness of the lens and the width of the mixing zone. The Rayleigh number R is strongly negatively correlated with the lens thickness and mildly positively with the width of the mixing zone. The aspect ratio G is positively correlated with both the lens thickness and the width of the mixing zone, but the range of G is quite small. The two groups A_t and D_m, that represent the transversal and diffusive mixing process, respectively, strongly influence the width of the mixing zone, and equally obvious hardly influence the thickness of the lens. Group A_r, representing the difference between longitudinal and transversal dispersivity, has no significant influence at steady state, in agreement with the analysis of the contributions of dispersive and diffusive mechanisms to the dispersive flux. The maximum fluid density F has a minor influence for most of the physically feasible range. Only as density approaches fresh water density, the lens size suddenly increases. Group C, representing the resistance at the boundary between the porous medium and the ditch, has a local effect only and is not of importance at the field scale.

Cases with very thin lenses have a truncated mixing zone since saline water reaches the soil surface as explained earlier. Standard deviations for such incomplete salinity distributions cannot be calculated using the spatial moments analysis mentioned earlier, without additional assumptions. These cases that occurred for groups M and R within the physically feasible ranges in Table 2.2, were therefore not elaborated further. A similar problem occurred for low values of F. Results were limited to salt mass fractions that result in a complete lens within the modelled domain.

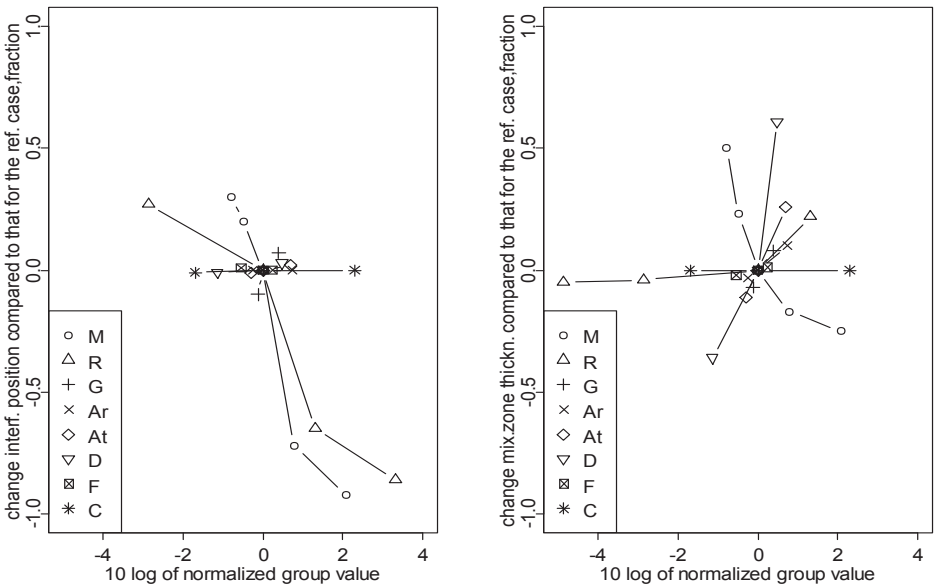

Fig 2.5: Sensitivity analysis of the dimensionless groups, using Table 2.2. Left the interface position change, where a positive change indicates a thicker lens. Right the thickness of the mixing zone, where a positive change indicates a wider mixing zone.

2.3.3 Dispersion and diffusion in the mixing zone

While in the literature, much attention has been given to sharp interface approximations of density induced flow problems, the thickness of the mixing zone has received much less emphasis. Important in the development of a rainwater lens and the mixing zone is the gradual change in the fluid motion from nearly perpendicular to the average mixing zone position ζ and the mixing zone at short times to nearly parallel to ζ at large times. These changes of the flow direction near the average mixing zone position have important implications for the dispersive mixing at this line.

Figure 2.3 shows the salinity distribution in the fresh-saline mixing zone during the transient phase (Figure 2.3b) and at steady state (Figure 2.3c). These figures show qualitatively that during the transient phase the mixing zone is considerably thicker than in the steady state. During the transient phase, fluid flow is directed through the average mixing zone position (see Figure 2.3b). Therefore, during this phase, longitudinal dispersion near the average mixing zone position will be significant (Underwood et al., 1992). As the steady state situation is approached, this is no longer the case (see Figure 2.3c) and transversal dispersion and molecular diffusion become dominant. Taking into account that the longitudinal dispersivities are an order of magnitude larger than the transversal dispersivities, it is understandable that from $t = 0$ (saline conditions) onwards, the width of the mixing zone at first increases, but decreases as the steady state is approached.

Another noticeable feature of the results shown in Figures 2.3b and 2.3c is the narrowing of the mixing zone in the direction of the outflow surface. This means that the increase of the thickness of the mixing zone by diffusive/dispersive spreading is more than compensated by the convergence of the streamlines towards the ditch. This is remarkable as the increasing velocity of the fluid as the ditch is approached implies an increasing dispersion as the ditch is approached.

Abarca et al (2007) considered the mixing zone in the dispersive version of Henry's benchmark problem (1964) in detail. They replaced diffusion of the mixing zone in the Henry problem by longitudinal and transversal dispersion to better approach reality and field observations. They, also, considered the steady state situation. They found that in their case, longitudinal dispersion was the controlling mechanism for the width of the mixing zone. The difference between the case of Abarca et al (2007) and our case concerns differences in the flow directions in the mixing zone. In our case, fresh and saline water flow in the same direction, whereas in the case considered by Abarca et al (2007), the flow is nearly perpendicular because a very sharp curvature occurs in the flow of the saline water near the interface. Therefore, we believe that the observation that longitudinal dispersion dominated for the Abarca et al case is not in contradiction to our observations for the steady state. Using our numerical results, we can support our qualitative assessment also quantitatively.

Apart from the differences in geometry and boundary conditions, three other factors need to be considered when comparing the analytical and the numerical solutions. First, in the numerical solution, the average mixing zone position ζ is defined as the first normalized spatial moment of the derivative of the salt mass fraction in the vertical direction. It is an assumption, that the sharp interface solution can be compared with this first spatial moment in case of a dispersed mixing zone. Equally well, a suitably normalized zeroth moment of the salt mass fraction could have been chosen, and would give different results in case of a skewed distribution of this fraction. Second, especially in the vicinity of the ditch, the distribution of the vertical derivative of the salt mass fraction in the vertical direction is not complete, but truncated, which results in deviations in the first spatial moment. Third, the calculation of the moments in the vertical instead of perpendicular to main flow becomes increasingly incorrect as the ditch is approached.

Aiming at hard, quantitative evidence of which factors affect the thickness of the mixing zone for the case considered here, we have closely considered the contributions of the different processes (longitudinal and transversal dispersion, molecular diffusion) in the mixing zone numerically.

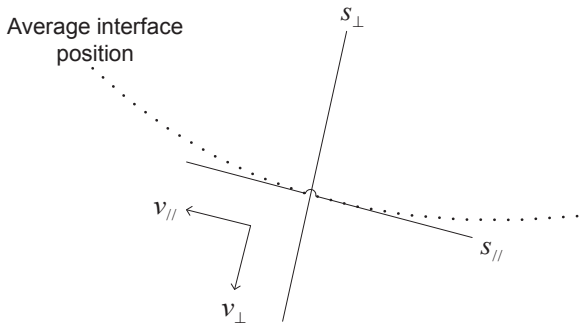

Figure2. 6: Local coordinate system, axes parallel and perpendicular to the average interface position

To that end, the position and width of the mixing zone were determined with the normalized first moment $\bar{z}$ and the variance σ of the vertical derivative of the salt mass fraction. The average mixing zone position, denoted by ζ in Figure 2.3, was constructed by determining the values of $\bar{z}$ as a function of the horizontal coordinate x. We then established a local coordinate system with axes $s_{//}$ and $s_\perp$, respectively parallel and perpendicular to the average mixing zone position, as shown in Figure 2.6. The velocity vector in the local coordinate system has components $v_{//}$ and $v_\perp$. In our notation, we distinguish on purpose between the subscripts $//$ and $\perp$ associated with the local coordinate system and the subscripts l and t associated with longitudinal and transversal dispersivities introduced in Eq. 2.8. Equations 2.7 and 2.8 can be transformed to the local coordinate system. The component $J_{//}$ in the parallel direction plays a role in transport of salt towards the outflow area, but is not of interest for the width of the mixing zone itself. Development and maintenance of the mixing zone is primarily influenced by the component $J_\perp$ perpendicular to the average mixing zone position.

$$J_\perp = -n\rho\left[D_{\perp\perp}\frac{\partial\omega}{\partial s_\perp} + D_{\perp//}\frac{\partial\omega}{\partial s_{//}}\right] \tag{2.19}$$

In the mixing zone, the gradient of the salt mass fraction in the $s_\perp$ direction will be much larger than that in the $s_{//}$ direction. Hence, the choice of the local coordinate system allows us to assume that the contribution of the salt mass fraction gradient in the direction parallel to flow can be neglected

$$\frac{\partial\omega}{\partial s_{//}} = 0 \tag{2.20}$$

so that Eq. 2.19 reduces to:

$$J_{\perp} = -n\rho\left[D_{\perp\perp} \frac{\partial \omega}{\partial s_{\perp}} \right] = -n\rho\left[D_m + \alpha_l \frac{v_{\perp}^2}{|v|} + \alpha_t \frac{v_{//}^2}{|v|} \right] \frac{\partial \omega}{\partial s_{\perp}} \qquad (2.21)$$

Earlier, we suggested that the influence of dispersion and diffusion on the thickness of the mixing zone depends on the phase of the lens development. In the transient phase, the average mixing zone position ζ moves, and the component $v_{\perp}$ normal to this average mixing zone position is significant. Hence, in this phase longitudinal dispersion can give a significant contribution to mixing in the mixing zone. Even for relatively small values of $v_{\perp}$ this is the case, because the longitudinal dispersivity is in general much larger than the transversal dispersivity. As the steady state is approached, flow normal to the average mixing zone position becomes less important and transversal dispersion and diffusion become relatively more important. The diffusive component in Eq. 2.21 is especially important near the stagnation point *A*, when at steady state the points *A* and Z have merged.

For an objective comparison of the different factors that contribute to mixing at the average mixing zone position, from Eq. 2.21 we derive the relative contributions of longitudinal and transversal dispersion and of molecular diffusion:

$$\frac{\alpha_l v_{\perp}^2}{D_m |v| + \alpha_l v_{\perp}^2 + \alpha_t v_{//}^2} \quad \text{relative contribution of longitudinal dispersivity} \qquad (2.22)$$

$$\frac{\alpha_t v_{//}^2}{D_m |v| + \alpha_l v_{\perp}^2 + \alpha_t v_{//}^2} \quad \text{relative contribution of transversal dispersivity} \qquad (2.23)$$

$$\frac{D_m |v|}{D_m |v| + \alpha_l v_{\perp}^2 + \alpha_t v_{//}^2} \quad \text{relative contribution of molecular diffusion} \qquad (2.24)$$

Using these expressions for, again, a rainwater lens that develops in an initially saline domain and using the local velocity vector components and the dispersivity values, we calculated the relative contributions along the numerically obtained average mixing zone position. The results are shown in Figure 2.7a for the transient situation that corresponds to Figure 2.3b and in Figure 2.7b for the steady state situation that corresponds to Figure 2.3c. The contributions of molecular diffusion, longitudinal and transversal dispersion to the mixing process are found to change as a function of time during lens development. During the initial growth of the lens, longitudinal dispersion indeed dominates (Figure 2.7a, $t/t_{ref} = 0.05$). We earlier attributed this to the large velocity components perpendicular to the average mixing zone position combined

with the fact that the longitudinal dispersivity is much larger than the transversal dispersivity. Only close to the ditch, where the flow is almost parallel to the average mixing zone position, longitudinal dispersion is of less importance. This is understandable as there streamlines are almost parallel to the average mixing zone position, causing transversal dispersion to dominate. An additional effect is also that convergence of streamlines may oppose the dispersion process. However, we do not further quantify the mixing close to the ditch, in view of the limitations we mentioned of determining the average mixing zone position on the basis of the first spatial moment in the previous section. For instance, in Eq. 2.22-2.24, the longitudinal and transversal velocity components $v_{//}$ and $v_{\perp}$ are needed and found by interpolating between nodal values. Near the ditch, the average mixing zone position is no longer parallel to the horizontal direction, which gives large numerical errors in the estimates of $v_{//}$ and $v_{\perp}$. This explains the erratic behavior of the different relative contributions near the ditch as shown in Figure 2.7.

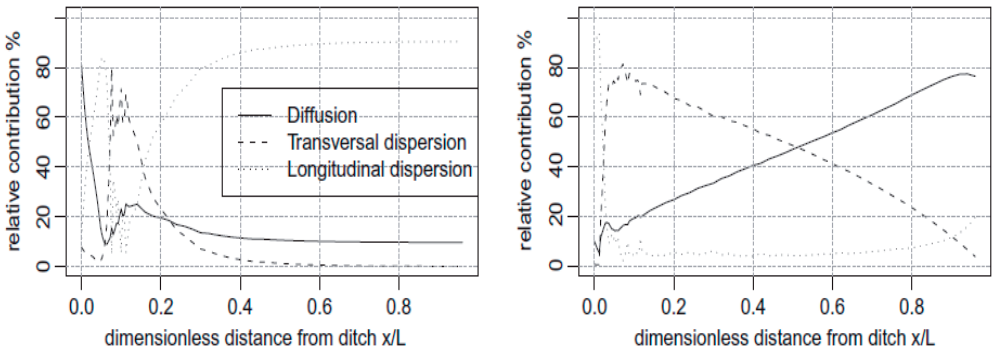

Figure 2.7: Dispersion and diffusion contributions (%) as a function of distance from the ditch, during lens development under reference conditions, a) transient phase (t/t_{ref}=0.05), and b) at steady state.

When the lens has reached its steady state shape, points *A* and *Z* coincide, point *B* has moved completely to the right, and the influence of longitudinal dispersion disappears almost entirely (Figures 2.3c and 2.7b). The dominance of diffusion close to the stagnation point *A* = *Z* is indicative of the small velocities in this region. Towards the ditch, the flow is mainly parallel to the average mixing zone position at all times, causing dominance of the transversal dispersion. Since the magnitude of the molecular diffusion coefficient is a constant (for a designated chemical compound), its relative importance can be viewed as a measure of the total dispersion coefficient.

In Figure 2.8, the relative contributions of longitudinal dispersion, transversal dispersion, and diffusion are shown as a function of time, for three scaled distances to the ditch. The time after which longitudinal dispersion looses its dominance, increases significantly with the distance from the ditch, which is consistent with the development of the flow pattern. Close to the ditch, the moment that water flow is

predominantly parallel to the average mixing zone position occurs earlier than farther away from the ditch. The influence of diffusion increases as a function of both time and distance from the ditch. Far away from the ditch, diffusion becomes dominant at early times due to the low velocities in this area. Of interest in Figure 2.8 is that the different relative contributions depend completely on flow pattern changes because dispersivities and the molecular diffusion coefficient are kept constant. That implies that the relative magnitudes of the dispersion contributions can be easily compared to absolutely (but not relatively) constant value of the molecular diffusion. For our reference case the total diffusive and dispersive mass flux is roughly two times larger than the diffusive mass flux.

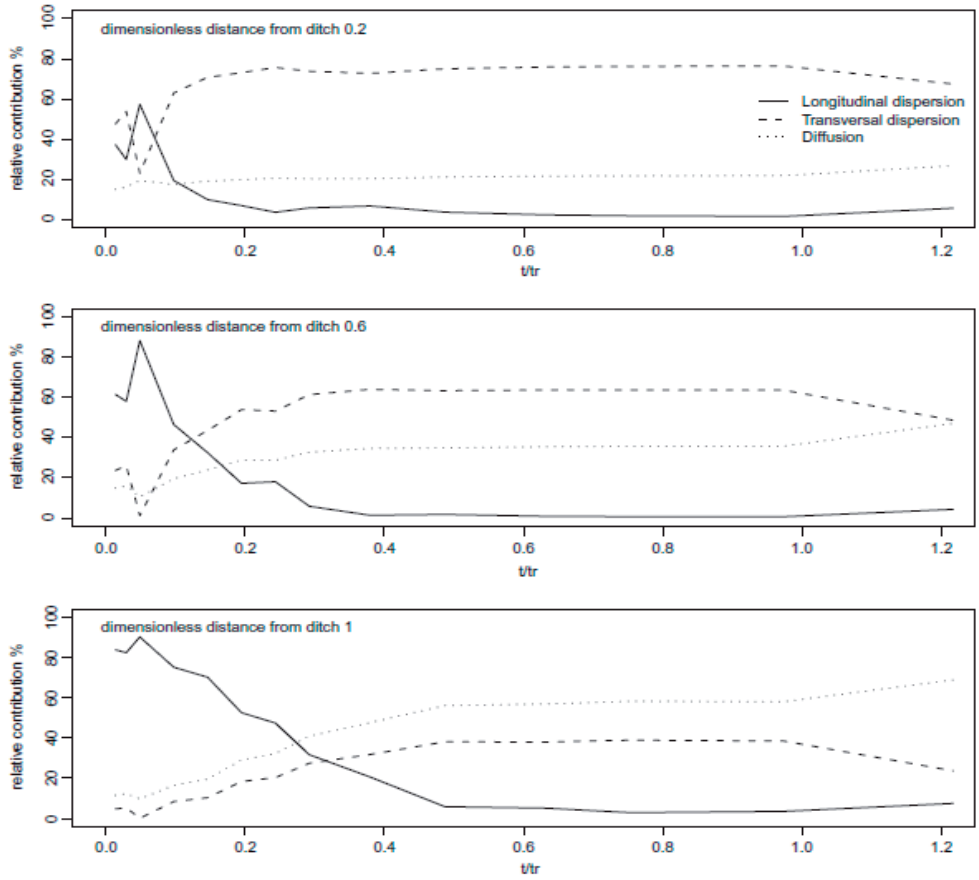

Figure 2.8: Relative dispersion and diffusion contributions (%) as a function of time at a scaled distance of 0.2 (upper), 0.6 (middle) and 1 (lower) from the ditch.

As Figure 2.8 indicates, it may be incorrect to attribute the dispersion at the average mixing zone position entirely to transversal dispersion or diffusion. Instead, it is appropriate to first estimate which of the contribution(s) may be neglected as instead of transversal dispersion also longitudinal dispersion and molecular diffusion may control mixing.

2.4 Conclusions

In this Chapter, we considered density affected flow of fresh water on top of saline water, as frequently encountered in coastal regions. Specifically, we considered the water movement and salt transport in a region drained by equidistant parallel ditches, initially entirely saturated with saline water, and subject to uniform, steady upward seepage of saline water at the bottom and steady rainfall at the top. This leads to the growth of a rainwater lens on top of the saline water, with a diffusive-dispersive mixing zone between the fresh water and the saline water. In view of the importance of the fresh water reserve of the lens, we focused on the impact of nine dimensionless groups of parameters on the thickness of the lens and of the mixing zone between the fresh and the saline water.

If diffusion and dispersion are ignored, there is a sharp fresh-saline interface instead of a mixing zone. In that case our numerical solution agrees well with the analytical solution of Maas (2007) for the closely related problem where the ditch is replaced by a horizontal seepage surface. Both the analytical solution of Maas and our numerical solution show that both the mass flux ratio (reflecting upward seepage relative to precipitation) and the Rayleigh number (reflecting density difference) have a significant effect on lens thickness. For our reference case, the lens becomes twice as thick in both the analytical and numerical solutions if the density difference is ignored. The agreement between the two solutions remains fine, though. If the mass flux ratio M approaches zero (by decreasing the upward seepage flux), the agreement between the analytical and numerical solutions deteriorates. We attribute this disagreement to the implicit assumption of the analytical solution, that for zero seepage flux, the saline ground water becomes stagnant. In reality and in the numerical solution this is not the case, as a rotating flow of salt water occurs as in the cases considered by Abarca et al. (2007) that, similar as upward seepage, pushes the mixing zone upward.

The mixing zone thickness depends mainly on the mass flux ratio M and the three dimensionless groups reflecting the diffusive-dispersive processes, which is no surprise. What is remarkable is that the mixing zone thickness decreases in the direction of the outflow surface (ditch), despite the increasing velocities and associated increasing dispersion in that direction at steady state. This can not be due to errors in calculating the mixing zone spatial moments, but is instead attributed to the convergence of streamlines of the mixing zone. Clearly, this effect is profound enough to be visible.

Starting from an initially completely saline domain, the mixing zone thickness grows in the intermediate stage of rainwater lens development and then decreases to its smaller steady state value, and this observation holds also for other initial conditions. To understand this development and the effects of dimensionless groups, we gave a detailed description of the flow pattern in three stages, i.e., initial saline situation,

transient growing rainwater lens, and steady state rainwater lens. In the early two stages the velocity field has a profound velocity component perpendicular to the mixing zone, whereas the steady state velocity field tends to be aligned parallel to the mixing zone, particularly in the region near the ditch. Since the transversal dispersivity is typically at least an order of magnitude smaller than the longitudinal one, this change in the flow pattern results in a thinner mixing zone in the steady state than at some stage during the transient phase. We explored this further by considering the different contributions to the diffusive-dispersive flux as a function of time, and at different locations. In this way, we could quantify these contributions and indeed see how their relative importance varies as a function of lens development. For our reference case, the individual dispersion fluxes that contribute to the mixing zone thickness are about equal to that of the molecular diffusion flux.

The mixing zone thickness increases as the mass flux ratio (i.e., seepage) decreases, which might intuitively not be expected as then also water velocities near the average mixing zone position decrease. The decrease of the dispersive flux due to smaller velocities is counteracted by the decrease in convergence of flow lines towards the ditch, caused by the smaller seepage flux.

In summary, we showed the applicability of the analytical solution for the lens thickness by Maas (2007), as well as its limitation as the mass flux ratio decreases. Whereas the lens thickness gives a first impression of the fresh water volume available for different purposes, also the mixing zone thickness affects this availability. This zone depends on the Rayleigh number and mass flux, and obviously on the diffusion/dispersion groups, but we show that transversal dispersion, as emphasized in other studies, may be less important if significant fluctuations of the lens thickness occur. Our quantification of the different mixing processes in comparison with molecular diffusion and the sensitivity analysis, sheds light on the mixing zone thickness for other geohydrological conditions.

3 SYSTEM RESPONSE TO VARIATIONS

ABSTRACT

In coastal zones with saline groundwater, fresh groundwater lenses may form due to infiltration of rainwater. The thickness of both the lens and the mixing zone, determines fresh water availability for plant growth. Due to recharge variation, the thickness of the lens and the mixing zone are not constant, which may adversely affect agricultural and natural vegetation if saline water reaches the root zone during the growing season. In this paper, we study the response of thin lenses and their mixing zone to variation of recharge. The recharge is varied using sinusoids with a range of amplitudes and frequencies. We vary lens characteristics by varying the Rayleigh number and Mass flux ratio of saline and fresh water, as these dominantly influence the thickness of thin lenses and their mixing zone. Numerical results show a linear relation between the normalized lens volume and the main lens and recharge characteristics, enabling an empirical approximation of the variation of lens thickness. Increase of the recharge amplitude causes increase, and increase of recharge frequency causes decrease in the variation of lens thickness. The average lens thickness is not significantly influenced by these variations in recharge, contrary to the mixing zone thickness. The mixing zone thickness is compared to that of a Fickian mixing regime. A simple relation between the travelled distance of the center of the mixing zone position due to variations in recharge and the mixing zone thickness is shown to be valid for both a sinusoidal recharge variation and actual records of daily recharge data. Starting from a step response function, convolution can be used to determine the effect of variable recharge in time. For a sinusoidal curve, we can determine delay of lens movement compared to the recharge curve as well as the lens amplitude, derived from the convolution integral. Together the proposed equations provide us with a first order approximation of lens characteristics using basic lens and recharge parameters without the use of numerical models. This enables the assessment of the vulnerability of any thin rainwater lens on saline, upward seeping groundwater to salinity stress in the root zone.

This chapter is based on: S. Eeman, S.E.A.T.M. van der Zee, A. Leijnse, P.G.B. de Louw and C. Maas. 2012. Response to recharge variation of thin rainwater lenses and their mixing zone with underlying saline groundwater Hydrology and Earth System Sciences (16), 3535-3549.

3.1 Introduction

Rain-fed areas may suffer from salinity in the root zone when salt groundwater is found at shallow depths. In low-lying coastal zones, saline water is often present at shallow depth, due to a history of flooding (Vos et al., 2008; Post, 2004), marine transgressions and sea spray (Stuyfzand et al., 1994). In such areas, infiltrating rainwater is the only source of fresh water, forming and maintaining thin rainwater lenses floating on top of the saline groundwater. Infiltration of rainwater is limited by upward seepage of the saline groundwater when the soil surface is below sea level as found in deltaic areas like the Netherlands (De Louw et al., 2011; Maas, 2007; Oude Essink et al., 2010), and foreseen due to future relative sea level rise in for example the deltas of the Nile and Mississippi (Jelgersma, 1996). The surface area of such coastal zones and delta regions is considerable and they are generally densely populated. Therefore, and in view of the usually good water supply and soil fertility conditions, their agricultural and ecological importance is significant. The integrity of rainwater lenses is threatened by both the expected sea level rise (Day et al., 1995; Lebbe et al., 2008) and the drainage of soil for agricultural reasons, which have caused subsidence of these low-lying areas and therefore increased the saline ground water pressure (Van de Ven, 2003). Studies by for example Zeidler (1997), Day et al. (1995), Habibullah et al. (1999), and Osterkamp et al. (2001) conclude that salinization in low-lying coastal areas in different parts of the world will cause changes in existing ecosystems and in some places loss of arable land over the next decades if no measures are taken. In all cases, water management will play a dominant role. To minimize adverse effects of salinization, water management and land use planning should be based on a proper understanding of the behaviour of thin fresh water bodies on saline groundwater and their response to temporal variability in recharge, whether seasonal, longer term, natural or human induced.

Related to the behaviour of thin lenses is the problem of the classical dune system, a thick lens of fresh water floating on top of more or less stagnant saline ground water. Fresh water bodies in dunes have received a lot of attention from Badon Ghyben (1888) and Herzberg (1901) and, more recently, by many others who derived analytical solutions for sharp interface steady state situations (e.g. Bakker, 2000; Bruggeman, 1999; Fetter, 1972, Van der Veer, 1977). Hantush (1968), Van der Veer (1977) and Bruggeman (1999) also provided sharp interface solutions for moving rainwater lenses in saline aquifers under different conditions. Maas (2007) derived a steady state approximation for lenses on top of upward flowing saline water, which is very similar to the relatively thin lenses considered in this paper.

For relatively thin lenses, a sharp interface approach is not appropriate since the mixing zone between the fresh and saline water is thick compared to the total lens thickness, as was demonstrated by De Louw et al. (2011). This mixing zone between fresh and saline water has been studied for several steady state situations by for

example Henry (1964), De Josselin de Jong and Van Duijn (1986), Paster and Dagan (2007), and Abarca et al. (2007).

Many case studies use numerical simulations to investigate mixing zones at different spatial and temporal scales. Of main interest is to identify the dominating process(ses) that influence the mixing zone and the delay of the response of the mixing zone, but results appear very dependent on the environmental conditions. Underwood et al. (1992) found for atolls that mixing was controlled by short-term fluctuations, driven by tidal pulses, whereas recharge drives the long term average ground water flow that determines lens thickness. However, Kiro et al. (2008) concluded that the lowering of the Dead Sea caused a delayed reaction in the mixing zone. This movement, very slow and small compared to tidal fluctuations, apparently needs more time to affect the mixing zone. In agreement with Kiro et al., Andersen et al. (1988) saw that small but long-term changes in groundwater level in a drinking water well area can significantly influence the position of the mixing zone, whereas annual variability did not have any influence. Cartwright et al. (2004) investigated the response of the mixing zone to tides and waves on a beach. Contrary to Underwood at al. (1992), they found that the effect of the diurnal tidal pulse (0.5 to 2 m sea level rise) did not influence the position of the centre of the mixing zone. However, they observed a nearly immediate and strong effect of the wave-induced groundwater pulse on the average position of the mixing zone during moderate storm events (wave heights ~4.5 m during 1-3 days). The higher amplitude and lower frequency enhance each other's effect on increasing the mixing zone. Cartwright et al. investigated much smaller spatial (horizontal and vertical) and temporal scales than Underwood et al. and Kiro et al., and neglected thickness variability of the mixing zone.

As these illustrations indicate, the response depends on the physical system parameters, the spatial scale and the duration and amplitude of temporal variations of the flux or water level. It is plausible, that it also matters whether such variations are forced at the perimeter of the system (e.g. tidal variations), and may therefore attenuate with distance from this perimeter, or are forced along the entire top boundary. The latter is of interest, if one wishes to consider variations in time of precipitation that leads to fresh water recharge.

Whereas rainwater lenses in larger dune areas generally have reaction times of years to even tens of years (e.g. Vaeret et al. 2012, Oude Essink,1996), for thin lens systems, we expect fast responses of the position of the mixing zone to recharge variability. The main responses of interest are the thickness of the lens and of its mixing zone. For a lens changing in thickness, flow lines are predominantly vertically oriented, perpendicular to the mean interface (Chapter 2). This agrees with observations (De Louw et al., 2011) and implies that mixing is controlled by longitudinal dispersion, which creates a thicker mixing zone compared to a transversal dispersion/diffusion dominated stable mixing zone. The combination of the position and width of the

mixing zone determines together with the capillary characteristics of the soil, whether saline water reaches the root zone during the growing season, and concern about the impact of root zone salinity on primary production is one of the motivations of this research.

Our objective is to relate changes of rainwater lenses and their mixing zone to hydrological characteristics of a field site and recharge variation. This relation can be used to determine under which circumstances water quality is affected in the root zone. Lens properties that describe the depth at which saline water is found, are the lens thickness and the vertical extent of its mixing zone. We analyse the effect of recharge variations with different duration and intensity on lenses with a different thickness and mixing zone thickness, using numerical simulations. The first step is to establish a relation between recharge variation and lens thickness. Secondly, the effect of variation on the mixing zone is investigated, and finally delay and amplitude of lens systems with different recharge variations is calculated. Together these aspects provide a useful tool for a fast analysis of lens variability under a given recharge pattern.

3.2 Theory and methods

3.2.1 Flow domain and system equations

The modelled lens system is comparable to that in Chapter 2. It is a vertical cross section of the flow domain between two ditches or drains (Figure 2.1). Recharge with fresh water (uncoloured) occurs at the upper boundary, while vertical upward seepage of saline water (grey-coloured) occurs at the lower boundary. All water entering the flow domain leaves through the ditches or drains. Such situations are common in deltaic lowlands, and field observations (Figure 3.1) illustrate that the resistivity, a measure of the salinity of the pore water, decreases gradually with increasing depth. The resistivity sequence found can be completely attributed to the salt concentration of the saline groundwater, which is for this case around two thirds of the salinity of sea water.

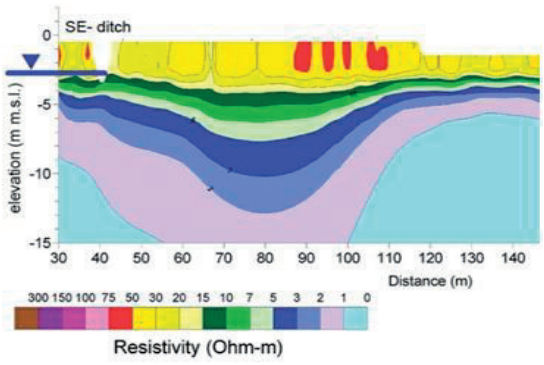

Fig. 3.1. Field measurements of resistivity with CVES (continuous vertical electrical sounding) of lens and mixing zone, measured on Schouwen- Duiveland, The Netherlands, September 2007 (taken from Goes et al., 2007; De Louw et al., 2011). The left part is a higher elevated sandy creek ridge, causing a thicker rainwater lens. The right part (110 to 140 m) is a thin lens on top of upward seeping saline groundwater, as schematized in (a).

In our analysis, the volume of fresh water in the lens includes the fresh water in the unsaturated zone. This is a reasonable approach because the unsaturated zone is thin (generally around 1 m), but also in view of our interest in the fresh water availability for plants. Lens thickness is defined as the distance between soil surface and the centre of the mixing zone, in the middle of the field. In the text, we refrain from mentioning this issue all the time, for brevity.

The equations for the water-saturated domain have been completely described in Chapter 2.2.2, Equations 2.1-2.4 (p. 14) Symbols and units are in the Nomenclature (p. vii and viii) . An overview and description of the 8 dimensionless groups formulated based on the system equations are in Chapter 2.2.4 as well, on p. 17. Lens thickness is particularly sensitive to changes in mass flux ratio M and Rayleigh number R (as is shown in Figure 2.5). The mass flux ratio M is the ratio between the mass fluxes of the lower (seepage) and upper (net recharge) boundary, the Rayleigh number R is the ratio of the characteristic density induced flux and the average discharge $\langle P \rangle$.

To assess the response of lens and mixing zone to variations in recharge, we adapted the top recharge boundary condition from Chapter 2.2.6 (p. 19-21). We use sinusoidal recharge variations (P_s) to model variations in recharge, while the average $\langle P \rangle$ replaces the constant P in M and R. This enables us to simply vary the main features of the recharge, such as average, duration, and intensity. Moreover, the absence of abrupt changes in sinusoids is numerically more attractive.

The boundary condition for the total mass flux at the upper boundary (fresh water precipitation) is given by

$$\rho q_z = \rho_0[\langle P \rangle + A \sin(2\pi f t)] \qquad (3.1)$$

We obtain the following two additional dimensionless groups by combining Eq. (3.1) and the reference values as elaborated in the steady state analysis of Chapter 2.

$$f_{Ps} = \frac{fLn}{\langle P \rangle} \qquad \text{and} \qquad A_{Ps} = \frac{A}{\langle P \rangle} \qquad (3.2\ \text{a,b})$$

Where $\langle P \rangle$ is the average of P_s, and the groups represent the dimensionless frequency and amplitude, respectively. In our analysis we will focus on these two groups, and the mass flux ratio M and the Rayleigh number R.

3.2.2 Model Schematization and parameter values

Only one half of a lens system is considered for reasons of symmetry. Besides the precipitation at the upper boundary, the boundary conditions and spatial discretization that we used are shown in Fig. 2.2 and discussed on p. 18-20 of Chapter 2. SUTRA (Voss and Provost, 2008) was used to carry out density-dependent numerical groundwater simulations, accounting for flow in the unsaturated zone.

Temporal discretization was controlled by criteria that limit the allowable changes in pressure, saturation and concentration per time step, and time step sizes were adapted accordingly. An overview of reference parameter values is given in Table 3.1. A longitudinal dispersivity of 0.1 m and a transversal dispersivity of 0.01 m were chosen. This choice is elaborated in Appendix I. Unsaturated soil parameters for a clay loam soil were used for the flow in the unsaturated zone. We tested the effect of different soil types on the lens thickness. This effect was negligible because the unsaturated zone is thin, and most of the time rather wet. For the initial conditions, steady state lenses were used that were obtained with a constant recharge rate of 1 mm day^{-1}.

The volume and thickness of rainwater lenses and the thickness of the mixing zone for the numerical simulations were quantified using spatial moments (Chapter 2). Spatial moments efficiently summarize the numerical results and have been used widely in other contexts, e.g. Acharya et al. (2005) and Paster and Dagan (2007). Govindaraju and Das (2007) discuss formulation and use of spatial moments. From the $zero^{th}$ spatial moment of the salt mass fraction over the modeled domain, the total volume of fresh water in the lens and mixing zone can be inferred. The spatial moments of the vertical derivative of the salt mass fraction (inset Fig. 1a) provide information on the position, thickness, and shape of the mixing zone and can also be used for field measurements, as shown by De Louw et al. (2011).

Table 3.1: Reference values of model parameters.

Parameter	ref. value	Parameter	ref. value
$\boldsymbol{g}$	9.81 m s^{-2}	γ	0.7
$\boldsymbol{n}$	0.3	κ	10^{-12} m^2
$\boldsymbol{D_m}$	10^{-9} m^2s^{-1}	μ	10^{-3} kg $m^{-1}s^{-1}$
$\boldsymbol{H}$	10 m	ξ	10^{-10} m
$\boldsymbol{L}$	25 m	ρ_0	1000 kg m^{-3}
$\langle \boldsymbol{P} \rangle$	1 mm d^{-1}	ρ_{max}	1014 kg m^{-3}
$\boldsymbol{S}$	0.5 mm d^{-1}	$\Delta\rho = \rho - \rho_0$	14 kg m^{-3}
$\boldsymbol{\alpha_l}$	0.10 m	ω_{max}	0.14%
$\boldsymbol{\alpha_t}$	0.010 m		

To assess the response of the lenses under different conditions to net recharge fluctuations, we varied the lens characteristics and the recharge. We varied average lens thickness by varying *M* and *R* (Table 3.2), which leaves all other groups constant (using reference parameter values as given in Table 3.1). Only *C*, the dimensionless conductance of the soil–ditch interface, changes as we vary *R*. Since the influence of *C* is very small (inset Nomenclature), its variation has a negligible impact on the results.

We focus on thin lenses because these are relevant for primary production in relation to salinity stress. We use the first spatial moment of dc/dz to determine lens thickness (see inset Fig. 2.1). For lenses thicker than 3 m and commonly observed recharge regimes, water with significant amounts of salt is very unlikely to reach the root zone (Chapter 2). For lenses that are thinner than about 0.8 m, the salt stress is likely to be so severe, that it limits plant growth to halophytic species.

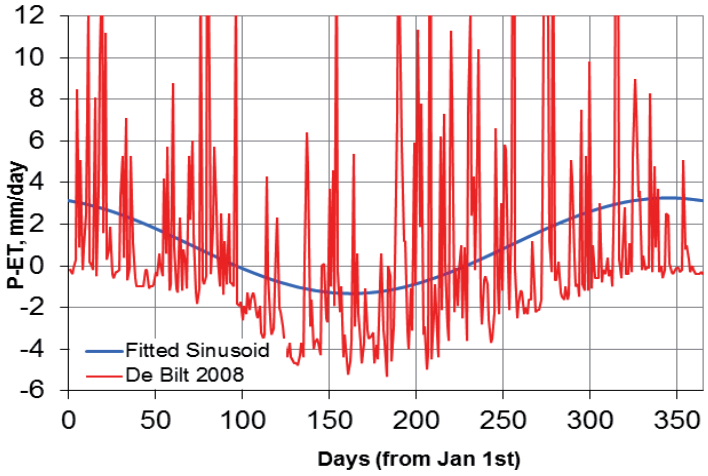

Fig. 3.2. Daily weather data from De Bilt, 2008, The Netherlands (KNMI) and a recharge sinus (fitted with average weather date from 1971–2000) used for numerical simulations.

To parameterize the sinusoidal recharge P_s we used variations from a reference P_s fitted to average Dutch weather data (De Bilt, 1971-2000, provided by the Royal Netherlands Meteorological Institute KNMI), see Fig. 3 and the bold values in Table 3.2. To quantify the influence of the amplitude and frequency of P_s on lens response, the amplitude was varied between 0.23 and 23.0 mm/d, while the period was varied from 1 year to 1 week (Table 3.2). Although an annual frequency is most often expected, higher frequencies were simulated for demonstrative purposes and because they have a resemblance with short-term precipitation events. $\langle P \rangle$, defined as the average of P_s was kept at 1 mm/day. The strongly fluctuating weather data from the KNMI (Fig. 3.2) are used to validate the approximation of the thickness of weather events the mixing zone that we will propose.

Table 3.2: Parameter variation of seepage (S), permeability (κ) and for the parameters of precipitation sinusoidal function (P_s with $\langle P \rangle = 1$, equation(5)), for which the reference situation (bold values) is De Bilt, www.knmi.nl).

Parameter	Simulated values						
S, (mm d^{-1})	**0.5**	1	2	5	8		
κ, (m^2)	10^{-13}	**10^{-12}**	10^{-11}	$5*10^{-11}$	10^{-10}		
A, amplitude of P_s (mm d^{-1})	0.23	0.92	**2.30**	3.45	4.60	11.50	23.00
f, frequency of P_s (y^{-1})	**1**	2	3	6	13	26	52

3.2.3 System delay using convolution

To investigate the delay between the variations in recharge and thickness response of thin lenses, we adopted a standard systems analysis, using the impulse response function and convolution of this function with the recharge signal (e.g. Olsthoorn, 2008). Practical solutions using convolution can for example be found in Maas (1994) and Bruggeman (1999). Although this approach is only valid for linear systems, while the system we consider here is nonlinear, we believe that this approach will give a good first order approximation, especially if we consider small variations in the recharge.

To be able to use convolution for estimating the lens response to variable recharge, an impulse response has to be determined. This impulse response function defines the reaction of the system to a unit impulse, i.e. an impulse for which the integral over time equals one. Instead of using an impulse input, we used a step function. Since the impulse is the derivative of the step function in time and the system is considered to be linear, the impulse response function will be given by the time-derivative of the response to the step function. We have used a 0.5 mm day^{-1} change in the recharge to establish the step response functions. To minimize the effect of nonlinearities, both a negative and positive change in recharge have been applied and the average of the absolute values of the responses has been used to determine the step response function. Results, as will be shown in the next section, illustrate that for simulations with the M and R-values of Table 3.2, the step response function $s(t)$ can very well be fitted by an exponential function of the form

$$s(t) = \Delta(1 - e^{-at}) \tag{3.3}$$

The impulse response function is then given by the derivative of the step response function

$$I(t) = \Delta\, a\, e^{-at} \tag{3.4}$$

For a variable recharge P_s in time, starting from an initial condition at time $t = 0$, namely the steady state lens with constant recharge $\langle P \rangle$, the response of the lens in terms of the lens thickness in the middle of the field is then given by the convolution integral

$$\bar{z}(t) - \bar{z}(0) = \int_0^t 2P_s(t - \tau)I(\tau)d\tau \tag{3.5}$$

where the recharge P_s needs to be given in mm day^{-1} and the factor 2 is a consequence of the determination of the step response for a change in recharge of 0.5 mm day^{-1}. For a sinusoidal recharge pattern

$$P_s = A\sin(2\pi f t) \tag{3.6}$$

we can now obtain analytical expressions for the amplitude Q and the delay T of the sinusoidal response of the lens

$$Q = \frac{2Aa\Delta}{\sqrt{(2\pi f)^2 + a^2}} \qquad T = \frac{1}{2\pi f} P_s \arctan\frac{2\pi f}{a} \qquad (3.7\ a, b)$$

as is shown in Appendix II.

3.3 Results

3.3.1 Volume variation of the lens

We define lens volume as the volume of soil pores filled with fresh water (saturated and unsaturated) for a slab of 1 m thickness perpendicular to the 2D-flow domain. We use the zeroth moment to calculate this volume. To obtain a quantification of lens responses for thin lenses to recharge that varies as a function of time, we investigated relations between the most important parameter groups. To this extent, we numerically simulated a large number of sinusoidal recharge variations (P_s) (Table 3.2). For a broad range of parameters (Table 3.1), we found responses that nearly linearly relate the amplitude (A) and frequency (f) to the volume variation of the lens. Volume variation is represented by a normalized volume deviation $V_n = (V_m - \langle V \rangle)/\langle V \rangle$, where V_m is the maximum and $\langle V \rangle$ the average lens volume. For a designated Rayleigh number (R), V_n is linearly related to the period $1/f_{Ps}$ where f_{Ps} is the dimensionless group representing the frequency of P_s (Eq. 3.2a).

In Fig. 3.3a is shown how an increasing period leads to a larger volume variation. Differences in slope are primarily caused by different mass flux ratios (M), since variations are relatively larger for thinner lenses, which have a larger M. Volume variation is to a lesser extent increasing with larger recharge amplitudes represented by dimensionless group A_{Ps} (Eq. 6b). Multiplying f_{Ps} and V_n and relating this to M, results in Figure 4b, where the slope now mainly depends on A_{Ps}.

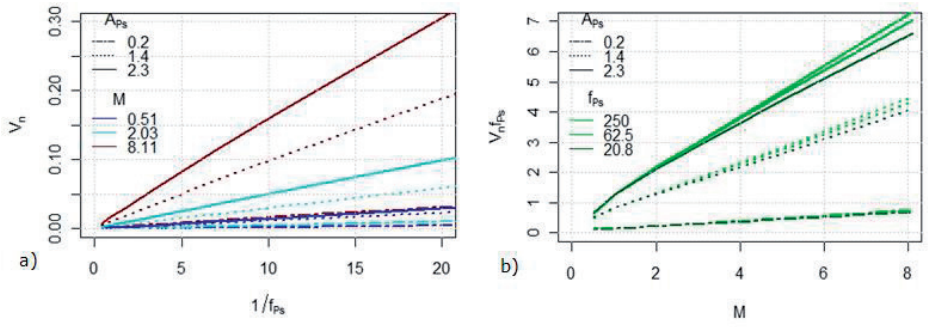

Fig. 3.3: (a) Linear relation between dimensionless recharge period $1/f_{Ps}$ and the normalized volume deviation V_n for $\langle P \rangle = 1$ mm day-1. (b) Multiplying f_{Ps} and V_n on the y-axis and relating this to the mass flux ratio (M) shows a linear relation dependent on A_{Ps} .

The results of Figure 3.3 lead us to multiply A_{PS} and M to obtain one linear relation for the most important parameter groups, shown in Figure 5a. The fitted linear relation is used to obtain an equation that relates lens deviation $\Delta V = V_m - \langle V \rangle$ to the average lens volume and three dimensionless groups

$$\Delta V = \langle V \rangle \frac{\beta M A_{PS}}{f_{PS}} \tag{3.8}$$

where $\beta = 0.87$ (95% confidence interval from 0.86 to 0.88) is the slope of the line shown in Figure 3.4a. The Rayleigh number R, which for practical situations mainly increases or decreases due to an increase resp. decrease in soil permeability κ, only has a minor influence (less than 10%), if we consider permeability ranges that seem plausible for drained agricultural fields.

Equation 3.8 shows that the deviation of lens thickness from its average is linear and positively influenced by larger seepage and larger recharge amplitude and the average thickness itself. Higher frequency, on the other hand, diminishes the deviation of lens response. This is consistent with the findings of Cartwright (2004), which indicated that higher amplitude and lower frequency enhance each other in their positive effect on lens deviation.

Although Eq. 3.8 is an empirical relationship, the advantage is that it describes the impact of quite a number of parameters (namely 11) over a wide range. The normalized lens deviation does not increase linearly with increasing MA_{PS} for very large values, as is shown in Figure 3.4b. For such conditions, saline water is being evaporated at the top boundary (or transpired by plants) and this decreases the response of the fresh water volume. The physical situation represented by these conditions implies presence of salt at the soil surface, disappearance of an actual rainwater lens, and consequently significant amounts of salt in the root zone. This will reduce primary production to a large extent.

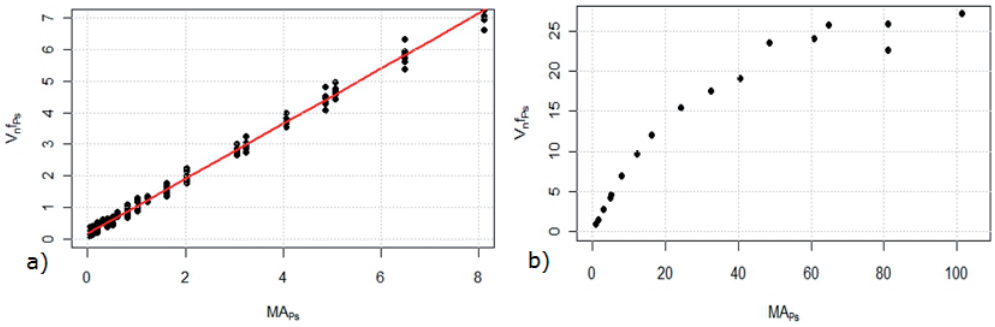

Figure 3.4: a) Relation between mass flux ratio M times A_{PS} and $V_n f_{PS}$ for $R = 11.87$. The red line shows the fitted linear model, $y = 0.87x + 0.18$ with an explained variance of 0.99. b) Indication that for larger values of MA_{PS} the relation is non-linear.

The average lens volume $\langle V \rangle$ calculated for the numerical simulations for which Eq. 3.8 holds, deviates less than 5% from the steady state lens that is formed when P_s is replaced by a constant recharge equal to $\langle P_s \rangle$. As we have shown earlier (Chapter 2), the center of the mixing zone of steady state lenses is well approximated by the analytical model proposed by Maas (2007). Figure 3.5 illustrates that the relation between the total lens volume and its thickness in the middle of the field is nearly equal for the numerical simulations and the approximation by Maas. Therefore, we can replace $\langle V \rangle$ in Eq. 3.8 by V_M, which can be calculated using the approximation of Maas (2007)

$$\frac{Z}{(L^2+Z^2)^{1/2}} = \frac{-S/P+\sqrt{(S/P)^2+4(1+S/P+R)}}{2\left((1+S/P+R)\right)} \tag{3.9}$$

in combination with his assumption of an elliptic lens shape this leads to a (half) lens volume (remember: our model domain is only half a lens in view of symmetry)

$$V_M = \frac{1}{4}\pi LZ \tag{3.10}$$

Combining Eqs. 3.10 and 3.9, we obtain for the lens response based on recharge data and field characteristics

$$\Delta V = V_M \frac{\beta MA}{Lf_{Ps}} \tag{3.11}$$

For lenses with an average thickness of more than 3 m the approximation of Maas overestimates the lens volume (Figure 3.5) derived from its thickness. This can be largely attributed to the outflow face in the model used by Maas, which creates a wider lens near the outflow region compared to the ditch outflow we model. For the lenses of interest here, as elaborated in Section 3.2, the difference between the volume-thickness relations of the numerically and analytically calculated steady state lenses is less than 5%. Therefore we can determine either and transform as required.

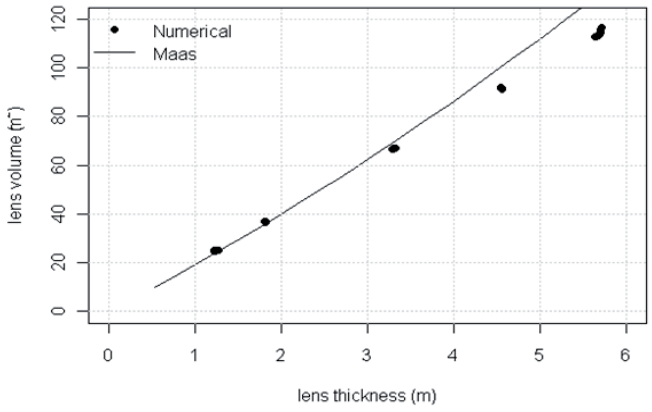

Fig. 3.5. The relation between lens thickness and lens volume according to the assumption of an elliptical lens shape (Maas, 2007, his Eqs. 5a–c, compare this paper Eq. 16) and the numerical simulations.

3.3.2 Thickness of the mixing zone

Since the mixing zones appear thick compared to total thickness of the rainwater lens when recharge varies as a function of time (Fig. 3.1, De Louw, 2011), an estimate of its average position is not sufficient. Temporary saline water in the root zone may be caused by a thick mixing zone, even when the average lens thickness covers the root zone.

We propose an analogy to a mixing zone that forms during the uniform motion of an initially sharp front through a porous medium. The width of the mixing zone for such a front depends on the distance it has traveled since $t = 0$. For a Fickian dispersion/ mixing regime, the standard deviation of a normally distributed concentration change is related to the diffusion/dispersion coefficient and time according to

$$\sigma = \sqrt{2Dt} \tag{3.12}$$

where a sharp interface at $t = 0$ is assumed. The standard deviation σ of the center of the mixing zone ($\bar{z}$), is calculated from the central moment of the concentration change distribution (inset Fig 2.1).

For a lens, the assumption of an initially sharp front is not met; however, we can derive a relation between the distance traveled in a certain period and the width of the mixing zone. First, we define χ_s as the traveled distance per sine-period of the center of the mixing zone ($\bar{z}$) in the middle of the field and $\langle|v|\rangle$ is the average absolute velocity of this interface for sinusoidal recharge variation (Cirkel et al., in preparation). Therefore

$$\chi_s = 4A_{\bar{z}} \qquad \text{and} \qquad \langle|v|\rangle = \chi_s f \tag{3.13 a,b}$$

where $A_{\bar{z}}$ is the amplitude of $\bar{z}$, as Fig. 7 shows. We approximate hydrodynamic dispersion $\boldsymbol{D}$ by the longitudinal dispersivity multiplied by the average absolute interface velocity. This is justified since mixing in vertically expanding and shrinking lenses is dominated by longitudinal dispersion (Chapter 2)

$$\boldsymbol{D} = \alpha_l \langle|v|\rangle \tag{3.14}$$

The combination of Eqs. (3.12-3.14) leads to a measure for the temporal average variance (a suitable measure for thickness) of a mixing zone when recharge variation is a sinusoid, denoted as $\langle\sigma_s\rangle^2$

$$\langle\sigma_s\rangle^2 = 2\alpha_l \chi_s f t \tag{3.15}$$

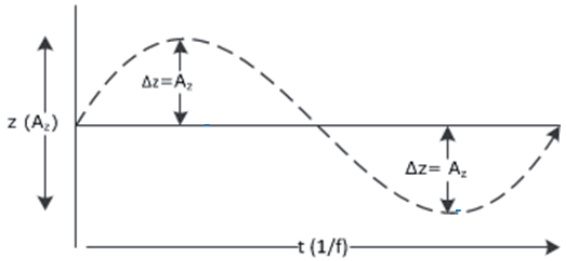

Fig. 3.6: Position (z) of mean interface as a function of time (t) for sinusoidal change, in support of Eq. 3.15.

Because of the dispersion, there is no time $t = 0$ with a sharp interface as assumed for Eq. 3.12. Therefore, mixing zone width will partly depend on its initial thickness and position. Numerical simulations show, however, that the relation between $\langle\sigma_s\rangle^2$ and $2\alpha_l\chi_s f$ is quite linear, as is illustrated in Fig. 3.7 for different mass flux ratios (M) and recharge curves (P_s).

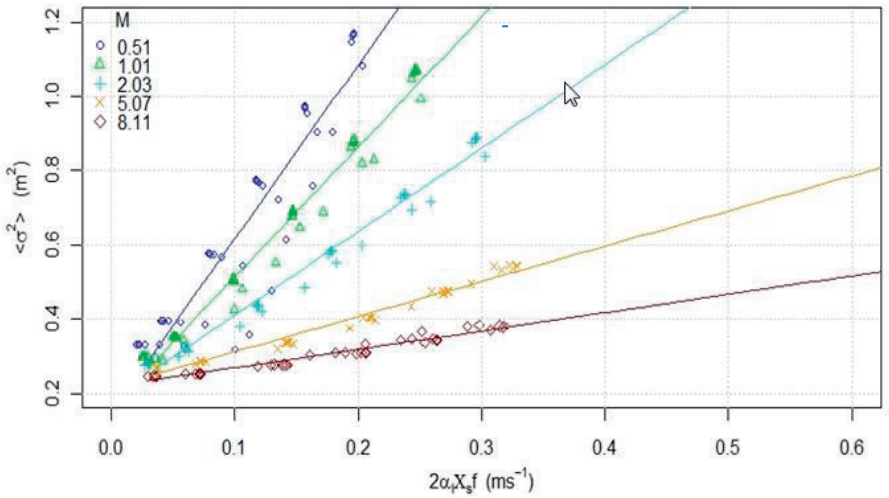

Fig. 3.7. Relation between the average variance of the mixing zone thickness and the longitudinal dispersivity and lens velocity, Eq. 3.15, including linear fitted lines. The explained variance is 0.85 for M =0.51, and larger than 0.96 for the other M values.

An explained variance for Eq. 3.15 of 0.85 is found for the smallest simulated mass flux ratio, whereas for other mass flux ratios, the explained variance is larger than 0.96. The different coefficients for the different mass flux ratios (M) can be explained by the increasing total flux in these simulations. $M = \rho_{max} S/\rho_0\langle P_s\rangle$ is varied by changing seepage S, which does not influence any of the other dimensionless groups. However, the total flux in the flow domain increases. This would lead to a wider mixing zone because larger fluxes lead to larger velocities. This mechanism is suppressed by streamlines that converge closer to the ditch where also velocity increases, as described in Chapter 2.

The approximation of net rainfall with a sinus ignores all irregular behavior (as is apparent in Fig. 3.2), and its suitability for this purpose therefore needs to be shown. Hence, we determined the thickness of the mixing zone also for a 15 year period of daily recharge data in De Bilt (KNMI, 2011) compared to a sinusoidal recharge curve P_s with the same average recharge, Fig. 3.8a.

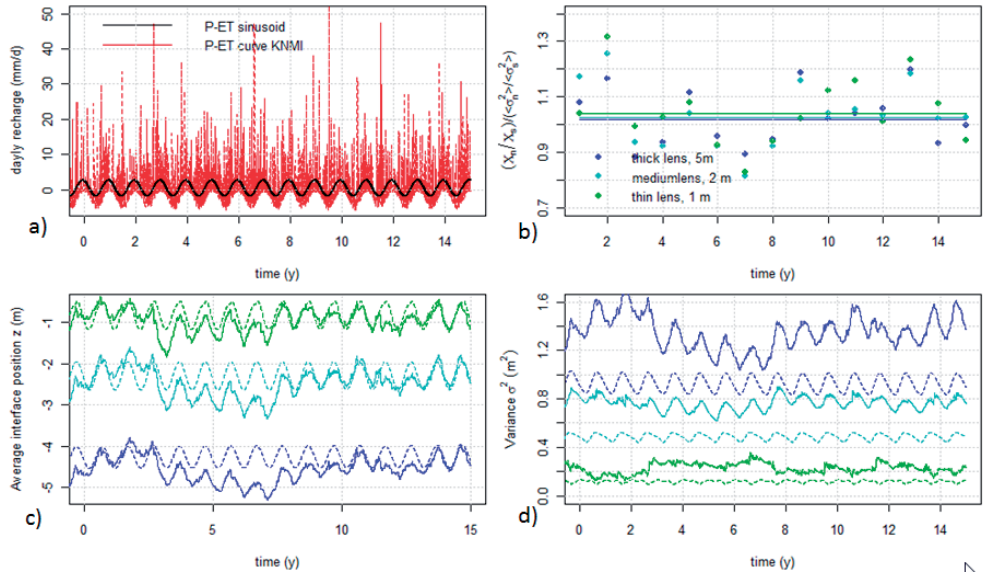

Figure 3.8: a) The recharge pattern of natural and sinusoidal recharge curves is shown. b) The ratio between the traveled distance and variance (Eq. 22b) for individual years (dots) and averaged over 15 years (lines). c) The center of the mixing zone for 15 yr of daily recharge ($\bar{z}_1$) and d) the associated variance ($\sigma_n{}^2$) for lenses with a different average thickness.

The travelled distance (χ_n) of the center of the mixing zone $(\bar{z})$ of the numerical simulation using daily weather data is calculated by

$$\chi_n = \left|\sum_{i=1}^{j} \bar{z}(t(i)) - \bar{z}(t(i-1))\right| \qquad (3.16)$$

The average variance of the lens when daily (i) recharge records are used, $\langle\sigma_n\rangle^2$, is calculated by

$$\langle\sigma_n{}^2\rangle = \frac{\sum_{i=1}^{j} \sigma_n^2(t(i))}{j} \qquad (3.17)$$

Assuming that the variance depends on the traveled distance for both the sinusoidal and the natural recharge signals, using annual frequencies (f) for both signals, we combine Eqs. 3.15 – 3.17 to

$$\frac{\chi_n}{\chi_s} = \frac{\langle\sigma_n\rangle^2}{\langle\sigma_s\rangle^2} \quad \text{or} \quad \frac{\chi_n/\chi_s}{\langle\sigma_n\rangle^2/\langle\sigma_s\rangle^2} = 1 \qquad (3.18\ \text{a,b})$$

In Fig. 3.8a, we show net recharge patterns that were used as input. Figure 9c shows the center of the mixing zone $\bar{z}$ and Fig 9d the associated mixing zone variance $\langle\sigma\rangle^2$. In Fig 3.8b the dots indicate the ratio according to Eq. 3.18b for individual years, for which significant deviations from the expected ratio of 1 are simulated. This can be attributed to erratic weather in terms of relatively dry or wet years and how these affect the initial conditions for the next year (Fig 3.8c and d). The average ratio over a period of 15 years is 1.01 to 1.03, which is a good indication that on average, the traveled distance is proportional to the mixing zone thickness. This method of relating mixing zone thickness to the traveled distance of the recharge signal is therefore suitable to estimate the mixing zone thickness for any rainfall pattern or for example the effects of irrigation. The only condition is that a sufficiently long period is used to minimize the effect of initial conditions. To estimate the width rather than the ratio obtained by Eq. 3.18, a numerical simulation would be needed to establish a reference situation, from which all variations can then be derived analytically.

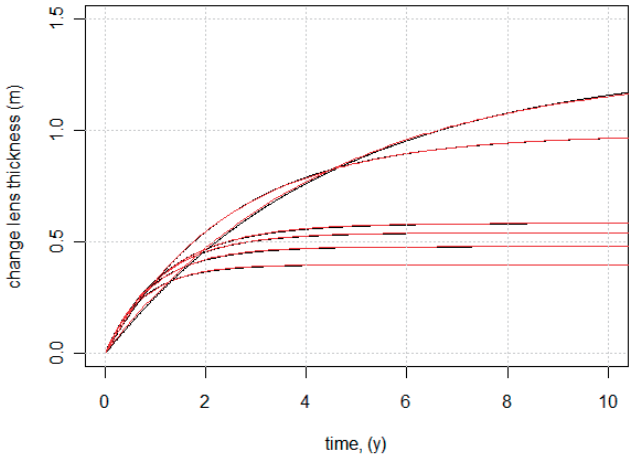

Fig 3.9: Change of lens thickness for a 0.5 mm -1 day change of a constant recharge, calculated for thin lenses with different M and R. Fitted with exponential Eq. 3.3 a determines the shape of the curvature and ΔZ is the ultimate value of the thickness change.

3.3.3 Delay and amplitude of lens response

The impulse response function was derived to apply convolution for thin lenses. We first derived the step response functions for a range of M and R (derived from numerical simulations), for small changes in constant recharge (0.5 mm d^{-1}), as shown for a few example curves in Fig. 3.9, where the total gain Δz and the shape parameter a were fitted according to Eq. 3.3. This leads to Fig. 3.10a and b in which a and Δ show a strong relation with M, and R has a limited influence on Δz and a negligible impact on a. Note that Fig. 3.10 is not limited to sinusoidal recharge curves: it only relates a change in lens volume created by a change in constant recharge to differences in M and R.

For sinusoidal recharge curves, we can relate these parameters to the amplitude of the lens and the delay of the lens response compared to the recharge sinus, using the derivation as found in the appendix. The delay of a lens, calculated from Eq. 3.7b was found to be always approximately 25% ($\pm$2%) of the period of the recharge variation ($1/f$), irrespective of M, R, A_{PS} and f_{PS}. This is expected and understandable. The maximum lens volume is reached at the moment that recharge equals outflow during a phase of declining recharge The same is found for the minimum lens thickness, which is reached when recharge equals discharge during a phase of increasing recharge. We compared this to the delay of the simulations used to establish Eq. 3.8, which leads to the same value, although the spread is slightly larger: 25% ($\pm$3%). Delays were determined for $at \gg 1$ to make sure Eq. 3.7 is valid (as elaborated in Appendix I).

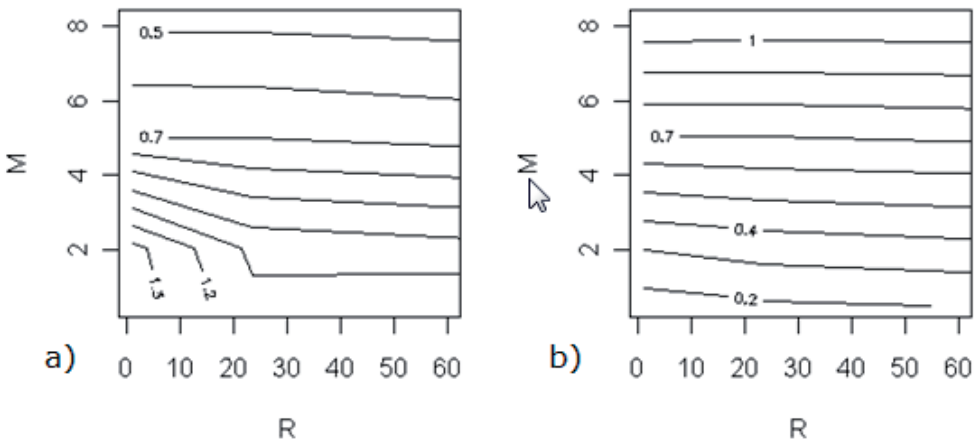

Fig 3.10: a) ΔZ and b) the term α of the exponential step response function, Eq.3.3 in relation to M and R.

Lens amplitudes determined from Eq. 3.7a, scaled with the average lens thickness, were compared to the numerical simulation results analysed in Section 3.3.1, again for $at \gg 1$. Differences are less than 5%. Lens amplitude is again only slightly influenced by R. The relations with M, A_{PS} and f_{PS} are shown in Fig. 3.11. A thinner lens (larger M), is more influenced by changes in A and f The enhancing effects of larger A and smaller f (Cartwright et al., 2004) is again confirmed. Only thin lenses are affected to an extent that may cause root zone salinization, with thickness variations of more than 30% for not extreme values of A and f (Fig. 12 c). Very clear from this analysis is that higher frequencies can only influence lens thickness significantly when amplitudes are extreme; their main effect is on the thickness of the mixing zone, as explained in Section 3.3.2.

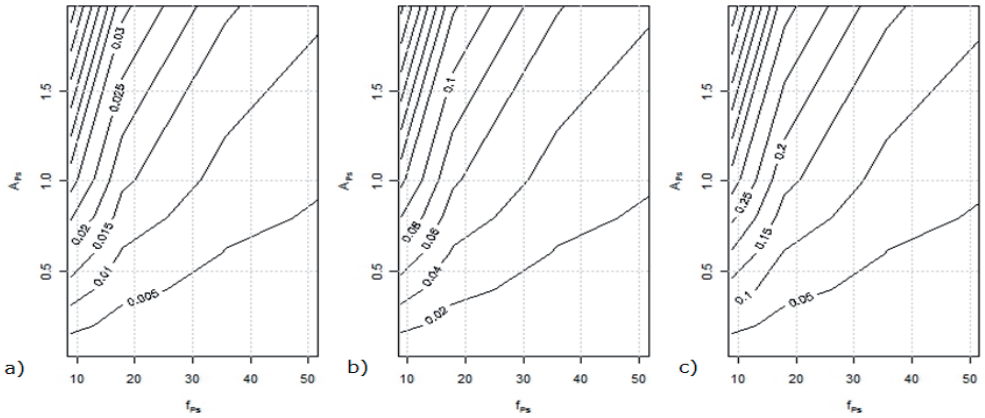

Fig. 3.11: Contours of change in lens thickness as a fraction of the average lens thickness as a function of frequency and amplitude. (a) M = 0.51, (b) M = 2.03, (c) M = 5.07. For the reference situation this leads to lenses with a thickness of 4.8, 2.3 and 1.1 m, respectively.

3.4 Discussion and conclusions

In this paper, we addressed the impact of temporal variations of net recharge at the soil surface on the thickness of, respectively, rainwater lenses and their mixing zone at the fresh/salt interface. We investigated the impact with numerical 2D simulations, varying dimensionless groups that follow from the basic governing flow and transport equations. The variations in both rainwater lens thickness and volume, and the mixing zone thickness, were related with simple linear functions of these dimensionless groups.

An empirical relation that was developed concerns the volume deviation of a thin rainwater lens from its average, in response to sinusoidal recharge variations (Fig. 4 and Eq. 3.8). This relation clearly shows the positive effect of recharge amplitude and the negative effect of recharge frequency on lens thickness variation. Because the average lens thickness is hardly influenced by the amplitude and frequency of the recharge variation, the relation can be combined with a steady state approximation of lens volume under saline seepage conditions (Maas, 2007), Eq. 3.9. This relation holds for parameter combinations appropriate for a realistic parameter values, and provides a simple, computationally fast estimate of the maximum and minimum lens thickness (Eq. 3.11).

The average mixing zone thickness over a longer period (>10 periodic recharge cycles) can be estimated from the traveled distance of the average mixing zone position, (Eqs. 3.15 – 3.18), for any recharge pattern. At least one reference simulation is required to derive an estimate of the absolute value of the thickness for any sinusoidal variation of recharge. The mixing zone analysis shows that the influence of short-term precipitation events on the thickness of the mixing zone is significant, in spite of their limited effect on lens thickness.

A first order approximation of the impulse response function for a thin lens was derived (Eq. 3.4), for which the parameters can be obtained from Fig. 3.10. With the convolution integral (Eq. 3.5) it is then simple to determine a first order approximation of the position of the mixing zone for arbitrary recharge variation in time. For sinusoidal recharge patterns, amplitude of the lens with respect to the recharge variations can be easily calculated (Eq. 3.7), whereas the delay turns out to be approximately 25% of the sinus period, independent of lens conditions. Both the shallowest position and the time of occurrence can be determined. The former indicates the rooting depth at which plants may take up saline water, the latter provides the moment during the growing season that saline water reaches this minimum depth. This combination can be used to assess possible crop damage. Results obtained by convolution are in very good agreement with numerically simulated results, which indicates that the approximation is very useful, even though the considered system is non-linear.

Together the proposed equations provide a first order approximation for all aspects of interest concerning salinity for thin rainwater lenses on saline, upward seeping ground water. The attraction of our analysis is nicely illustrated by considering the impact of more realistic erratic rainfall (measured daily time series) on mixing zone thickness. Whereas most of the analysis was for regular sine variation, also for erratic rainfall, the mixing zone thickness and its variation at first order are well reproduced. The approach will be most successful when based on one or a few numerical calculations to establish a good set of reference parameters for the specific field- and soil type (including parameters for the unsaturated zone), especially to determine the thickness of the mixing zone. The approach can be used to develop a tool for upscaling to, for example, a more regional analysis of salt sensitivity of agricultural soils. For such an analysis, additional geological and geographical parameters, in particular the layering of soil (De Louw et al, 2011) and spatially different drainage levels may have to be accounted for.

4 FIELD OBSERVATIONS OF RAINWATER LENS DYNAMICS

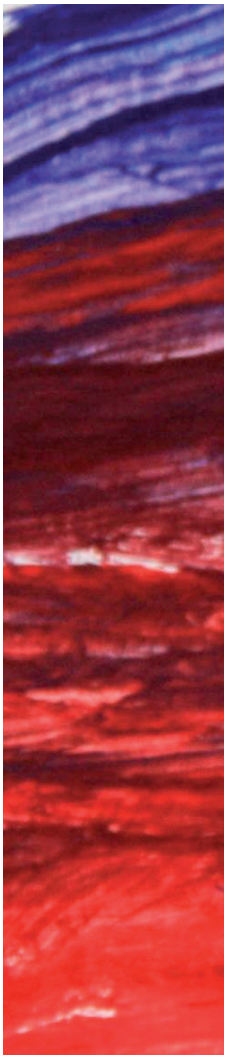

ABSTRACT

Thin rainwater lenses near the land surface are often the only source of freshwater in agricultural areas with regionally-extensive brackish to saline groundwater. The seasonal and inter-annual dynamics of these lenses are poorly known. Here this knowledge gap is addressed by investigating the transient flow and mixing processes in rainwater lenses beneath two tile-drained agricultural fields in the Netherlands. Evidence of rainwater lens dynamics was systematically collected by monthly ground- and soil water sampling, in combination with daily observations of water table elevation, drain tile discharge and drain water salinity. Based on these data, and numerical modeling of the key lens characteristics, a conceptual model of seasonal lens dynamics is presented. It is found that variations in the position of the mixing zone and mixing zone salinities are small and vary on a seasonal timescale, which is attributed to the slow transient oscillatory flow regime in the deepest part of the lens. The flow and mixing processes are faster near the water table, which responds to recharge and evapotranspiration at a timescale less than a day. Variations of drain tile discharge and drain water salinity are also very dynamic as they respond to individual rain events. Salinities of soil water can become significantly higher than in the groundwater. This is attributed to the combined effect of capillary rise of saline groundwater during dry periods and incomplete flushing by infiltrating freshwater due to preferential flow through cracks in the soil. The results of this study are the key to understanding the potential impact of future climate change and to designing effective mitigating measures such as adapting tile-drainage systems to ensure the future availability of freshwater for agriculture.

This chapter is based on: P.G.B. de Louw, S. Eeman, E. Vermue, G.H.P. Oude Essink, V.E.A. Post. 2013. Rainwater lens dynamics and mixing between infiltrating rainwater and upward saline groundwater seepage beneath a tile-drained agricultural field. Journal of Hydrology 501: p. 133-145.

4.1 Introduction

In many coastal areas worldwide, groundwater is brackish to saline because of the combined effects of seawater intrusion and marine transgressions (e.g. Post and Abarca, 2010; Werner et al., 2013). In such areas, freshwater lenses recharged by rainwater are often the only water resource available for agriculture and drinking water. The best-known type of freshwater lens is the Badon Ghijben-Herzberg (BGH) lens (Badon Ghijben, 1889; Herzberg, 1901), which develops in areas with saline groundwater where recharge creates an elevated water table in areas like dune belts along the coast (e.g. Stuyfzand, 1993; Vandenbohede et al., 2008), below islands (e.g. Chidley and Lloyd, 1977; Underwood et al., 1992), and even in inland desert areas (e.g. Kwarteng et al., 2000).

Another type of a rainwater-fed lens forms in areas where saline groundwater migrates to the surface by upward groundwater flow (referred to here as seepage), such as the coastal area of the Netherlands (De Louw et al., 2011; Velstra et al., 2011) and Belgium (Vandenbohede et al., 2010) and the Po-delta, Italy (Antonellini et al., 2008). They differ from BGH-lenses in that the upward moving saline groundwater limits the penetration depth of rainwater, and thus the volume of the freshwater lens (Chapter 2, De Louw et al., 2011). Field measurements by De Louw et al. (2011) in the south-western delta of the Netherlands showed that the mixing zone between infiltrated rainwater and upward seeping saline groundwater occurs within 2 meters below ground level (BGL) and that nearly all mapped lenses lacked truly fresh groundwater (chloride concentration < 0.3 g L^{-1}). These lenses are the object of the current study, and are referred to as rainwater lenses. For the purpose of this study, the vertical extent of the rainwater lens is bounded by the water table and the depth below which no rainwater penetrates (B_{mix}, which is the depth at which the salinity equals the salinity of regional groundwater, Fig. 4.1). With this definition, the rainwater lens is not purely a freshwater lens, and salinities within the rainwater lens vary both in space and in time.

The dynamic behaviour of salinities within rainwater lenses and the soil moisture in the unsaturated zone above them is of great importance from an agricultural perspective. It is expected that lens thickness and mixing zone properties are not steady state and will respond to temporal recharge variations at intra- and inter-annual timescales, as well as to seepage variations on a longer timescale. Due to their limited size and vicinity to the land surface, rainwater lenses are vulnerable to changing precipitation and evapotranspiration (which control recharge) patterns. During dry periods, saline groundwater can reach the root zone via capillary rise, affecting crop growth (Katerji et al., 2003; Rozema and Flowers, 2008).

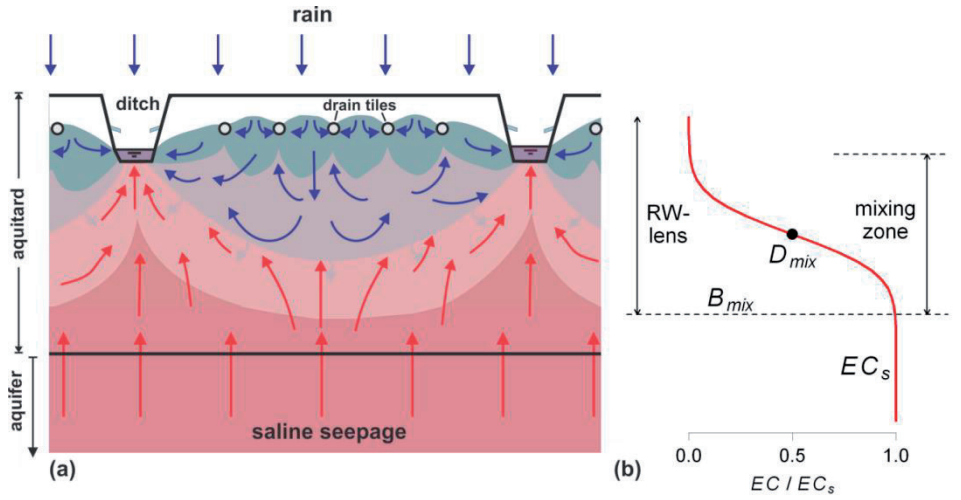

Fig. 4.1: a) Schematic cross-section visualizing the conceptual model of a rainwater lens in an area with upward seepage of saline groundwater. b) Vertical profile of the electrical conductivity (EC) of groundwater at an arbitrary point in the rainwater lens. The vertical extent of the rainwater lens at any point is from the base of mixing zone (Bmix) to the water table. The depth of the centre of the mixing zone (Dmix) is at the point where the EC is 50% of the seepage water salinity (ECs).

Besides recharge and seepage, another important factor that controls the size of the rainwater lens is tile drainage (De Louw et al., 2011; Velstra et al., 2011). Adapting drainage systems has been proposed as an effective water management strategy to mitigate the predicted adverse consequences of increased drought and sea level rise (e.g. Poulter et al., 2008). The latter may enhance upward seepage rates (Chapters 2 and 3,Maas, 2007; De Louw et al., 2011), thus negatively impacting the freshwater volume stored in rainwater lenses.

Successful implementation of any measure to make the rainwater lenses more resilient to future climate change requires knowledge of their dynamic behaviour. So far, research into lens dynamics has mainly been focused on BGH-freshwater lenses (e.g. Badon Ghijben 1889; Herzberg, 1901; Meinardi, 1983; Underwood et al., 1992; Collins and Easley, 1999; Bakker, 2000; Stoeckl and Houben, 2012). Stoeckl and Houben (2012) examined the development and flow dynamics of freshwater lenses by physical experiments on laboratory scale. Underwood et al. (1992) examined the dynamic behavior of the mixing zone of a BGH-lens of a generalized atoll groundwater system and found that mixing is controlled by oscillating vertical flow due to tidal fluctuation, while recharge determines lens thickness. On Jeju Island (Korea), measurements showed small tidally-induced variations, but no long-term seasonal variation of the fresh-salt water interface (Kim et al., 2006). In BGH-lenses the response to recharge variations is in the order of decades (e.g. Vaeret et al., 2012; Oude Essink, 1996). Rotzoll et al. (2010) observed thinning rates of 0.5 to 1.0 m y^{-1} in thick freshwater lenses in Hawaii due to long term groundwater withdrawal and reduced recharge.

In the absence of long-term field data for rainwater lenses, their response at intra-annual and inter-annual timescales remains poorly characterized and understood. De Louw et al. (2011) reported that, since temporal variations were not measured, they could not conclusively determine if the noted absence of fresh groundwater was a transient or a permanent feature of the rainwater lens. Velstra et al. (2011) used DC resistivity measurements to delineate rainwater lenses in the northern coastal area of the Netherlands and found seasonal variations in lens-thickness. However, the use of geophysics to monitor temporal variations of shallow subsurface resistivity is difficult due to the limited resolution, impact of unsaturated zone conditions and non-unique interpretation of the measurement data (Goes et al., 2009). In Chapter 3, a theoretical relation between lens thickness variations and sinusoidal recharge variations was developed, but not corroborated with measured data. To understand the rainwater lens field behaviour, direct measurements of groundwater and soil water salinities are much needed.

The intent of the present study was to address the knowledge gap that exists on the temporal dynamics of rainwater lenses. To this end, a comprehensive set of data was collected at two tile-drained agricultural fields in the Netherlands. The data consisted of groundwater and soil water salinities, groundwater levels, drain tile discharge and drain water salinity, precipitation and evapotranspiration. The main objectives were (i) to obtain direct, field-based evidence of rainwater lens dynamics, and (ii) to quantify the temporal variations of the flow and mixing processes within the rainwater lens. The main focus was on the control of recharge and tile drainage. A numerical flow and transport model was used to complement the collected field data and to support the development of a conceptual model of rainwater lens dynamics.

4.2 Study area

Two of the 27 agricultural sites examined by De Louw et al. (2011) were selected to monitor the rainwater lens dynamics and mixing behaviour between March 2009 and January 2011. These sites were referred to as sites 11 and 26 in De Louw et al. (2011) but here as site A and B, respectively. The sites were selected primarily because of their representative hydrogeological conditions and rainwater lens characteristics, typical for the saline seepage areas of the south-western part of the Netherlands (De Louw et al., 2011). Practical considerations, such as accessibility and nearby electricity supply, also played a role. Monitoring sites A (latitude 51°42'04''N, longitude 03°51'26''E) and B (latitude 51°43'44''N, longitude 03°47'57''E) are both situated on the Schouwen-Duivenland island in the south-western part of the Netherlands (Fig. 4.2a). The mean annual precipitation and potential Makkink evapotranspiration for the period 1980-2010 are 815 mm and 613 mm, respectively (data from the Royal Netherlands Meteorological Institute KNMI). Groundwater is predominantly saline, and originates from Holocene transgressions during the periods 7500 BP to 5000 BP

and 350 AD to 1000 AD (Vos et al. 2008; Post et al., 2003). Upward seepage of saline groundwater occurs where the land surface lies below mean sea level (MSL).

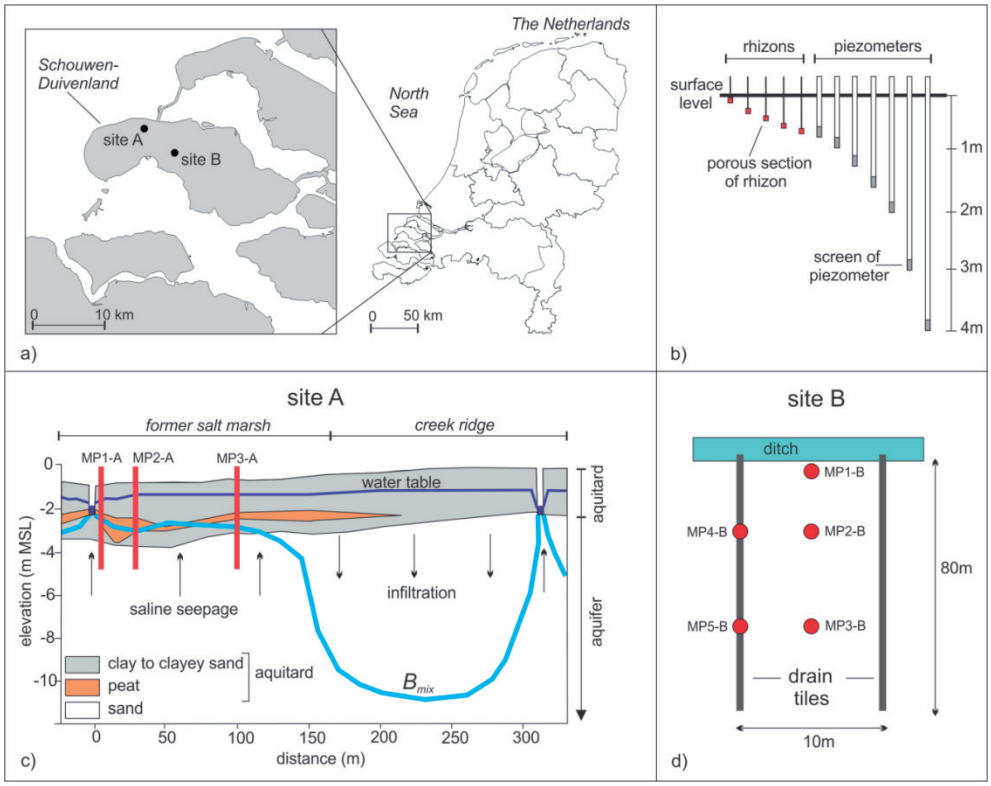

Fig. 4.2: a) Map showing the location of study sites; b) Schematic diagram showing the depths below ground surface of the rhizons and piezometers installed at each measurement point. The minimum and maximum distances between installed piezometers and rhizons of a measurement point are respectively 0.5 and 2.5 m; c) Cross section at site A showing the geology, water table, vertical flow direction, the base of the rainwater lens (Bmix, De Louw et al., 2011) and the locations of the measurement points (red vertical lines); d) Plan view of site B showing the location of the measurement points, the ditch and the drain tiles.

Site A is a 300 m long agricultural field located at the mixing from a former salt marsh to a tidal creek paleo-channel (Fig. 4.2c). Due to differential subsidence by sediment compaction, the land surface elevation of the paleo-channel (-0.2 m MSL) is presently above that of the salt marsh sediments (-0.7 m MSL). The field is bordered by ditches with a surface water level which is maintained at an depth of 1.3 m BGL, and the field is tile-drained at a depth of 1.0 m BGL with a horizontal drain separation of 10 m. Fine-grained to medium coarse-grained sand is found between 2.5 m and 30 m BGL, which belongs to a regionally-extensive aquifer. The aquifer is confined by 2.5 m of heterogeneous low-permeability sediments comprised of peat, clay and sandy clay at the former salt marsh and sandy clay to clayey sand at the creek ridge (Fig. 4.2c). As freshwater head gradients between 1.5 m and 4 m depth were considerably larger than the relative density difference that accounts for the buoyancy effect, the vertical

flow direction (but not the magnitude) can be inferred directly from the head measurements (Post et al., 2007). At the former salt marsh, the measured heads were permanently higher in the sandy aquifer at 4 m depth than at 1.5 m depth in the aquitard, resulting in a continuous upward groundwater flow (De Louw et al., 2011, Fig. 4.2c). At the creek ridge, the freshwater head was lower at 4 m depth than at 1.5 m depth, indicating downward flow. Due to these different vertical flow patterns, the rainwater lenses below the former salt marsh are thin ($1.5 < B_{mix} < 3$ m) compared to the creek ridge ($4 < B_{mix} < 10$ m) (De Louw et al., 2011). Only the data collected in the former salt marsh zone with permanent upward seepage is presented in this paper.

Site B is located in a former salt marsh at an elevation of -2.0 m MSL and is bordered by a ditch with a surface water level maintained at 1.1 m BGL (Fig. 4.2d). Drain tiles with a length of ~80 m are located at a depth of 0.70 m BGL with a horizontal separation of 10 m. The upper 2.5 m of the subsoil consists of silty clay and a 0.10 - 0.15 cm thick peat layer at about 0.5 m depth. Between 3.0 m and 4.5 m BGL a sequence of clayey fine sand and sandy clay occurs. These low-permeability sediments form a semi-confining unit, below which the same regionally-extensive sandy aquifer as at site A is found. Head gradients indicate that permanent upward seepage occurs everywhere below the agricultural field, and the rainwater lenses have a thickness between 1.5 and 2 m (de Louw et al., 2011). Shrinkage cracks in the clayey top soil were observed during the driest months of the year (May – October).

4.3 Methods

4.3.1 Monitoring network

The monitoring networks of site A and B consisted of measurement points at various distances from the north western (site A) and western (site B) ditch, at which time-series data of groundwater salinity, soil water salinity, water table elevation and hydraulic head were collected at different depths (Fig. 4.2c and d). The measurement points were located between two subsurface drain tiles, except for MP4 and MP5 of site B, which were positioned within 0.2 m of a drain tile to assess the effect of tile drainage (Fig. 4.2d).

At each measurement point a cluster of piezometers was installed (Fig. 4.2b). Each cluster consisted of 6 or 7 piezometers with 0.16 m long screens at depths (bottom of screen) of 0.8 m, 1.0 m, 1.3 m, 1.6 m, 2.0 m, 3.0 m and 4.0 m BGL. Piezometers with pre-fabricated bentonite plugs of the same diameter as the auger borehole were used to avoid preferential flow. The electrical conductivity (EC) of groundwater samples was measured in the field every month for a period of 22 months (March 2009 – December 2010). Before taking groundwater samples for measurement, all the standing water was extracted from the piezometers. The piezometers were then allowed to re-fill with groundwater, which could take up to several hours due to the

low permeability of the sediments. Errors in the order of 1-5% were associated with the EC measurements due to calibration difficulties in the field.

At each measurement point a cluster of soil moisture samplers (rhizons from Rhizosphere®) were installed to obtain soil water samples (Fig. 4.2b). The porous section of the rhizons had a diameter of 2.5 mm, a length of 100 mm and an average pore size of 2.5 μm. Each cluster contained 5 rhizons at depths (measured from the bottom of the porous section) of 0.15 m, 0.30 m, 0.45 m, 0.60 m and 0.75 m BGL. Suction was applied for at least 4 hours, after which the soil water was collected and the EC was measured in the field. When the amount of collected water was insufficient for an EC measurement, demineralized water was added and the measured EC was corrected for dilution. Soil water was sampled monthly on the same days as the groundwater was sampled, for a period of 17 months (July 2009 – December 2010).

At all measurement points, the hydraulic head at 4 m depth was recorded between March 2009 and January 2011 with a 1-hour frequency using data-logging pressure transducers (Schlumberger Water Service Divers®). Measured heads were converted to equivalent freshwater heads using the equations presented in Post et al. (2007). The water table elevation was inferred by measuring the water level in a piezometer with a 1.0 m long screen installed at a depth between 0.5 m and 1.5 m BGL.

At site B the drain tile discharge (Q_{drain}) and salinity (EC_{drain}) were measured from February 2010 to January 2011. The ends of 2 drain tiles (Fig. 6.2d) were connected and the discharge water was collected in a container (1 m × 0.6 m × 0.6 m). A known volume of water was pumped from the container automatically with a water-level-controlled-pump, and the number of pumping events per hour was recorded automatically. These recordings were multiplied by the pumping volume to obtain Q_{drain}. Water level fluctuations in the container were measured with a pressure transducer to verify the pumped volumes and the inferred Q_{drain}. The EC of the collected drain water was measured hourly in a small compartment installed in the pipe connecting the 2 drain tiles using a CTD-diver from Schlumberger Water Service®.

Precipitation (P) was measured at both sites with a tipping bucket rain gauge which reported rainfall at 1-hour intervals. Daily sums of the potential Makkink (1957) evapotranspiration (ET_p) were obtained from the nearest meteorological station of the KNMI (Wilhelminadorp, at 23 and 19 km from site A and B respectively). The obtained ET_p data is assumed to be representative for both field sites since the data of KNMI show that evapotranspiration patterns in the Netherlands are rather uniform (Sluijter et al., 2011). The retention characteristics of the soil were determined based on samples taken from 0.2 and 0.4 m BGL following the method described in Stolte (1997).

4.3.2 Numerical modeling

Spatial and temporal discretization

A rainwater lens between two drain tiles under the field conditions of site B was simulated using the variable-density flow and transport code SEAWAT version 4 (Langevin et al., 2007). The setup of the model is shown in Fig. 4.3a. A cross-section perpendicular to the drain tiles was modelled, which had a length of 10 m and a thickness of 4.5 m, i.e., the thickness of the aquitard at site B. Drain tiles were implemented at the left and right boundaries at 0.7 m BGL (Fig, 4.3) through the MODFLOW drain package (Harbaugh et al., 2000). The side boundaries were no-flow and no-solute flux boundaries. All inflows, i.e. recharge and vertical upward seepage, were applied at the top and bottom model boundaries, respectively. Water could leave the system by tile drainage and evapotranspiration. The mesh consisted of 40 columns of 0.25 m, 1 row of 0.25 m, and 45 layers of 0.1 m.

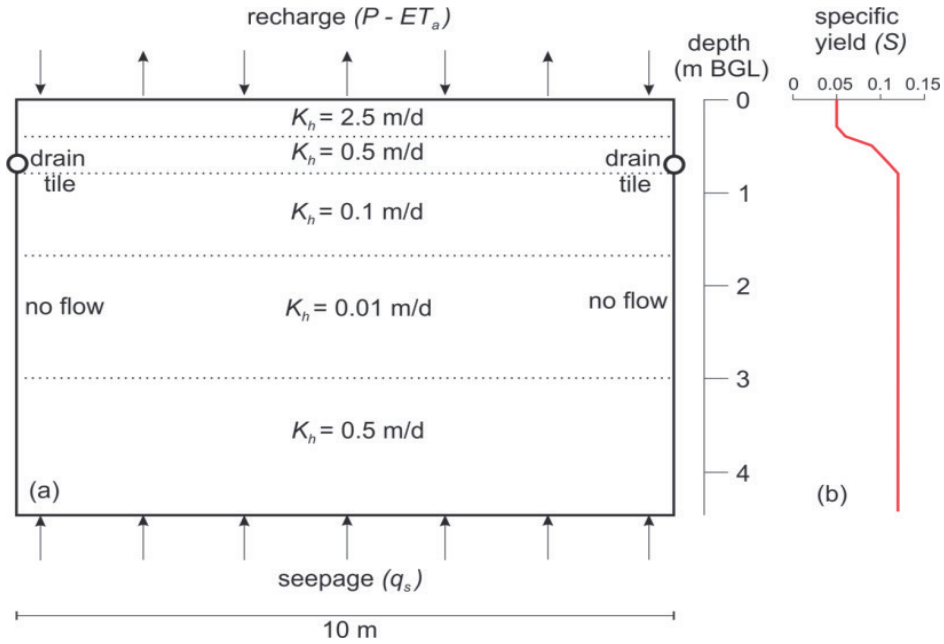

Fig. 4.3: a) Schematic representation of the setup of the SEAWAT-model of the rainwater lens between two drain tiles at site B. b) The specific yield (S)-depth relation is derived from measured water table fluctuations and precipitation data using Eq. (4.1).

Simulation time spanned a period of 20 years. The same sequence of daily varying recharge, calculated using the meteorological data of 2009 and 2010 as detailed below, was repeated 10 times. After some initial simulations it was found that subdividing each stress period of 1 day into 20 flow time steps provided adequate simulation of the water table fluctuations. The flow time steps were automatically subdivided into a number of transport time steps according to the Courant number which was not allowed to be greater than 1 (Langevin et al., 2007).

Hydraulic parameters

The hydraulic parameters varied with depth based on the lithological strata that were encountered in the auger holes (Fig. 4.3a). The Dutch Geohydrological Information System (REGIS II, 2005) contains an extensive database of hydraulic conductivity measurements of soil materials in the south-western part of the Netherlands, and provides a range of horizontal (K_h) and vertical hydraulic conductivity (K_v) for each material type. The values of K_h and K_v that were adopted after calibration lie within the range of values in REGIS II. The hydraulic conductivity anisotropy factor (Kh / Kv) was set to 5 for the entire model (REGIS II, 2005; De Louw et al., 2011).

The moving water table was simulated through MODFLOW's cell wetting and drying option. With this option, model cells are made inactive when the head falls below the bottom of the cell. The cell becomes active again (that is, it rewets) once the head in the underlying cell rises above the cell's bottom (Harbaugh et al., 2000). For the highest active cells a specific yield (S) was used to account for storage changes due to a fluctuating water table, whereas a confined storage coefficient was used for all fully-saturated cells below. The use of a specific yield parameter to simulate water table fluctuations is a gross simplification of the conditions in the field, as it does not take into account the dynamic conditions in the unsaturated zone, which vary continuously as a result of rainfall, evapotranspiration and tile drainage. Different strategies have been proposed in the literature to account for this (e.g. Acharya et al., 2012), but here the following approach was used in this study to determine S. For selected periods throughout the year, S was quantified based on measured water table fluctuations and rainfall amounts using:

$$S = \frac{\sum_{t=1}^{n} P(t)}{(h(n) - h(1))} \tag{4.1}$$

where h is the water table depth (m BGL), P is the daily rainfall (m d^{-1}), and n represents the number of days considered for the calculation. 12 periods of continuous increasing water levels ranging in length between 2 and 5 days were selected. A relation was found between S calculated according to Eq. 4.1 and the water table depth, which was implemented in the model by letting the specific yield vary with depth (Fig. 4.3b). A constant value of S of 0.12 was applied at a depth below 0.7 m BGL. Above this depth, S decreases to 0.05 for the upper 0.3 m. The values of S were not adjusted during calibration.

Seepage

The vertical seepage flux from the aquifer into the aquitard was estimated based on measured data of site B for a period of 343 days (6 February 2010 - 13 January 2011), based on a salt mass balance for the tile drains:

$$\sum_{t=1}^{n} q_s(t) = \frac{\sum_{t=1}^{n} (Q_{drain}(t) \cdot EC_{drain}(t))}{EC_s \cdot A} \tag{4.2}$$

where n = 343, q_s is the vertical seepage flux (m d^{-1}), Q_{drain} is the measured drain tile discharge (m^3 d^{-1}), A is the surface area that contributes to Q_{drain} (m^2), and EC_{drain} and EC_s (mS cm^{-1}) denote the drain and seepage water salinity, respectively. This assumes that all dissolved salt that is discharged by the drain tiles originates from seepage and that no storage of salt occurs during the considered period. With these assumptions, the vertical seepage flux calculated according to Eq. 4.2 was q_s = 0.29 mm d^{-1}.

Recharge

To calculate the recharge, daily values of the actual evapotranspiration (ET_a) are required, which, in principle, could be based on reported values of the potential Makkink (1957) evapotranspiration ET_p for the KNMI meteorological station in Wilhelminadorp multiplied by a crop factor f. The value of f is unknown, and it was found that the model outcomes had a high sensitivity to this parameter. Therefore, the daily values of ET_a were determined based on water balance considerations instead. Using the same data as for the estimation of q_s, the total ET_a between day 1 and day 343 was first calculated according to:

$$\sum_{t=1}^{n} P(t) - \sum_{t=1}^{n} ET_a(t) + \sum_{t=1}^{n} q_s(t) = \sum_{t=1}^{n} \frac{Q_{drain}(t)}{A} \tag{4.3}$$

Eq. 4.3 was solved for $\sum_{t=1}^{n} ET_a(t)$ using measured values of P and Q_{drain}, and values of q_s based on Eq. 4.2. Subsequently, a surrogate crop factor f_s for the considered period was calculated by:

$$f_s = \frac{\sum_{t=1}^{n} ET_a}{\sum_{t=1}^{n} ET_p} \tag{4.4}$$

The calculated value of f_s was 0.69, and accounts for all processes that reduce ET_p, such as crop type, growth stage and plant stress due to limited soil moisture availability and the presence of salt in the root zone. Daily values of ET_a were then obtained by the multiplication of f_s with the daily values of ET_p. Finally, daily recharge fluxes for the model were obtained by subtracting the daily values of ET_a from P. Daily recharge could be either positive or negative with this approach, and was applied to the highest active model cells.

Salt transport

Chloride (Cl) was used to represent salinity in the model and a linear relation between density (ρ) and Cl concentration was assumed. To compare the model-calculated concentrations with the field measurements, modeled Cl concentrations (g L^{-1}) were converted into ECs (mS cm^{-1}) using the linear relation derived from measured Cl - EC pairs of 79 groundwater samples taken at site A and B (De Louw et al., 2011): EC = 2.78Cl + 0.45. Water entering across the bottom model boundary was assigned a Cl concentration of 12 g L^{-1} based on measured data. The same Cl concentration was used as the initial Cl concentration in all model cells, allowing a rainwater lens to develop in the saline groundwater body.

The negative recharge that was applied in the model when $ET_a > P$ constitutes a sink for both water and solutes. Conceptually, negative recharge is considered to represent water loss from the saturated zone by capillary rise. In the field, depending on the salinity of groundwater at the water table, variable amounts of solutes are thereby moved into the unsaturated zone and temporarily stored. During recharge events, the solutes residing in the unsaturated zone are flushed. To replicate this behaviour in the model, a Cl concentration of 1.25 g L^{-1} was assigned to the water entering the system as recharge. This value was chosen such that the total salt mass leaving the model by capillary rise equaled the total salt mass entering the model by recharge.

Preliminary model runs showed that in order to reproduce the width of the mixing zone, longitudinal and transversal dispersivity values of 0.1 m and 0.01 m, respectively, were adequate. These values are commensurate with values adopted in numerous case studies in comparable settings (e.g. Stuyfzand, 1993; Lebbe, 1999; Van Meir, 2001; Oude Essink, 2001a; Vandenbohede and Lebbe, 2007). The molecular diffusion coefficient for Cl in porous media was assumed to be $8.6 \cdot 10^{-5}$ m^2 d^{-1}.

Model calibration

The model was calibrated manually by optimizing the fit between the simulated and measured (i) salinity-depth profiles at and between the two drain tiles, (ii) daily observations of Q_{drain}, (iii) EC_{drain}, and (iv) water table elevation. The Nash-Sutcliffe coefficient (*NSC*, Nash and Sutcliffe, 1970) was used to quantitatively evaluate the dynamic model performance:

$$NSC = 1 - \frac{\sum_{t=1}^{n} (o_t - s_t)^2}{\sum_{t=1}^{n} (o_t - \bar{o})^2} \qquad (4.5)$$

in which o_t represents the observed and s_t the simulated value for day *t,* and $\bar{o}$ the mean of the observed values. The model output for the twentieth year (corresponding to the year 2010) was used to compare to the field data.

The outcomes of the calibrated model were used to analyze vertical flow velocities, transient path lines and travel times towards the drain tiles. The path lines and travel times were calculated by forward-tracking particles placed at the centre of every model cell, using the post-processing package MODPATH version 3 (Pollock, 1994).

4.4 Field observations

4.4.1 Groundwater salinity and rainwater lens thickness

Fig. 4.4 shows the salinity of the water in the saturated and unsaturated zone as a function of depth for all monitoring locations. The data show the existence of a 1 – 1.50 m wide mixing zone at a depth D_{mix} (= centre of mixing zone with a salinity half that of seepage water) of around 1.5 m BGL, and B_{mix} of around 2.2 m BGL. Only location MP2-A had a wider mixing zone (about 2 m), with B_{mix} at about 3.3 m BGL. Below the mixing zone the salinity stayed constant with depth until a depth of at least 25 m BGL (De Louw et al., 2011). The salinity below B_{mix} is therefore considered to be representative of the salinity of the groundwater (EC_s) that constitutes the vertical seepage. At site A the average EC_s for MP1-A and MP2-A was 44 mS cm^{-1} (σ^2 = 0.88) while at site B the average EC_s for all five locations was 34 mS cm^{-1} (σ^2 = 1.12). The EC_s for MP3-A was lower (about 37 mS cm^{-1}) than for the other two locations at site A. This is probably due to the presence of the nearby thick freshwater lens that laterally mixes with the upward flowing saline groundwater in the aquifer (Fig. 4.2c).

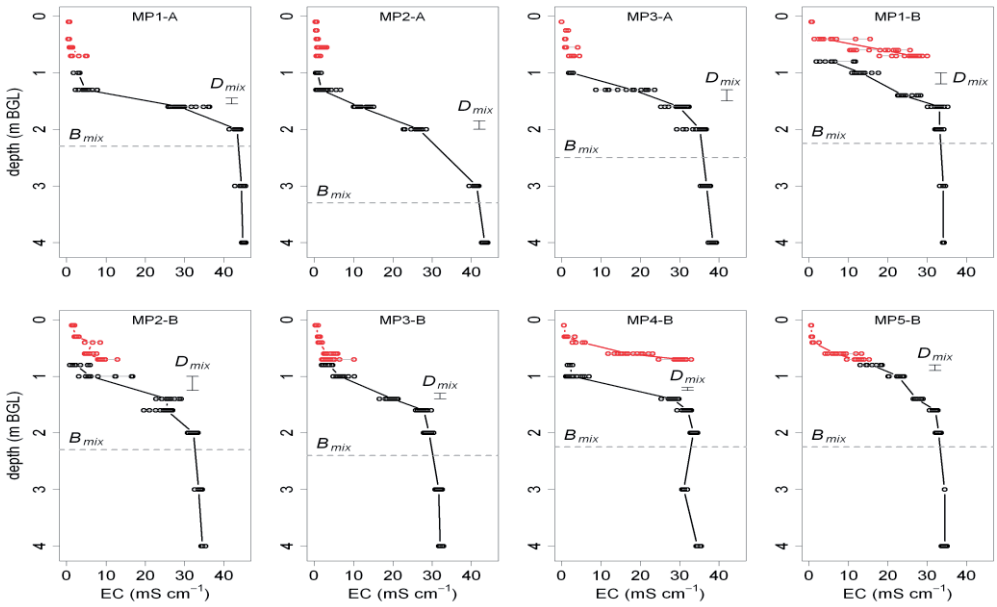

Fig. 4.4: Depth profiles of soil water salinity (in red) and groundwater salinity (in black) for sites A and B, based on monthly measurements during the period March 2009 – December 2010. The individual measurements are indicated by dots and median values are connected by a full line. The amplitude of the displacement of Dmix during the monitoring period and the depth of Bmix is indicated for each measurement point.

The scatter of the data points in Fig. 4.4 shows that the temporal salinity variations are significantly larger around D_{mix} than around and below B_{mix}. The variations below B_{mix} were smaller than the accuracy of the EC-readings. A seasonal trend of groundwater salinity was found for some of the shallow screens: groundwater salinities decreased when the water table rose and vice-versa for sampling depths of 1.3 m and 1.6 m at MP1-A and MP2-A, 0.8 m, 1.0 m and 1.3 m at MP3-B and 1.0 m at MP4-B (Fig. 4.5d-f). Although salinity variations were less pronounced for larger depths, the data suggest that at sampling depths of 2 m and 3 m at MP1-A and MP2-A, 1.6 m and 2 m at MP3-B, and 1.3 m and 1.6 m at MP4-B, salinities show the opposite trend, i.e., they increased with increasing water level, and decreased with decreasing water level (Fig. 4.5g-i).

Despite the observed temporal salinity variations at each sampling depth, the mixing zone location and width remained almost unchanged (Fig. 4.4). The maximum displacement of D_{mix} of all salinity profiles was between 0.05 m and 0.25 m and B_{mix} stayed virtually at a fixed position throughout the entire 22-month measurement period (Fig. 4.4). Water table fluctuations, on the other hand, were highly dynamic, and changed in response to individual rainfall events as well as on a seasonal timescale (Fig. 4.6). As a result, the rainwater lens thickness was highly dynamic as well, and varied by up to 1.2 m per year.

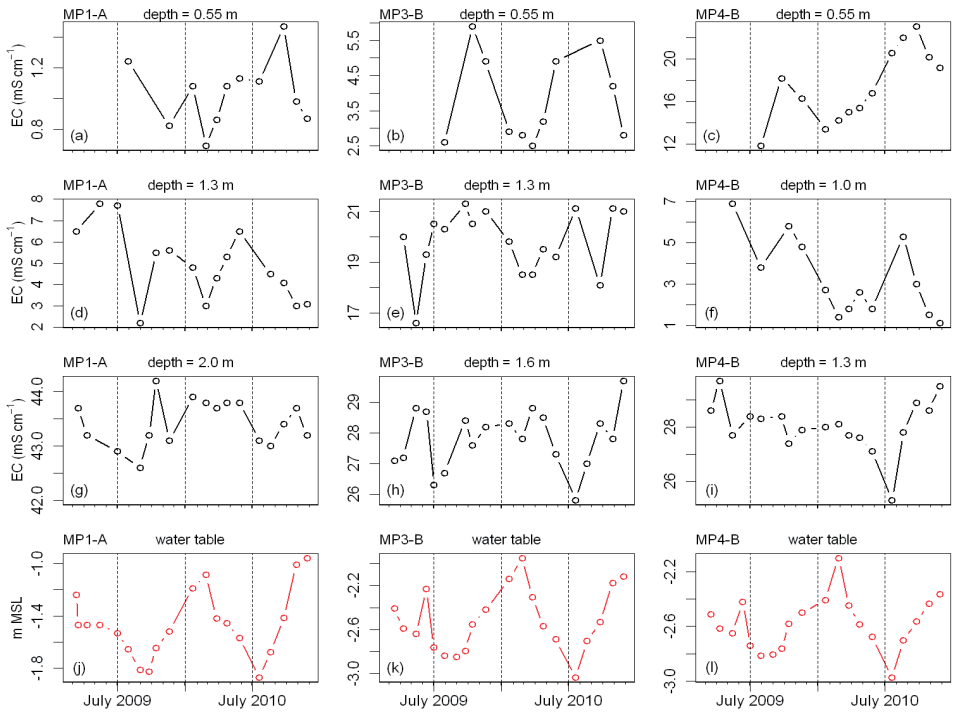

Fig. 4.5: Graphs showing time series for measurement points MP1-A (left panel), MP3-B (middle panel) and MP4-B (right panel) of (a-c) soil water EC at 0.55 m, (d-i) groundwater EC at two different depths and (j-l) water table elevation.

4.4.2 *Soil water salinity*

In general, soil water salinities increased with depth at both sites, but soil water salinities are notably higher at site B than at site A (Fig. 4.4). At site A, salinities within the root zone (sampling depths 0.15 m, 0.25 m, and 0.4 m) were always below 1.7 mS cm^{-1}, while they reached up to 15 mS cm^{-1} at site B. It should be noted though that extracting soil water was more difficult at site A and therefore data of dryer periods could not be obtained, except for sampling depth 0.55 m of MP1-A. Another conspicuous difference is that for three locations at site B soil water salinities were much higher than in the saturated zone (Fig. 4.4), which was not the case at site A.

For the sampling depths where sufficient samples could be collected throughout the year a clear seasonal trend in soil water salinity was observed. Selected examples of this seasonal behaviour are shown in Fig. 4.5a-c. Higher soil water salinities occurred during periods with low water tables (Fig. 4.5j-l), low P and high ET_a.

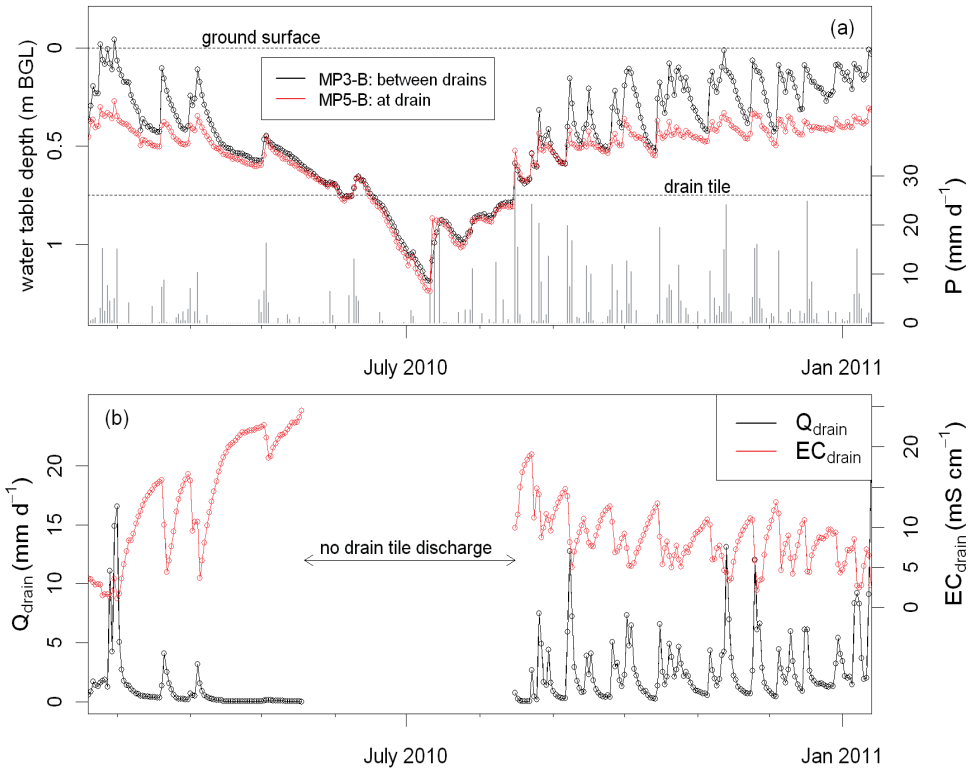

Fig. 4.6: Graphs showing times series at site B of (a) the water table at a drain tile and between two drain tiles and daily precipitation P, and (b) Qdrain and ECdrain. Water table elevations above the ground surface indicate conditions of surface ponding.

4.4.3 Drain tile discharge and drain water salinity

Fig. 4.6 shows the observed Q_{drain} and EC_{drain}, as well as the water table at a drain tile and between two drain tiles. The data cover a period of almost 1 year. Drain tiles carried discharge when the water table was above the drain tile level, and the discharge increased when the water table rose due to precipitation. EC_{drain} varied with Q_{drain}, where an increase of Q_{drain} caused a rapid and pronounced decline in EC_{drain}, followed by an increase of EC_{drain} when the discharge decreased. Fig. 4.7b shows that EC_{drain} was linearly correlated with water table depth, with EC_{drain} decreasing when the water table was rising. EC_{drain} never exceeded 25 mS cm^{-1} or fell below 2 mS cm^{-1}. The largest salt loads (discharge times salt concentration) occurred during peak discharge events (Fig. 4.7d) when drain water salinities were low.

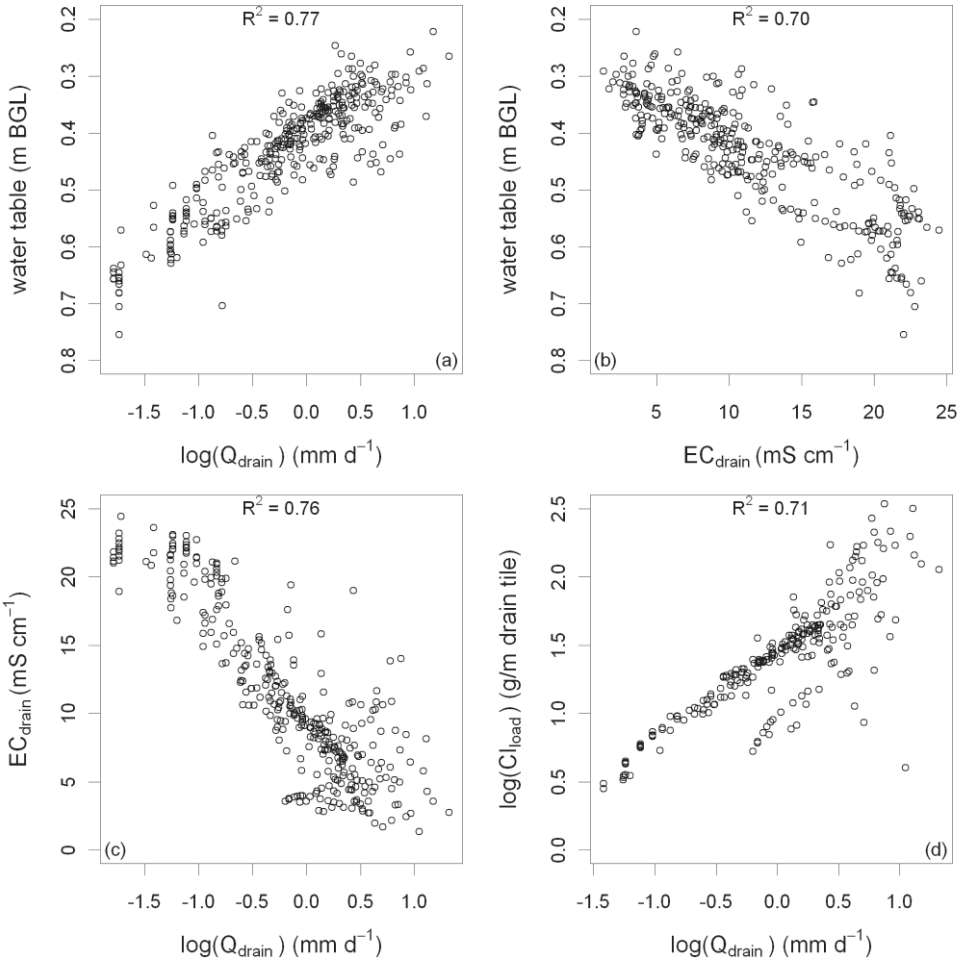

Fig. 4.7: Scatter diagrams showing measurements at site B of (a) the water table elevation at MP5-B versus log(Qdrain), (b) the water table elevation at MP5-B versus ECdrain, (c) ECdrain versus log(Qdrain) and (d) log(Clload) versus log(Qdrain). The salt load Clload is expressed in g Cl discharged per m drain tile.

4.5 Model outcomes

Because the model started with initial Cl concentrations of 12 g L^{-1} a spin-up time was required during which the rainwater lens developed. It was found that after 8 years the total solute mass in the model between consecutive 2-year recharge cycles changed < 0.1%, indicating that there was no long-term change in the lens volume. Fig. 4.8 shows the comparison between the observed and model-simulated dynamics of Q_{drain}, EC_{drain}, and the water table elevation between the drain tiles during the measurement period. Also shown are the time-averaged observed and simulated salinity-depth profiles at and between the drain tiles. The simulated dynamics of Q_{drain} correspond well to the observed dynamics (NSC = 0.65) (Fig. 4.8a). In order to achieve this fit, high values of K_h (2.5 m d^{-1}) needed to be assigned to the upper 0.4 m of the subsoil. Cracks were observed at the surface, in particular during summer, and these are believed to be the cause for the relatively-high K_h value for this soil type. The adopted values of S (0.05 – 0.09) were adequate to reproduce the observed response of the water table elevation and Q_{drain} to recharge.

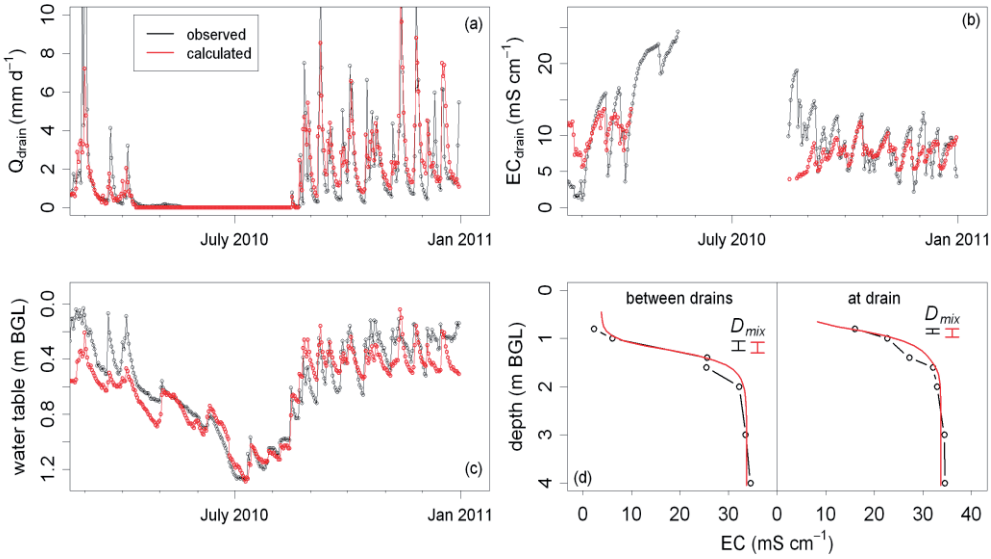

Fig. 4.8: Graphs showing the comparison between observed and calculated a) Qdrain, b) ECdrain, c) water table between the two drain tiles, and d) salinity-depth profiles at and between the two drain tiles. The observed and calculated variation of Dmix is indicated as well.

During calibration it was found that with a constant f_s = 0.69, the simulated water table fell too deep in the summer. Simulations with f_s = 0.60 for the summer half of the year (15 April – 14 October) and f_s = 1.0 for the winter half of the year (15 October – 14 April), resulted in a much better fit with the observations whilst leaving the total ET_a for the period unchanged. The justification on physical grounds for this approach is the reduction of ET_a in summer due to limited soil moisture availability and salt stress. In an analogous way, q_s was set to 0.16 mm d^{-1} for the winter half of the year

and to 0.42 mm d^{-1} for the summer half of the year, which is commensurate with the observed change in the difference between the head at 4 m depth and the water table. With these adjustments, the observed water table could be satisfactory simulated (*NSC* = 0.81) (Fig. 4.8c).

The observed dynamics of EC_{drain} could only be partially reproduced by the model (NSC = 0.01 for the entire period of available data; 0.42 for the period after 15 September 2010). The largest discrepancies between simulated and observed values occurred directly after the summer period when drain tiles start discharging again and simulated values of EC_{drain} are lower than observed (Fig. 4.8b). This is believed to be attributable to the fact the salinity of the recharge water after a period of drought is higher in the field than the constant Cl concentration of 1.25 g L^{-1} used in the model. Attempts to increase the simulated EC_{drain} after periods of drought and EC_{drain} dynamics throughout the year, such as by adopting higher K_h and lower S-values for the upper soil, different salinities of recharge for summer and winter, smaller cells around the drain tile and lower dispersivity values, resulted in little improvement, or a significant worsening of the fit for the other metrics.

4.6 Discussion

4.6.1 Groundwater dynamics

The time-series data showed that D_{mix} did not vary more than 0.25 m during the measurement period. The temporal depth variation of D_{mix} showed a seasonal trend rather than a response to individual rain events, with a deeper D_{mix} during the winter half of the year when the water table was high (Fig. 4.9a). The small vertical displacement of the mixing zone explains the observed seasonal salinity variations in the rainwater lens, which are illustrated in the next example. The salinity gradient around D_{mix} is about 4 mS cm^{-1} and 3 mS cm^{-1} per 0.1 m depth interval for sites A and B, respectively (Fig. 4.4). From this it can be inferred that a vertical displacement of D_{mix} of only 0.05 - 0.25 m results in seasonal salinity variations of 2 - 10 mS cm^{-1} for site A and 1.5 – 7.5 mS cm^{-1} for site B, which is in accordance with the observations (Fig. 4.5) and model results (Fig. 4.9b). The upward and downward movement of D_{mix} and seasonal salinity variations suggest that there exists a seasonally oscillating flow regime.

2 mm d^{-1} and 5-10 mm d^{-1}, respectively. These small velocities and the fact that the flow alternates in vertical flow direction result in little vertical displacement, which explains why the seasonal variation of D_{mix} is only small. The numerical experiments in Chapter 3 showed much larger seasonal displacements of D_{mix} (0.5 - 1.0 m per year). This is probably due to the fact that they considered a different hydrogeological setting, i.e., a sandy aquifer without the presence of a low-permeability aquitard on top allowing for much larger vertical flow velocities than in cases rainwater lenses develop within an aquitard.

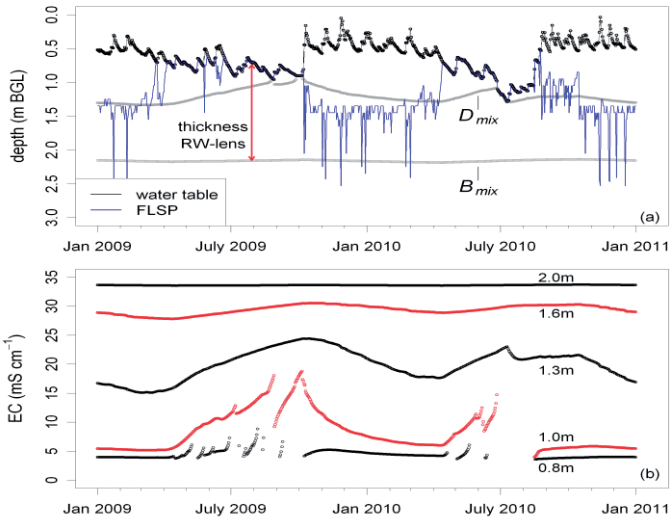

Fig. 4.9: Graphs showing model results between the drain tiles: (a) time series of the water table, Dmix, Bmix and the vertical flow stagnation point (FLSP) for a period of two years (2009-2010), (b) temporal variations of groundwater salinity at different depths. No results are shown for depths of 1.0 m and 0.8 m when model cells were above the calculated water table and hence inactive.

Beyond this, the calibrated model was used to determine the temporal dynamics of the vertical flow stagnation point (FLSP), which is the point below which the flow switches from having a vertical downward to a vertical upward component (De Louw et al., 2011). The FLSP at the point between the drain tiles shows a clear correlation with the elevation of the water table (Fig. 4.9a), whereby a rising water table resulted in a deeper FLSP. The FLSP responds rapidly to water table fluctuations. Flow is downward for a large part of the rainwater lens when the water table is high, but when the water table falls below the drain tile all flow in the rainwater lens is upward (Fig. 4.9a).

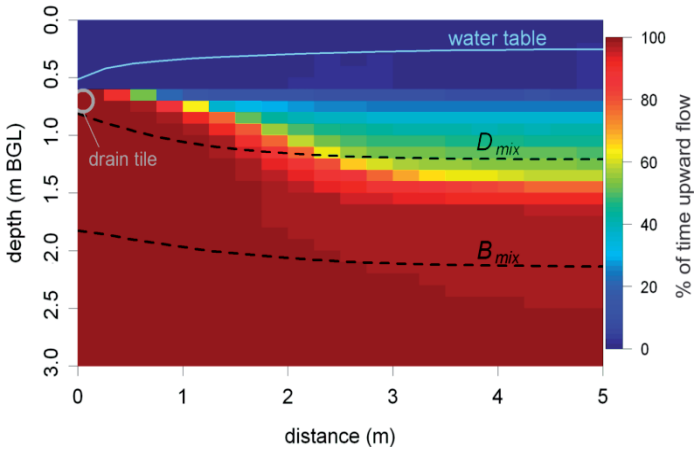

Fig. 4.10: Contour plot that shows for every model cell the percentage of time during which groundwater flow has an upward flow component (determined for a period of two years, 2009 - 2010). The average positions of Dmix and Bmix for the modeled period 2009-2010 are indicated as dashed lines.

The oscillatory flow regime is further believed to be a driver for the mixing of infiltrated rainwater and saline groundwater in a rainwater lens (De Louw et al., 2011). This is illustrated by the transient path lines within the rainwater lens (Fig. 4.11a). Path lines started from different locations within the rainwater lens show that certain regions of the subsurface sometimes receive inflow from (i) recharge across

the water table, (ii) saline groundwater from seepage, or (iii) a mixture of the two. Path lines originating in the fresh- and saltwater zone cross each other over time, indicating mixing. The bends of the path lines indicate seasonal changes of periods with different recharge; path lines are predominantly horizontally oriented during winter when there is a significant flow towards the drain tile, and nearly vertical flow occurs during summer when the water table dropped below drain tile elevation. The oscillatory regime is most dynamic for the zone 2.5 - 5 m from the drain tile (Fig. 4.10). Closer to the drain tile, flow between B_{mix} and D_{mix} is upward for most of the time (Fig. 4.10). Nonetheless, both observations and simulations highlight the presence of a mixing zone below the drain tile. The calculated path lines show that this mixing zone groundwater results from mixing of rainwater with seepage at larger distance from the drain tile subsequently flowing towards the drain tile. Fig. 4.11b shows that within the rainwater lens (i.e., above B_{mix}) the maximum travel time towards the drain tiles is 3.5 years.

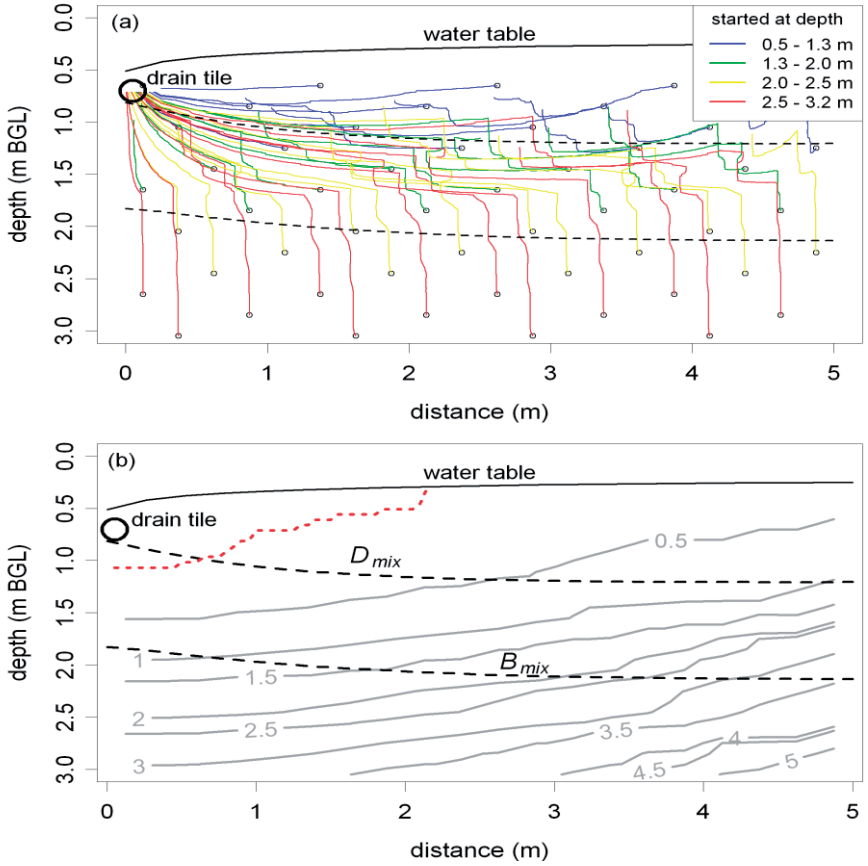

Fig.4.11: Cross sections showing (a) transient path lines started at 1 January 2009, at different locations in the cross section, (b) travel time to the drain tile (in years). The red dotted line delineates the bottom of the zone around the drain tile that contributed to a rainfall-driven drainage event with duration of 7 days (11 - 17 November 2010). The average positions of Dmix and Bmix for the modeled period 2009-2010 are indicated as dashed lines.

4.6.2 Soil water dynamics

Important mixing processes occur in the zone where the water table fluctuates and conditions alternate between saturated to unsaturated. For both sites A and B this zone extends from ground surface to 1.3 m BGL. When the water table falls, water with variable dissolved salt concentrations is retained as soil water, which will mix and become diluted with infiltrated rainwater when the soil saturates again. The temporary storage of salt in soil water has an important damping effect on groundwater salinity variations when the rainwater lens grows by the recharge by rainwater. For example, the average fillable porosity (Acharya et al., 2012) of the top soils of site B is ~0.07 (S in Fig. 4.3), while the average total porosity (i.e. the volumetric soil moisture content at saturation) is ~0.49. Consequently, infiltration of 1 mm of rainfall leads to the saturation of ~14 mm of soil. Assuming instantaneous mixing when the soil gets saturated, the salinity of this saturated part will then equate to 0.07 / 0.49 = 1/7 times the salinity of the infiltrated water plus 0.42 / 0.49 = 6/7 times the salinity of resident soil water. The salinity of the mixture will thus be close to that of the soil water before saturation since the resident soil water is diluted by only a small amount of infiltrated water. This shows that the salinity of groundwater recharge is controlled by mixing processes in the unsaturated zone, which is believed to be the explanation for the observed absence of truly fresh groundwater at site A and B (Figs. 4.4 and 4.5) and most other locations measured by De Louw et al. (2011).

The average salinity of soil water increases gradually with depth from low values near the land surface to the groundwater salinity at the water table, except at the monitoring points MP1-B, MP2-B and MP4-B at site B. At these locations the soil water at 0.55 and 0.70 m BGL were found to have higher salinities than the groundwater at 0.80 and 1.0 m BGL (Fig. 4.4). This is attributed to the co-existence of macro-pores (e.g. cracks) and small pores in the top soil, and the following mechanisms are thought to operate. Infiltration of rainwater occurs preferentially through the macro-pores, whereas capillary rise of water is strongest in the smallest pores. The smallest pores also can retain soil water against increasingly negative soil water potentials during summer. When the water table lowers, the concurrent loss of soil moisture due to drainage and evapotranspiration is, at least partially, compensated by capillary rise. At the same time, the salinity of the groundwater just below the water table becomes more saline as the water table fall 'decapitates' the lens and the vertical separation between the water table and the base of the rainwater lens becomes smaller. The salinity of the soil water in the small pores thereby increases with time during summer, as the water that rises by capillary effects becomes ever more saline. This effect is much smaller or even absent in the macro-pores. The high salinities in the small pores can persist during the infiltration events, as infiltration of rainwater occurs preferentially via the macro-pores, by-passing the soil aggregates in which the smaller pores reside. Pulses of relatively freshwater can recharge the rainwater lens in this way, while high salinities persist in the unsaturated zone.

4.6.3 Drainage dynamics

Under no conditions during the measurement period did the drain water consist solely of saline seepage water, which can be inferred from the fact that EC_{drain} never reached the EC of the seepage water of about 35 mS cm^{-1} for site B (Fig. 4.6). This can be explained by the presence of a mixing zone below the drain tile (Fig. 4.4; MP4-B and MP5-B) and the path lines in the rainwater lens (Fig. 4.11a) which indicate that groundwater flowing towards the drain tiles is mixed groundwater.

The seasonal timescale of variation of groundwater and soil water salinity contrasts starkly with the high-frequency dynamics of EC_{drain}, which responds almost instantaneously to individual rain events (Fig. 4.6). Cracks are thought to play an important role in this dynamic behaviour, facilitating the rapid infiltration of rainwater and responses of drain tile discharge and salinity to rainfall. Velstra et al. (2011) found similar fast responses and also allotted this to the existence of cracks in the clayey top soils. The dynamics of EC_{drain} (Fig. 4.6) indicate a fast mixing of infiltrated rainwater and mixing zone groundwater. Particle tracking analysis shows that path lines originating from different depths converge and mix in the drain tile (Fig. 4.11a). This is further illustrated in Fig. 4.11b in which the red dotted line the region delineates (based on particle tracking) that contributes to a rainfall-driven drainage event with duration of 7 days (11 - 17 November 2010). For this event about 80% of the discharged water came from above the drain tile level with a low salinity close to that of rainwater, and about 20% came from below the drain tile level with salinities representative of the mixing zone. The linear relation between the water table and drain water salinity (Fig. 4.7b) implies that a higher water table leads to a larger fraction of infiltrated rainwater and a smaller fraction of mixing zone groundwater in drain water. However, the measurements also showed that despite the lower fraction of saline groundwater in drain water, the absolute amount of saline groundwater drained increases with water table elevation (Fig. 4.7d). From this it is inferred that during a water table rise, an increase of the flow of saline groundwater from the mixing zone towards the drain tile is triggered, which is confirmed by the model results (not shown). Drain water will therefore never consist of solely rainwater which explains why EC_{drain} never fell below 2 mS cm^{-1} (Fig. 4.6).

4.7 Conclusions

In this study, the temporal dynamics of thin rainwater lenses and the mixing between rainwater and saline seepage were investigated using field measurements at two tile-drained agricultural fields in the south-western part of the Netherlands and numerical simulations for one of the sites. Upward saline seepage limits the size of the rainwater lens and the freshwater availability for agriculture purposes. The base and the centre of the mixing zone were found at a depth of 1.8 – 3.3 m BGL and 0.8 – 1.8 m BGL, respectively. For the first time, field-based evidence of rainwater lens dynamics was

systematically collected by monthly ground- and soil water sampling, in combination with daily observations of water table elevation, drain tile discharge and drain water salinity. These observations were reproduced by the numerical model. Based on the field data and numerical modelling of the key lens characteristics, a conceptual model of rainwater lens dynamics and mixing behaviour was presented of which the most important characteristics are summarized below.

The thickness of the rainwater lens varied up to 1.2 m due to water table fluctuations in response to individual recharge events. The position of the center of the mixing zone D_{mix} showed a much smaller change (< 0.25 m), and fluctuated at a much longer, seasonal time scale. The base of the rainwater lens stayed virtually at the same position. The small variations in the position of the mixing zone can be explained by the slow transient oscillatory flow regime in the deepest part of the rainwater lens. This oscillatory flow regime also controls the mixing between infiltrated rainwater and seepage water in a rainwater lens.

The flow and mixing processes are much faster near the water table, which fluctuates on a daily basis in response to recharge and evapotranspiration, and conditions alternate between saturated to unsaturated. When the water table falls, most of the water with variable dissolved salt concentrations is retained as soil water, which will mix and become diluted with only a small amount of infiltrated rainwater when the soil saturates again. The salinity of the mixture will thus be close to that of the soil water before saturation, which explains the observed absence of very fresh groundwater. Although the mixing processes are fast, the temporary storage of salt in soil water has an important damping effect on groundwater salinity variations when the rainwater lens grows due to the recharge by rainwater.

Salt migrates upwards into the root zone by capillary rise of the groundwater at the water table. As the water table falls during the summer, the water rising through the capillaries originates from deeper parts of the rainwater lens and is therefore more saline. Salinities of soil water can become significantly higher than in the groundwater due to the unsynchronized effects of capillary rise of saline water during dry periods and the flow of infiltrated rainwater during wet periods being restricted to cracks in the soil.

Preferential flow through cracks is thought to play an important role in the rapid response of the drain tile discharge to individual rain events. Groundwater of variable salinity, originating from different parts of the rainwater lens, as well as infiltrated rainwater, contributes to the drain tile discharge in proportions that vary on a timescale of hours to days, and this causes the dynamic behaviour of drain water salinity.

The small dimensions and dynamic behaviour of the rainwater lenses, especially the rapid removal of recharge through drain tiles and the loss of freshwater by

evapotranspiration, make them vulnerable to climate change. rainwater lenses may be expected to shrink due to evapotranspiration during drier summers, which are expected to become more frequent under future climate change (Van den Hurk et al., 2006), but the projected increase in winter precipitation may not compensate for the lens shrinkage because the tile-drainage system efficiently discharges the recharge. Alternative tile-drainage configurations that promote prolonged retention and storage of infiltrated freshwater in rainwater lenses could be a way to mitigate the potential adverse effects of future climate change. The optimal design of such configurations will be the subject of future research.

5 CATION EXCHANGE PROCESSES IN A DYNAMIC MIXING ZONE

Abstract

In coastal-zone fields with a high groundwater level and sufficient rainfall, fresh-water lenses are formed on top of saline or brackish groundwater. The fresh and the saline water meet at shallow depth, where a transition zone is found. This study investigates the mixing zone that is characterized by this salinity change, as well as by cation exchange processes, and which is forced by seepage and by rainfall which varies as a function of time. The processes are first investigated for a one-dimensional (1D) stream tube perpendicular to the interface concerning salt and major cation composition changes. The complex sequence of changes is explained with basic cation exchange theory. It is also possible to show that the sequence of changes is maintained when a two-dimensional field is considered where the upward saline seepage flows to drains. This illustrates that for cation exchange, the horizontal component (dominant for flow of water) has a small impact on the chemical changes in the vertical direction. The flow's horizontal orientation, parallel to the interface, leads to changes in concentration that are insignificant compared with those that are found perpendicular to the interface, and are accounted for in the 1D flow tube. Near the drains, differences with the 1D considerations are visible, especially in the longer term, exceeding 100 years. The simulations are compared with field data from the Netherlands which reveal similar patterns.

This chapter is based on: S. Eeman, P.G.B. de Louw and S.E.A.T.M. van der Zee. 2016. Cation exchange in a temporally fluctuating thin fresh-water lens on top of saline groundwater. Journal of Hydrogeology: p. 1-19.

5.1 Introduction

Deltas worldwide are areas in which fresh and saline water meet and mix. Because of the generally dense population in coastal areas, the availability and quality of fresh water is important for drinking water and agricultural production. This availability and the threats caused by salinization have received worldwide attention over the last few years, for example Alvarez *et al.* (2015) describe the main causes of salinization in coastal zones. The consequences of an increasing sea level and climate change for salinization of coastal zones has been investigated over the past years by Giambastani (2013), Langevin *et al.* (2013), Colombani *et al.* (2014), Feseker (2007) and De Louw *et al*. (2011, 2013) for deltas in Italy, Florida (USA), Argentina, Germany and The Netherlands respectively. Scott *et al.* (2015) investigated the development of shallow brackish water in Bangladesh. Lenses, formed by infiltrating rainwater 'floating' on saline groundwater, are often a major source of fresh water. The fresh-water lenses, sometimes called Badon Ghijben-Herzberg (BGH) lenses (Badon Ghijben, 1889; Herzberg, 1901) after the first investigators of these fresh water bodies, are formed by rainwater in areas that are somewhat elevated with respect to mean sea level (MSL), and have an annual precipitation surplus. These lenses are found on (barrier) islands (e.g. Underwood *et al.*, 1992), and in dune areas (e.g. Stuyfzand, 1993; Vandenbohede *et al.*, 2008; Röper *et al.*, 2012). In low-lying areas, with a soil surface close to mean sea level (MSL), thin lenses are found, on top of upward seeping saline groundwater (Maas, 2007; Eeman *et al.*, 2011; De Louw *et al.*, 2011). Also in the absence of saline groundwater, lenses can be formed on deeper, upwelling groundwater and differ from that groundwater by its chemical signature, in a way that can be ecologically relevant (Cirkel *et al.*, 2014).

These thin lenses, referred to as fresh or rainwater (RW) lenses, are studied because of their vulnerability during expected future droughts. Sensitivity (Eeman *et al.*, 2011), occurrence and spatial variability (De Louw *et al.*, 2011) and response to recharge variations, including delay and damping, have been investigated in detail (Eeman *et al.*, 2012). Geological and topographical variations have been shown to have a major impact on the thickness of RW lenses (De Louw *et al*., 2011).

In Chapter 4 we studied the dynamics and related mixing in two agricultural fields in Zeeland, The Netherlands, and these sites are studied in this chapter as well. The rainwater lens is defined in the same way as in Chapter 4, p. 57 and Fig. 4.1 which implies that rainwater lenses generally do not contain truly fresh water. They range from brackish (mostly 0-2 g Cl/l, but in some cases up to 8 g Cl/l) at the groundwater level (GWL), to saline (> 10 g Cl/l) at a depth of 2-4 m.

The ion exchange associated with this dynamic mixing process affects the hydrochemistry that determines the water quality in the root zone as well as the drain water composition. European regulations, such as the EU Water Framework Directive,

and the vulnerability of deltaic systems in view of climate change demand a better understanding of chemical processes in RW lenses (Bates *et al.*, 2008).

Although the authors are not aware of any published studies on hydrochemical processes in thin RW lenses in areas with saline seepage, hydrochemical processes have been studied in thick BGH lenses because of their influence on drinking water quality. Stuyfzand (1993) investigated the hydrochemistry of dune and adjacent areas, where mixing of saline and fresh water is an ongoing, although slow process. He found that hydrochemical processes in mixing zones are in a transient state, even where groundwater flow is relatively stable, due to the slow kinetics of dissolution and precipitation processes. Marconi *et al.* (2011) and Mollema *et al.* (2013) showed for small coastal wetlands and forests in the Po delta and the Ravenna area, respectively, both in Italy, that the hydrochemical conditions are different. Both used the Base Exchange index (BEX index) of Stuyfzand (2008) to characterize the water types found, and concluded that the combination of land use, climate and sea level rise is causing salinization in the aquifers in this area. Mollema *et al.* (2011) point out the influence of seepage of hypersaline water on coastal fresh water systems caused by artificial drainage of agricultural land.

Hydrochemical conditions in RW lenses differ from those in a BGH lens, where mixing occurs at a much larger depth, often with anoxic conditions and relatively steady situations. RW lenses, on the contrary, are much more affected by oxic rainwater that mixes with anoxic seepage water. They are also a much smaller size than BGH lenses in horizontal (10s of meters instead of 100s of meters) and vertical (less than a few meters instead of 10s-100s of meters) planes, causing travel times of less than 5 years (De Louw *et al.*, 2013) instead of decades to centuries (Stuyfzand, 1993; Vaeret *et al.*, 2011; Oude Essink,1996).

Foppen *et al.* (1995) stressed that the role of drains in hydrochemical processes needs elucidation. A clear demonstration of the importance of RW-lenses on the local hydrogeochemistry of regions with upward groundwater seepage is given by Cirkel *et al.* (2014). They show the resilience to eutrophication by fresh groundwater, saturated by calcite and rich in sulphate, due to the precipitation of pyrite and calcite invoked by processes in the organic matter rich top soil. In another study, Cirkel *et al.* (2015) simulated the movement and shape of oscillating solute fronts with a significant change in concentration, taking into account exchange of Na^+ and Ca^{2+}. They found that the transition zone thickness is unaffected by the ion-exchange process, but the concentrations of individual cations change profoundly within the zone, influenced by the phase of oscillation. Hence, such patterns may also be expected in case of fresh-salt gradients. Many other studies focus on exchange processes (e.g. Bolt *et al.,* 1976), however, these studies concern steady flow situations.

The objective of this study is to investigate the dominant hydrochemical process (ion exchange) as affected by mixing and fluctuations of rainwater infiltration and upward saline seepage. Such situations abound in practice in coastal regions (with fresh/salt gradients), but are similar with those in brook valleys (with different chemical signatures of shallow and deeper groundwater) and even with drinking water well extraction/injection cycles. For lenses, the gradients as affected by mixing, fluctuating flow directions and exchange, are ecologically and agronomically important. Because a preliminary analysis of field data revealed spatiotemporal complexity, this study focused on a simplified one dimensional vertical situation, to begin with: the development of the fluctuating transition zone in the solution and the soil adsorption complex where seepage and infiltration water meet. The main ions, Na^+, Ca^{2+}, Mg^{2+} and K^+ are considered, which is an extension of the work by Cirkel *et al.* (2015). This extension is not trivial, because consideration of more cations leads to much more combinations of initial and boundary conditions that affect the mixing zone. Using the insights obtained with this first model assessment, a more complicated two dimensional flow pattern was analyzed, using parameters typical for a site in Zeeland in the Netherlands. Theory based on geochemistry and numerical transport modeling was in this way applied to the chemically complex, cyclic situation of a 2D tile drained field.

5.2 Field work campaign

The geography and hydrology of the two field sites (Fig. 4.2 c and d) have been elaborated in Chapter 4 (p. 59-61). At sites A and B (Fig. 4.2c and d), 14 and 11 sampling locations were selected, respectively, in March and May 2009. These were chosen based on the expected differences between locations near and in between drains and ditches and illustrated as MP (measurement point) in Figure 4.2c and d at different depths between 1 and 4 m (Fig 4.2b). In the field, O_2, temperature, pH, EC and alkalinity were measured directly. Cation-samples were collected and analyzed in the lab. Concentration measurements were done using Ion Chromatography (SO_4^{2-}) and ICP-AES (Na^+, K^+, Ca^{2+}, Mg^{2+}). In this study, we used only a limited number of the measurements, from the dominating cations Na^+, K^+, Ca^{2+}, Mg^{2+} and the pH and SO_4^{2-}, for the sampling sites and depths that can be related to the drainage profile described in the previous section. For site A, results of MP 1,4 and 6 were used and for site B for MP 2,3,4 and 5.

Table 1: Composition of Water use for input, based on field measurements and equilibrium calculations.

	Unsaturated zone water	Seepage water A	Seepage water B		Unsaturated zone water	Seepage water A	Seepage water B
Species	mmol/kgw	mmol/kgw	mmol/kgw	**Species**	mmol/kgw	mmol/kgw	mmol/kgw
Na	3.4	319.9	270.5	**SO4**	0	10.3	7.5
K	0.26	6.9	4.7	**CO2**	1.6	2.3	0.96
Ca	3.4	18.1	15.2				
Mg	1.8	21.1	30.6	**pH**	7.0	6.7	7.1

Cl	7.9	375.4	344.5	**pe**	14.8	14.6	14.7

The data in Table 5.1 reveal a significant difference in salinity between the locations. Dilution due to mixing with rain or river water as the sediment formed causes site A to have a concentration of approximately two thirds of seawater salinity, whereas at site B this is only half. This mixing with other water sources can also explain the relative abundance of magnesium in the soil at site B.

In June 2009, soil samples were taken at both sites at depths of 55, 95, 135, 165 and 195 cm at MP 3 and 4 at site A (Fig 4.2c) and MP 3 and 5 at site B (Fig 4.2d).Cores were analyzed in the lab according to Tan (1996). The concentration of exchangeable cations (Na^+, K^+, Ca^{2+}, Mg^{2+}) and effective CEC (cmol+/kg) were determined by ion displacement using an adapted version of the unbuffered compulsive exchange procedure, as proposed by Gillman (1979). ICP-AES was used to measure concentrations of the exchangeable ions. Results were corrected for the presence of excess salts in the examined cores.

5.3 Theory and methods

In this chapter, we present the used flow and transport models, describe the input for the hydrochemical model, and introduce the theoretical concept used to interpret model results.

5.3.1 Flow and transport models

To understand and visualize the flow patterns and exchange processes in the studied fields, the data gathered in the field were used as the basis to construct two hydrochemical flow and transport models. The PHT3D software package (Prommer *et al*., 2010) is used to combine the possibilities of flow and transport from MODFLOW and MT3D (Zheng *et al.*, 1999), with the calculation of the chemical processes by PHREEQC2. For a 1D column, exchange and how this is influenced by alternating flow direction and input of recharge from the top and seepage from the bottom is visualized. With a 2D model we represent the study site B, where flow towards drains and constant upward seepage of saline water creates different mixing patterns and associated cation exchange processes (Chapter 2) compared to the 1D column. Although there is a difference in the density of the unsaturated zone water and the seepage water, this has been neglected in the models, since it was shown in Chapter 4.2 (p.60) and by Post *et al.* (2007) that the studied field systems are controlled by head gradients and geology, hence buoyancy effects are not significant.

1D column basic model

1D vertical column MODFLOW model was made, consisting of 41 square cells with sides of 0.1 m (Figure 5.1), resembling the flow-tube concept used by PhreeqC2. All side boundaries were no-flow and no-solute flux boundaries. Inflow and outflow, due to alternating flow directions, were limited to the top (recharge) and bottom (seepage) boundaries. Inflow from the top results in an equal amount of outflow at the bottom and vice versa. The column remains completely filled with water at all times, and effective porosity was set to 35%. Apart from porosity, hydrogeological parameters do not influence this artificial model, since water is forced by the flux conditions at top and bottom boundaries . This column does not represent a particular site, and its aim is to illustrate the effect of fluctuations on a fresh-saline front in a basic way. The flow was calculated using stress periods of one day and transport and chemistry time steps were one hour.

Figure 5.1: 1D column model of 4.1 m long, consisting of 41 cells of 0.1 m, to investigate basic exchange processes under conditions of alternating flow direction.

For an initially saline column, filled with seepage water, three different alternating flow patterns were applied to investigate both the influence of the average flux and variations around the average. The patterns, shown in Figure 5.2 for a period of two years, are repeated to calculate the processes in the column for 300 years. This long period is needed since ion exchange progresses very slowly compared to flow and transport. The water compositions of seepage and recharge water are based on observations from study site B and A respectively and elaborated in the next section.

Figure 5.2: Flux patterns used in the column simulations. Positive values relate to downward flow.

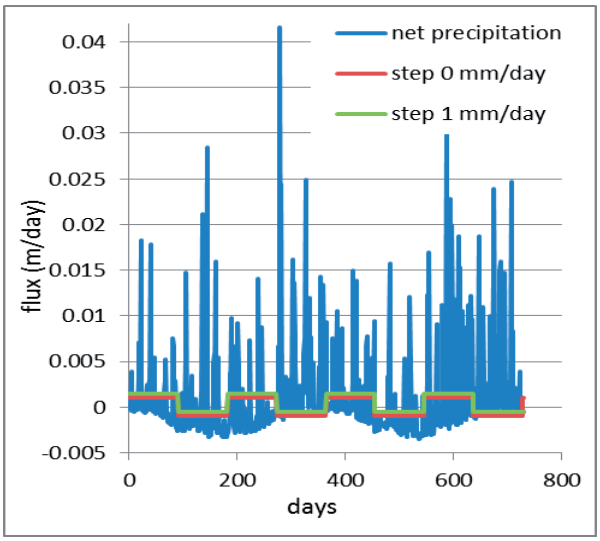

The first simulation, (red line in Figure 5.2), applied an average zero flux and a step-wise change of flow direction of 1 mm/day downward (recharge, implying outflow of saline water at the bottom) and 1 mm/day upward (seepage, leading to outflow of relatively fresh water at the top). Alternation of flow direction occurred every 3 months. The mixing in this simulation resembles the process in the center of the mixing zone, Chapter 4. The second simulation (green line in Figure 4) was similar, only the average flux is 1 mm/day downward, comparable to the mixing in the top of the mixing zone in Chapter 4. We used again a step-wise 3-monthly change of flow direction of 1.5 mm/day downward and 0.5 mm/day upward. The third simulation used the daily precipitation measured at field site B, combined with Makkink evaporation data from the nearest KNMI weather station, also on a daily basis (Wilheminadorp, 17 km away). The average flux of these data is 1 mm/d downward, equal to the second step-model. The amount of evaporation in this case equals the amount of seepage water coming from the bottom. The blue line in Figure 5.2 shows the variation around this average.

2D field model of profile between drains

The two dimensional model of site B is linked to the 1D model, and an extension from the model presented in Chapter 4. Soil hydraulic properties for this model are illustrated by Figure 4.3. Spatial domain and discretization as well as geohydrological conditions and boundary conditions were elaborated in Chapter 4. Total porosity at the site was measured at 49%, effective porosity was estimated at 25%, in line with findings of Stephens et al. (1998). Vertical upward seepage into the model is calculated based on field measurements, at a value of 0.29 mm/day. Recharge and evaporation used are the same as described for the third simulation of the 1D model: field measurements combined with KNMI data from Wilhelminadorp. Recharge and the specific yield relation were applied as described in Chapter 4.

5.3.2 Hydrochemistry models

The water quality in the rainwater lenses at site B is evaluated by combining field data and lab measurements with the flow and transport models, using the hydrochemical package PHREEQC2 (Parkhurst *et al.,* 1999).

The data from site B are the most valuable, due to the setup of the measurements above and between drains, the larger number of data at these MPs, and the calibration of the transport model based on drain data (Chapter 4). Although the 1D simulation is a generic one rather than a site specific representation, the hydrochemical data from site B were adopted for the seepage water. In the 2D field model of site B, this composition was used as well.

Initially, all models are filled with saline seepage water. The initial composition of the cation exchange complex in the models was calculated with PHREEQC2, using the

composition of the seepage water based on averages of the different MPs on both sites and representative CEC values for the upper 2 m of the profiles were used. The small amount of available soil data, 2 locations per site, did not justify more detail. The CEC was on average much larger for site A (0.5 eq/l) than for site B (0.13 eq/l), which is explained by the substantial amount of peat in the subsoil of site A (a layer of approximately 0.7 m thick, see Figure 4.2c). The upward seeping water entering the model at the bottom equals the seepage water quality that initially fills the model.

The water entering the model at the top is similar to rainwater, but enriched in Ca^{2+} while passing the unsaturated zone, according to the unsaturated water sample from site A. The reason that we used a sample from site A here is that no suitable sample of unsaturated zone water was available at site B. The unsaturated zone water in the calculations was assumed to be equilibrated with CO_2 and calcite, to determine the composition of the input recharge water in the model. CO_2 pressure was determined using the average partial pressure of the 5 samples that were taken on site A, according to Henry's law (NIST, 2015). Results for the three water types used as input for the models are in Table 5.1.

Significant chemical precipitation is very unlikely to occur in view of the very small (<1) saturation indices (SI) of the unsaturated zone and seepage water at both sites for Calcite and Dolomite. For all other minerals, the SI was negative. To rule out errors due to the impact of chemical precipitation, this was tested in preliminary simulations. We saw no significant impact on model outcomes and therefore and chemical precipitation has not been accounted for. If dissolution or precipitation occurs, this is likely to be a non-equilibrium process (particularly for dissolution). This will affect the concentrations of the cations. However, it modifies but does not in essence change the processes. Another important aspect, the effect of DOC/SOM mediated redox processes was not accounted for. This does not imply that we consider this an insignificant process. However, DOC-facilitated transport may affect the solute balances, but not the impact of cation exchange as a predominant mechanism in the root zone.

5.3.3 Analysis of the simulations

To describe exchange processes, we use the Gaines-Thomas equation, which is available in PHREEQC2, and for Na^+ and Ca^{2+} is given by

$$\frac{\sqrt{[Ca^{2+}]}}{[Na^+]} = K_{GT}\frac{\sqrt{[Ca{-}X_2]}}{[Na{-}X]} \qquad (5.1)$$

where X stands for surface site. To interpret the outcomes of the hydrogeochemical models, we make the system dimensionless as was proposed by Cirkel *et al.* (2015), using C for the total concentration of cations in solution , f for the fraction of dissolved species i with concentration c_i and N for the fraction of the cation exchange complex occupied by adsorbed species i

$$C = \sum_i c_i \quad ; \quad f = \frac{c_i}{C} \quad ; \quad N = \frac{i_{adsorbed}}{CEC} \qquad 5.2$$

To investigate the modelled and observed changes in soil water and exchange complex due to varying lens thickness, we consider the one dimensional oscillation, as recently investigated by Cirkel *et al.* (2015), comparing relative normalized amounts of Ca^{2+} in solution (f) and on the complex (N). As explained in the transport section, initial conditions are saline. The Ca^{2+} enriched rainwater that reaches the groundwater (Table 5.1) is often found in coastal zones, due to the marine history of the sediment (Appelo *et al.*, 2005). As this Ca^{2+} enriched water enters the flow domain, two changes occur: (1) the salinity decreases and (2) the fraction f_{Ca} in solution increases. We describe only the results for the three main cations, Ca^{2+}, Mg^{2+}, and Na^{+}, and after preliminary calculations decided to ignore K^{+} in view of its tenfold smaller concentrations (Table 5.1) and accordingly small impact. In the total concentration C, however, K^{+} is included.

5.4 Results

5.4.1 Transport in a 1D-column with time varying boundaries

To understand the results obtained for the column simulations, we first present our concept and illustrate it in Figure 5.3. Due to the decrease of salinity, the preference of the cation exchange complex for Ca^{2+} increases (Bolt *et al.*, 1976; their Figure 7.5) and some of the dissolved Ca^{2+} adsorbs, whereas some Na^{+} desorbs. The increase of $f_{Ca^{2+}}$ also causes Ca^{2+} to adsorb. The net effect is therefore that it may depend sensitively on the quantity of incoming Ca^{2+} and on the quantity that is exchanged with Na^{+} due to the two changes in the solution (different cationic ratios and different salinity), whether the net effect is an increase or a decrease of $f_{Ca^{2+}}$. However, in either case, the fraction $N_{Ca^{2+}}$ of Ca^{2+} on the complex increases. Next, as the fresh/salt interface oscillates, the original saline solution displaces the fresh water that infiltrated, causing some re-adsorption of Na^{+} but also removing in this process some of the desorbed Na^{+} from the soil at the top of the flow domain. If we consider a full oscillation, some Na^{+} will be removed and some Ca^{2+} will have entered the flow domain, and particularly at shallow depths, the salinity will decrease somewhat. In Figure 5.3b, that schematically depicts the trajectory of Ca^{2+} changes, the impact of changing salinity and cationic composition are illustrated.

As fresh water enters at the top, the changes are largest there (red line). However, due to dispersion, and particularly if the net downward flux is positive, these changes will propagate downwards (green line). Gradually, the fraction of Ca^{2+} in the solution and at the cation exchange complex will increase and to which level this occurs depends on the salinity profile that will develop between the fresh incoming and saline initially present pore water.

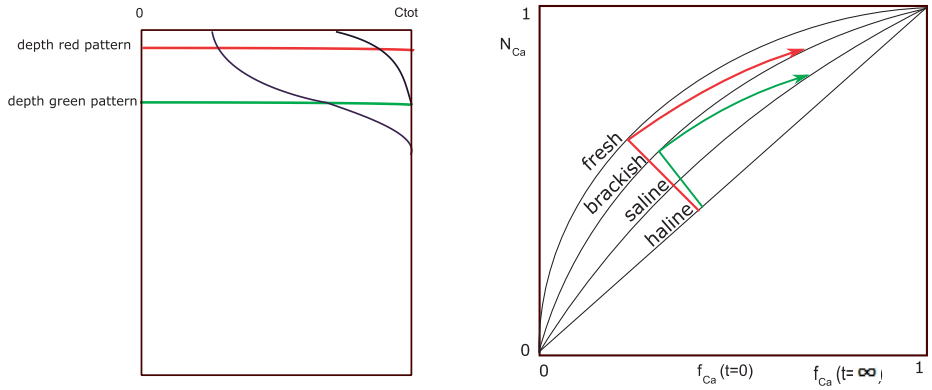

Figure 5.3: a) (left) showing a vertical profile with 2 observation depths and b) (right) showing the corresponding relation between N' and f' as both waters start mixing due to an alternating flow direction.

Situation 1: Alternating flow, no net flux

Figure 5.4a illustrates the development of dimensionless adsorbed (N) as a function of dissolved (f) fractions of divalent Ca^{2+}, Mg^{2+} and Na^{+}, for the simulated regular alternation (every three months) of flow direction (1mm/day), without net displacement of water. The initial saline situation is indicated by the black circle. Different colors correspond with different depths. Figure 5.5a shows the relation between the dissolved fractions f and the total concentration in the water, C, for the same simulation.

The complex, depth dependent pattern of Figure 5.4a can be interpreted on the basis of sequential processes. For the top of the domain (zero depth), the major short term impact of incoming water is that the total salt concentration decreases, increasing the preference of the adsorption complex for divalent Ca^{2+} and Mg^{2+} at the expense of monovalent Na^{+}. Both divalent cations therefore adsorb and their f-values decrease. Because the distribution ratio (amount of cations at the complex divided by their amount in solution, is large ($\frac{CEC}{C}$ = 16.5 in this model) , the change in N-values is small compared with the change of f -values. Na^{+} on the other hand, initially shows an increase in f, as it is exchanged due to the preferentially adsorbing divalent cations. As the infiltrating fresh water reaches only a limited depth, and due to dispersion, the decrease of salinity is smaller for larger depths. This is recognizable in the smaller short term impact at larger depths. After a relatively small number of oscillations, the fluctuation of the total salt concentration stabilizes, though at a different level for each depth.

On the longer term, another process becomes important and that is the cation exchange, caused by the different f -values of initially present and incoming fresh water. As Table 5.1 and Figure 5.4 reveal, Ca^{2+} is far more abundant in the incoming fresh water than Na, and also more abundant than Mg. Accordingly, the f -value of

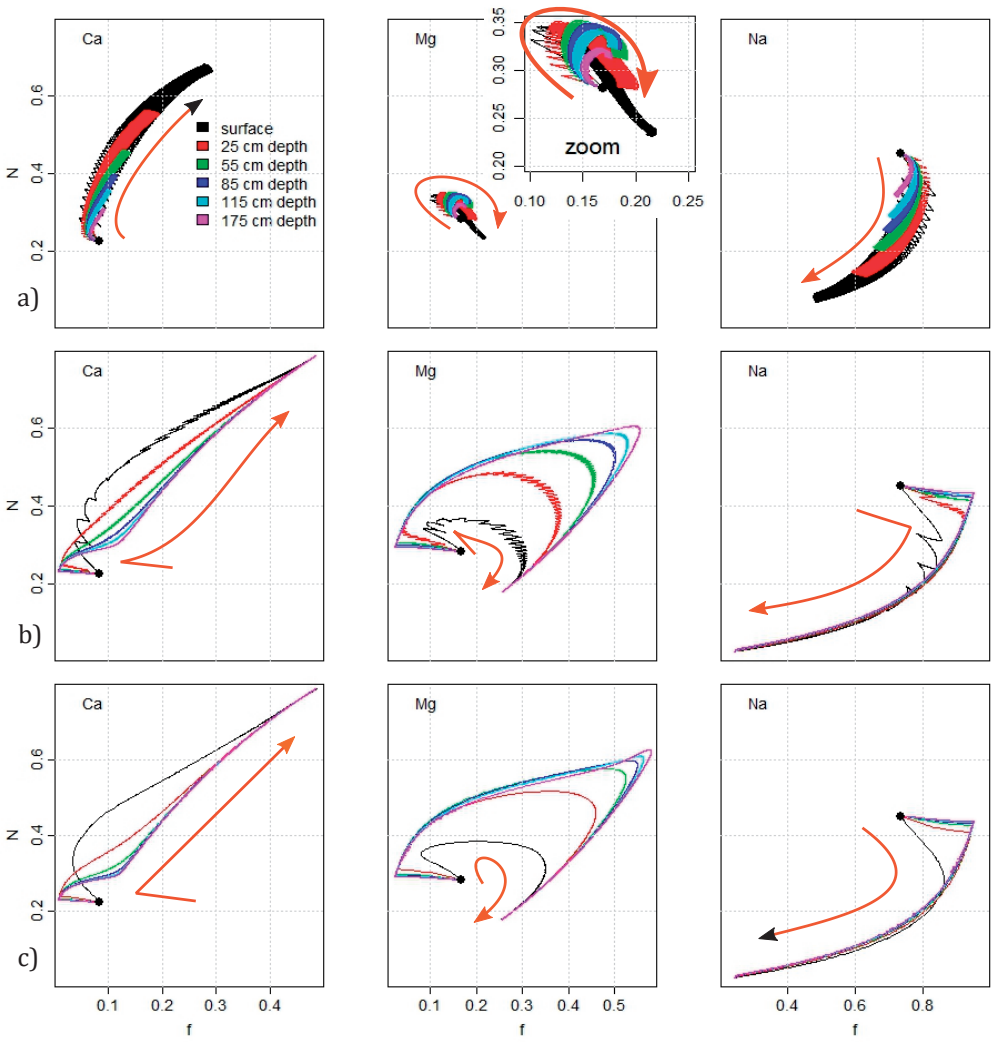

Figure 5.4: Adsorbed (N) vs. dissolved fractions (f) of Ca^{2+}, Mg^{2+}, and Na^{+} at different depths, for a simulation of 300 years. Arrows illustrate the overall direction of change as a function of time. Top: a) Step-wise change of flow direction every 3 months (average 0 mm/day), Middle: b) Step-wise change of flow direction every 3 months (average 1 mm/day downward). Bottom: c) Flow direction determined by actual net precipitation/evaporation simulation (average net precipitation 1 mm/day), where the amount of evaporation equals the amount of seepage entering from the bottom.

Ca^{2+} starts to grow, and Ca^{2+} adsorbs, predominantly at the expense of Na. This is also the case for Mg^{2+}, that likewise exchanges with Na^{+} at the complex, but to a lesser degree than Ca^{2+}. At the long term, when Na^{+} has been by and large expelled from the exchange complex, Ca^{2+} starts to outcompete also Mg^{2+}, and the N -value of Mg^{2+} declines again. As is apparent from Figure 5.4 for Mg, the maximum N -value attained increases with increasing depth. This is partly the result of passing Mg^{2+} that is desorbed higher in the soil profile, and partly due to the complex interplay of changing concentrations of Ca^{2+}, Mg^{2}, Na^{+}, and total salinity.

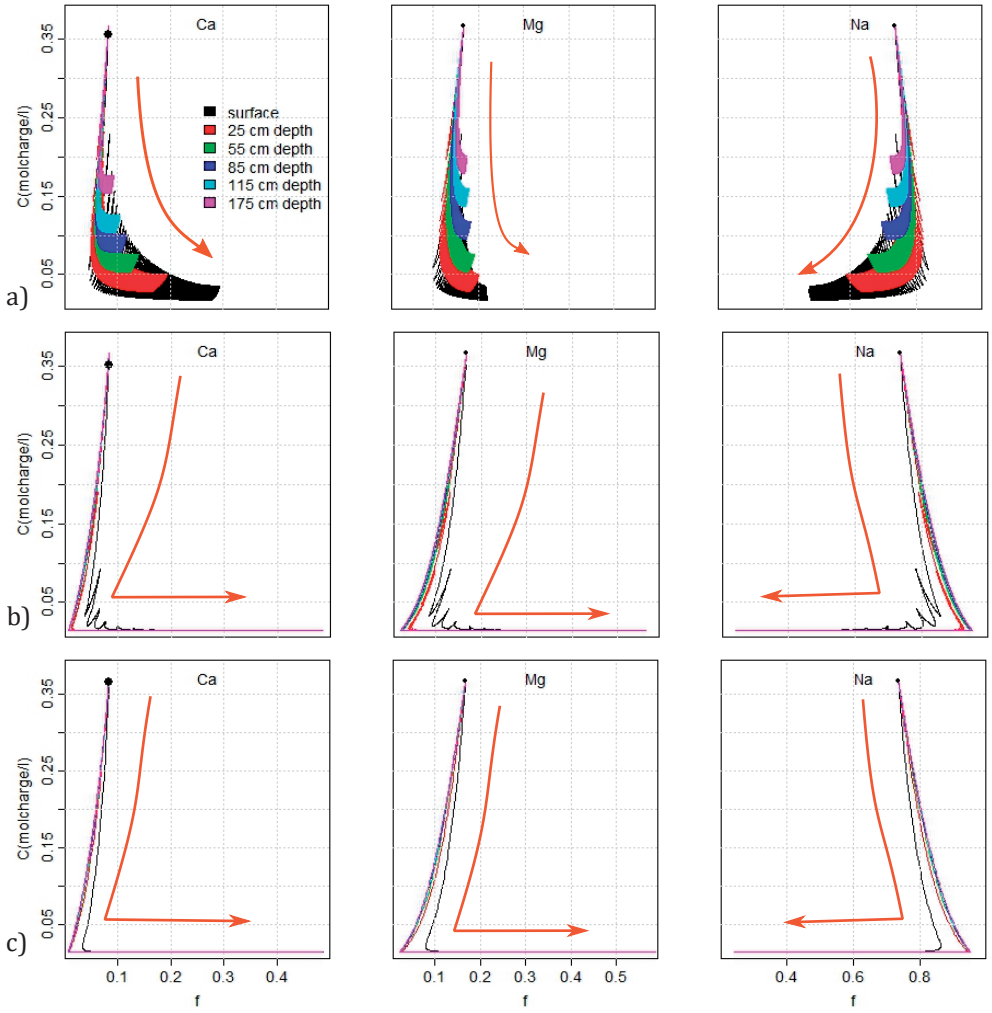

Figure 5.5: Fractions f of dissolved Ca^{2+} (left), Mg^{2+} (middle and Na^{+} (right) versus the total amount of dissolved salts at different depths, for a simulations of 300 years. Top: a) Step-wise change of flow direction every 3 months (average 0 mm/day), Middle: b) Step-wise change of flow direction every 3 months (average 1 mm/day), the sharp angle is reached after approximately 10 years, depending on depth. Bottom: c) Actual net precipitation simulation (average 1 mm/day), the sharp angle is reached after approximately 5 years, depending on depth.

Figure 5.5a is in agreement with the above interpretation: on the short term (related with the half cycle of 3 months), f -values decrease and increase sequentially, due to varying salinity, where the salinity variation is depth dependent. As divalent cations in soil build up their mass, which is possible due to the nonlinearity of the cation exchange, the f -values of Ca^{2+} and Mg^{2+} increase and that of Na^{+} decreases. But this happens strongly retarded in time, due to the large distribution ratio. Figure 5.6a more clearly shows that the composition of the complex N shifts from Na^{+} towards Ca^{2+}, while Mg^{2+} increases only slightly. The changes at larger depth are almost negligible.

Situations 2 and 3: Alternating flow with net downward flux

Figures 5.4b and c again illustrate the development of divalent Ca^{2+} and Mg^{2+}. The net water displacement is 1 mm/day based on the regular pattern of alternating flow every 3 months (situation 2) or on alternation triggered by meteorological data (situation 3), as described in the methods section.

Although the processes for situation 1 (Figures 4-6, a) are similar to situation 2 and 3 (Figures 4-6, b and c), the differences are striking: the saw-tooth pattern is far less distinct in case of a net water displacement and the changes occur over a different range of f and N values. This illustrates the importance of net water displacement, which clearly dominates over the changing flow direction that occurs on the timescale of months.

For Figures 5.4b and c, the major short term impact is still determined by the decrease in total concentration due to the incoming water. Na^+ initially increases in the solution (f) since the changing isotherm causes Na^+ to be pushed of the complex by Ca^+ and Mg^+. The large decrease in f of Ca^+ and Mg^+ compared to a much smaller decrease of N for Na^+ due the large distribution ratio is visible as well. However, in this case this effect is significant to a depth of 1.5 m, since the infiltration reaches progressively deeper due to the net water displacement in the downward direction.

On the longer term, the oscillations in f are absent, because the salinity at the top of the domain never reaches the initial situation again, a direct consequence of the net downward flux. Compared to the zero net displacement simulation, Figures 5.4b and c show a rather smooth development of the exchange process between monovalent Na^+ and divalent Mg^{2+} and Ca^{2+}. The initial differences in the N - f trajectory for the considered depths disappear and the patterns converge to the same one, with a delay related to depth. The interplay of concentrations is slightly different for the regular oscillation (Fig. 5.4b) and the natural precipitation simulations (Fig. 5.4c). Changes in N occur faster at larger depths for the precipitation model, and the maximum concentration of Mg^{2+} increases sharper with depth when compared to the regular model. This can be explained by the shorter periods of upward flow, that cause less reversal of the exchange process compared to the 3-monthly alternating flow direction, causing also a difference in the balance between the 3 main cations.

Figure 5.5b and c confirm the interpretation of Figure 5.4. Total concentration C drops quickly for both simulations, due to the incoming fresh water and does not visibly increase again. However, relative concentrations of Ca^{2+} and Mg^{2+} develop much slower, continuously increasing for Ca^{2+} and decreasing again after a maximum for Mg^{2+}. The larger velocity of exchange with depth for the natural precipitation simulation is shown by the left panels of Figure 5.5b and c, where the lines showing the deeper positions are more developed in the bottom (precipitation) than in the middle (regular) panel. Just as Figure 5.4, Figure 5.5 shows a much smoother development of N, f and C for more realistic flow patterns (given the recharge-

seepage situation in the field) compared to the artificial zero-displacement simulation. This difference is not so explicit in Figure 5.6b and c. The temporal dominance of Mg^{2+} with increasing depth is illustrated clearly for the complex. Due to the exchange of Ca^{2+} higher in the column, less is available at larger depth, causing more Mg^{2+} to exchange with Na^{+}.

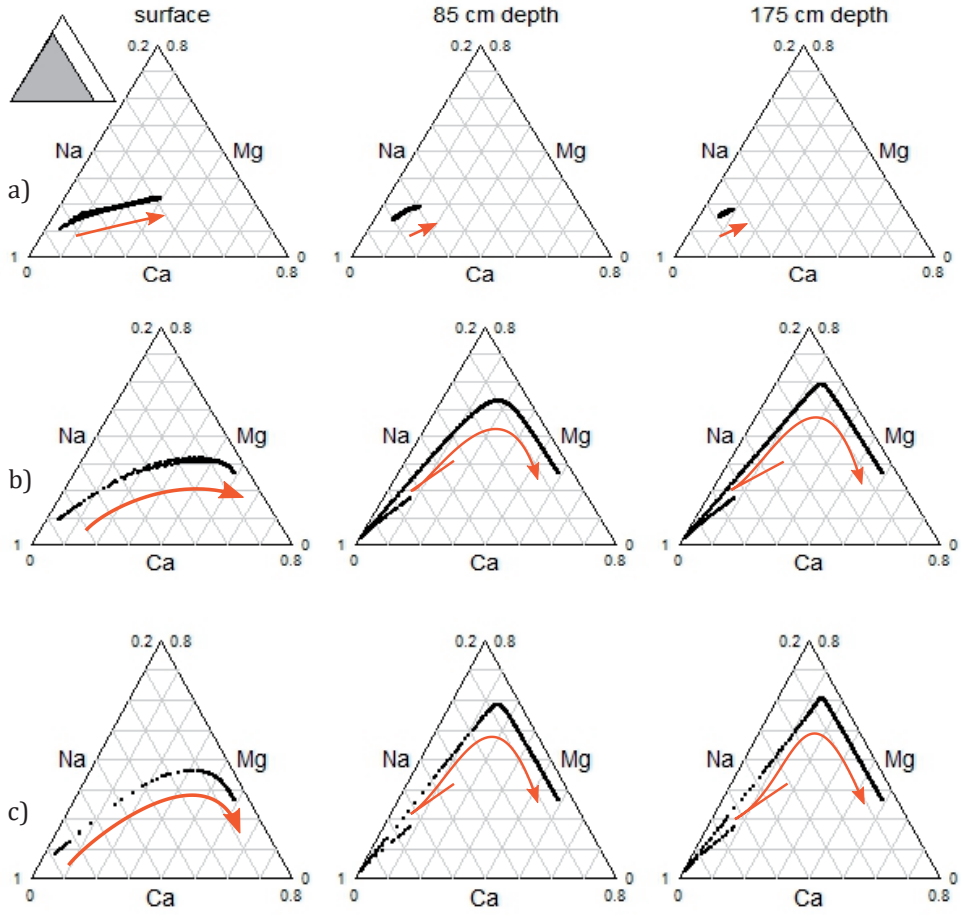

Figure 5.6: Triangle plot showing the dissolved fractions (summing to 1, ignoring K^{+}) for the three simulations. a) Top: Step-wise change of flow direction every 3 months (average 0 mm/day). b) Middle: Step-wise change of flow direction every 3 months (average 1 mm/day). c) Bottom: Actual net precipitation simulation (average 1 mm/day). Composition in the top layer (left), at 1 m depth (middle) and at 2 m depth (right)

Movement of the front

In Figure 5.7 the movement of the total concentration front is shown for the three simulations. Figure 5.7a shows solid lines for the front position in situation 1 after 3 months of downward flow, and dashed lines for the position of the front after 3 months of upward flow. Sets of solid/dashed lines are shown after each 5 years interval. After 50 years, the lines approach their equilibrium position with a broad mixing zone that covers the entire considered domain. This is in line with the smooth development in Figures 5.4 and 5.5a. Figures 5.7b and c, situation 2 and 3 respectively, show that the net downward flux causes a fast downward progression of the front. In both figures, solid lines are drawn for each year, showing that for the regular oscillation simulation (middle) the domain (until 4 m depth) is almost completely filled with fresh water after 10 years. For natural precipitation, this is even faster the case, already after 5 years. This is also visible in Figures 5.4 and 5.5b and c, where the sharp angles show that decrease in C ends as the fronts have passed.

For all cases, Figure 5.7 confirms that the short term impact of the oscillating front both with and without net downward flux can be attributed to the movement of this front, whereas the long-term impact occurs after the front has reached its steady state position in situation 1, or has passed in situation 2 and 3. Figure 5.7b and c show that natural precipitation (bottom) causes faster flushing than the regular model with average downward flux of 1 mm/day (middle), in line with the interpretation of figures 5.4 and 5.5. The middle panel also shows that the bottom will not completely freshen in the regular case with a three-months alternation. A zone of approximately 15 cm at the lower boundary is refilled with seepage water each cycle (0.5 mm/day, 35% porosity, 91 days) and is therefore a consequence of putting the boundary at -4 m.

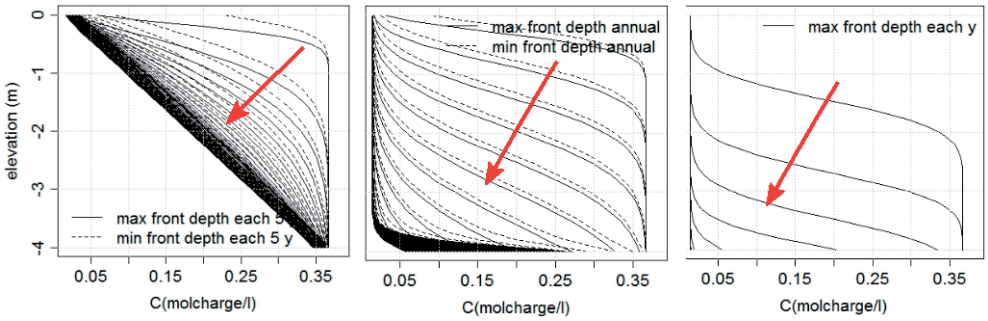

Figure 5.7: a) left: Front movement for the simulation with 0 mm average. The solid lines, approaching the lower limiting straight line, show the development of the front developing each 5 years, for 3 months of upward and downward flux. The dotted lines, approaching the upper limit of the black diagonal bar show the upper limit front that develops after ca. 50 years, the lower end of this bar are the limit after 3 months of downward flow. b) middle: Front movement for the 1 mm downward average step simulation. The solid lines show the annual progress of the front. c) right: Front movement for the 1 mm downward average precipitation/evaporation simulation. The solid lines again show the annual front progress.

5.4.2 *Transport and exchange in a drained field model*

Whereas the one-dimensional simulations give an impression of the complexity of the geochemical interactions, they also neglect a crucial aspect: the dimensionality of flow in real situations. Since strictly vertical flow may be a good approximation halfway two drains, closer to the drains the water movement may be dominated by horizontal flow (Chapter 2). Therefore, in this section we investigate whether this affects the transport.

Exchange process

Figures 5.8-5.10 illustrate the results for the 2-dimensional field cross section. The results for the middle of the field (the 'hydrological divide' HD) and half way that position and the drain are very similar, and therefore only the midfield position is shown. The explanation for these similar results is found in the shape of the mixing zone between fresh and salt water, which is almost horizontal, apart from the 2 m nearest to the drain. There is a significant difference between the horizontal flow components at the HD, where it is almost zero, and halfway between the drain and the HD, where the horizontal flow component dominates. The reason that the horizontal flow component has a limited impact on the composition of the mixing zone compared with the one-dimensional cases is that this incoming water has more or less the same composition as the water that it pushes away sideward. For the vertical flow component, this is not the case, as higher and lower water is fresher and more saline, respectively. Near the drain, the gradient of the mixing zone increases, and flow lines are forced to converge (see also Chapter 2), leading to increased mixing of water types, less freshening and a slower progress of the exchange between Na^{+}, Ca^{2+}, and Mg^{2+}.

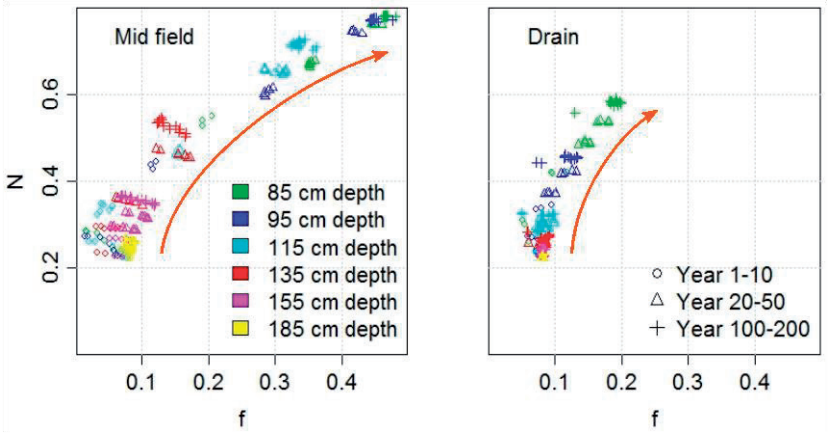

Figure 5.8: Site B: Development of the ratio of dissolved vs adsorbed Ca2+ for different depths over time. The left figure shows the situation in the middle of the field, being the middle of Figure 4.3, The right figure shows the situation next to the drain (at 70 cm depth), near the right boundary of Figure 4.3. Points are drawn each 10 days, to include variation within years. The clay layer starting at 170 cm depth forms a boundary, below which little fresh water is found, shown by the very small changes at 185 cm depth after 200 years.

For Ca^{2+}, the exchange over time and depth are visualized from 85 to 185 cm in Figure 5.8. The drain is at 70 cm depth and the clay layer with low permeability (1mm/d) starts at 170 cm depth (Figure 4.3). Above the drain, the profile is mostly water-unsaturated, which leads to inactive cells in the model, for which the chemical balance is not calculated. The top of the relatively impermeable clay layer is a geohydrological barrier. Little fresh water enters this layer, as shown by Figure 5.11a. This agrees with the lower limit of the mixing zone found at approximately 2 m depth according to Chapter 4 and therefore also valid for Mg^{2+} and Na^{+}.

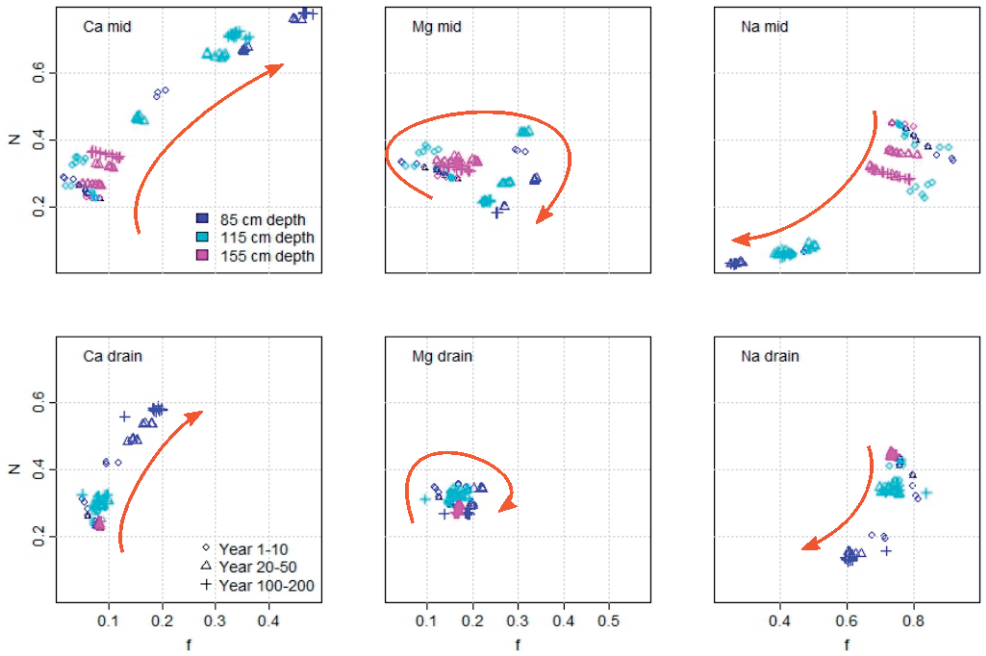

Figure 5.9: Site B model: Graphs for the N-f ratios of Ca^{2+} (left), Mg^{2+} (middle) and Na^{+} (right) in the middle between drains (top) and near the drain (bottom).

When we compare the top panels of Figure 5.9 with the bottom panels of Figure 5.4, the similarity is striking. Both the short and long term processes described for the 1D domain are very recognizable in the case of a 2D field situation with drains and upward seepage instead of a 1D-domain in which the saline and fresh water are artificially pumped up and down. Even the velocity of the exchange for Ca^{2+} is rather similar when the region just below the top of the saturated zone (85 cm depth) is compared to the 25 cm depth line in the 1D-domain. At larger depth, the exchange is slower than for the 1D-domain. This can be explained by the decreasing vertical displacement with depth due to the constant upward flow of the seepage water. The situation deeper is more comparable to the top panels of Figure 5.4, since net vertical displacement becomes very small. The water in the middle of the mixing zone moves mainly horizontally towards the ditch. This is in line with the findings in Chapter 4 concerning the dynamics of the mixing zone.

For Mg^{2+}, the temporary increase of adsorption on the complex at larger depth is not as profound for the field situation. A slight temporary increase of Mg^{2+} is still visible, but the relative availability of Ca^{2+} compared to Mg^{2+} at larger depth seems larger in a field situation than for a 1D column. This corresponds with the difference in flow pattern between 1D and 2D: whereas the seepage water, containing Mg^{2+} is forced to flow upward in the column, it follows a nearly horizontal flow direction in the mixing zone for a field situation (Chapter 4) Less Mg^{2+} is therefore supplied after the rainwater lens is established, compared to the 1D situation with alternating flow directions.

Movement of the front

For the 2 sides of the simulated domain, the HD (left) and near the drain (right), fronts ranges are illustrated in Figure 5.10 for site B. There is a limited bandwidth in which the total concentration (C) front varies dependent on weather and season. Near the drain, its depth of 0.7 m below the soil surface is determining for the depth of the mixing zone, whereas in the middle of the field, the clay layer between 1.7 and 3 m depth provides a lower limit for the front (Figure 4.3).

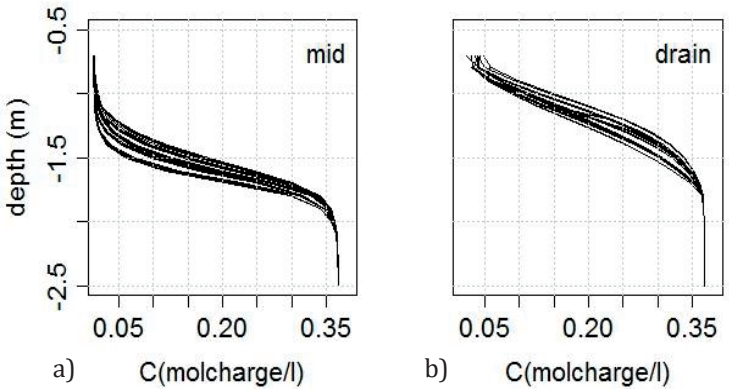

Figure 5.10: Front positions in the middle of the field a) and at the drain b) for the Site B model. Lines were drawn each week for 200 years. Line that seems "cut off" are caused by drying out of the model in a dry period.

Model and field data

Figures 5.11a shows the field data for total concentration, which in Figure 14b are used to illustrate the match between the 2D model and the field data. The comparison is reasonable: the mixing zone is at the same depth for the field and the data, and for both the model and field, a shallower mixing zone and higher total concentration towards the phreatic level are found near the drain (black and red) compared to the middle between drains (green and blue). This shows that the chemical model captures the main features occurring in the field, since flow and transport were calibrated on drain data presented in Chapter 4. For site A, not enough data were available to calibrate the 2D model, therefore only the field data and drain depth are shown at the same scale.

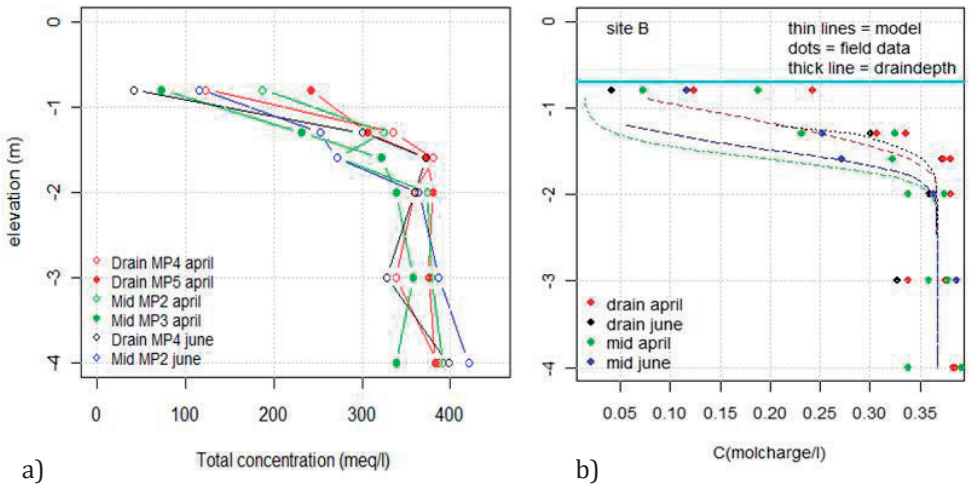

Figure 5.11: Left: a) Field measurements of total concentration (sum of concentrations of Na, Ca2+, Mg2+ and K+). Locations of MPs are in Fig 4.2. This Figure can be compared to the Cl-fronts illustrated in Chapter 4, Figure 4.4, only cations instead of anions are given for this case. Right: b) Comparison of field observations and the 2d simulation for site B. The lines in different colours show the model outcomes for the same date as the field measurements with the same colour.

5.4.3 *Influence of hydrogeological and chemical differences on the exchange process*

Since we have the composition of the saline end members for 2 sites, B and A, as well as CEC values for both soils, we can make a qualitative assessment of the influence of geohydrology and chemical composition.

We assume the calcium enriched precipitation is equal for both sites, based on measurements at site A and similarity of the amount of shells found in both top soils. Based on the pore water composition and CEC (Section 5.3.2), the equilibrium situation was calculated for the complex and the unsaturated zone water. Although this equilibrium situation may not be reached, it provides us with a direction of change for the complex composition for both sites. The equilibria for the saline start, differing per site, and "end" situation on the complex are illustrated for the different ions in Figure 15a.

Magnesium is far more abundant in the seepage water of site B than at site A (Section 3.2), illustrated by Figure 15b. Magnesium has increased compared to the initial situation, as explained in section 5.1 and 5.2. However, the initial difference between sites remains up to this point. Table 2 compares the simulated ranges for shallow depth, coarsely schematized, of *N* illustrated in Figure 12 with the measured fractions of Na^{+},Ca^{2+}, and Mg^{2+} at site B, where the sample at 1.6 m depth is from MP3 (see Figure 2d), between drains, and the sample at 3 m depth is taken near a drain, at MP5.

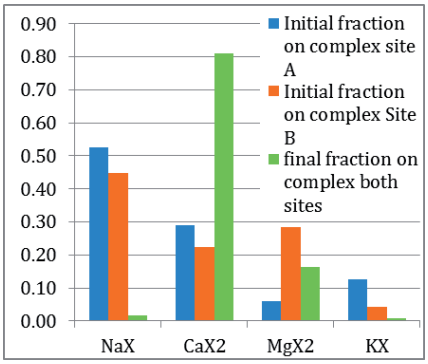

a)

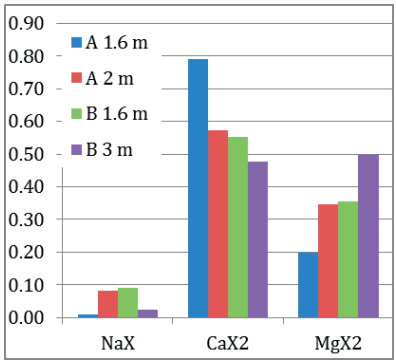

b)

Figure 5.12: a) Left, Fractions (N) of equivalents of Na+, Mg2+, K+ and Ca2+ on the complex, in equilibrium with seepage water (blue and orange) and unsaturated zone water (green). b) Right, presents the current fractions on the complex for the field samples at two depths for both sites (averaged over 2 tested sub-samples). NaX and CaX2 are both clearly in between the seepage and unsaturated zone equilibrium, A at 1.6 m depth is close to the unsaturated zone status. MgX2 shows higher levels, which is in line with preferential exchange of Na+ for Mg2+, followed by exchange of Mg2+ for Ca.

Table 6.2 provides us with two clear suggestions concerning the relation between the situation at site B and our model. First is that although the depth of the simulated values presented in Table 6.2 (1.15 m) is shallow compared to the observation depths (1.6 and 3 m) the N values are comparable to the expected situation after approximately 120 years. This indicates that the field situation has developed over a longer time than the simulated time, which is in line with the work of Vos et al. (2003) as cited in Section 2. A very precise comparison in not possible since water management (dikes, polder levels) as well as geohydrological conditions (sea level rise, land subsidence, e.g. Post et al., 2007) varied over time.

Table 6.2: Comparison of approximate simulated N value at 115 cm depth (upper 3 rows) and observed (bottom 2 rows) fractions on the complex of site B. Differences in depth are caused by limited data availability.

	CaX2		MgX2		NaX	
	mid	drain	mid	drain	mid	drain
Model Start	0.2	0.2	0.3	0.25	0.5	0.5
Model after 100 y	0.5	0.4	0.4	0.35	0.25	0.3
Model after 200 y	0.8	0.6	0.2	0.25	0	0.1
Depth of observation	1.6 m	3m	1.6 m	3m	1.6 m	3m
Observed	0.55	0.48	0.35	0.5	0.09	0.03

Secondly, the drain impact on water flow cannot already have influenced the composition of the exchange complex of soil. After all, these drains were installed only decades ago, little compared to the timescale of significant exchange variations according to the simulations. For the same reason, it may be understandable that even at the depth of 3 meters the composition of the exchange complex has changed,

towards a fresher situation then would be expected based on the simulations. Apparently, fresh water has been able to reach a much larger depth somewhere during the geological formation of the land.

5.5 Discussion and conclusions

In this paper, we investigated the cation exchange and transport in thin rainwater lenses on top of upward seepage of saline water in case of an alternating flow pattern caused by recharge, evaporation, saline seepage and horizontal flow towards tile drains. Because a preliminary analysis of field data revealed quite some complexity, we first studied an abstracted, one-dimensional analog. After interpreting these results, it was possible to understand the cation exchange occurring in a more realistic two-dimensional case that better represents field conditions.

The one dimensional models show the exchange that develops over time, starting from an initially saline situation with alternating inflow of calcium enriched rainwater from the top and saline water from the bottom:

- On the short term, a large change in solution composition is caused by the initial salt shock: fresh water enters the saline water filled domain.
- On the longer term, gradual increases of calcium on the complex and in the solution are caused by the larger affinity of the complex for calcium in fresh water and the gradual supply of calcium by the fresh water.
- Magnesium initially increases on the complex at the cost of sodium, however, as calcium in the solution gradually increases, it outcompetes magnesium on the complex.

Differences between the oscillation patterns of the 1D models illustrated:

- Oscillations of flow direction in combination with a zero net flux leads to a strongly oscillating pattern and, ultimately (i.e. after centuries) to a disperse front with a stable alternation.
- Oscillations with a 1mm/day net downward flux behave similar for an artificial step model and a natural net precipitation pattern. Both lead to a rather fast passage of the fresh/saline front up to just above the bottom of the column. Exchange progresses fast compared to the zero net displacement situation, but decrease sharply in velocity with depth.

The field model with drains spaced at distances of 10 m, and constant upward seepage of saline water can be interpreted using the 1D models:

- Up to a depth below surface of ca. 1.2 m: a sequence and velocity of exchange comparable with the 1D model with natural net recharge

- The limited downward movement of the front, inhibited by the constant upward seepage of saline water, causes the process at depths > ca. 1.2 m to resemble the 1D model with zero net flux.
- The horizontal flow component is shown to have little influence on the exchange of saline and fresh ions, which can be understood from the fact that only vertical flow causes changes in pore water composition.

Comparison of field data with the model for site B shows that the main features of the field are represented:

- In line with the findings of De Louw *et al.* (2011, 2013), the mixing zone position depends largely on the presence of aquitards combined with the position of the drain.
- Comparing observations and model results, the exchange process seems to have progressed towards freshwater equilibrium for rather long; even at larger depth (3 m) the exchange has progressed considerably.
- After functioning 30-40 years, the drains have only changed the composition of the pore water and not yet that of the soil complex.

Analysis of main cation concentrations in the soil of both study sites reveals:

- Both for site A and B, observed complex composition confirms the expected increase of calcium, decrease of sodium, and intermediate increase of magnesium.
- The initial difference in magnesium between the sites remains intact up to now, illustrating a long-term effect of the composition of the seepage water on the complex.
- Both sites show that there is no equilibrium, however, the complex has developed a lot from the initially saline conditions towards a fresh water dominated complex

History for both study sites is known only approximately. After initial lens formation since 1300 AD, intensified deeper drainage at the beginning of the 20th century was followed by tile drainage between 10 and 40 years ago. Given these big changes over the last century, and the ongoing changes in polder systems, both in water management (e.g. drainage level) and external changes (e.g. increasing seepage caused by relative see level rise and climate change), a real equilibrium is unlikely. In this paper, cation exchange has been emphasized. However, in case of large amounts of organic matter (e.g. peat layers). Also redox and chemical precipitation-dissolution reactions may complicate the hydrochemistry of the subsoil.

6 VEGETATION STRESS AND SALINE GROUNDWATER

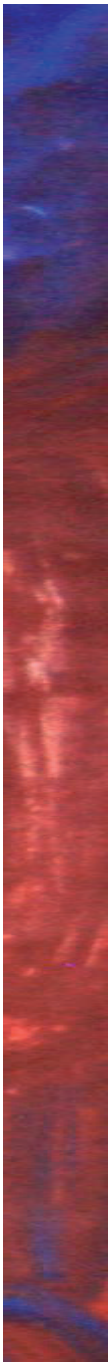

ABSTRACT

Sustainability of agriculture and natural vegetation in coastal zones with saline groundwater is of concern in view of climate change and sea level rise. A first order assessment was made of the influence of saline groundwater on vegetation development. For two time series of twenty years for a Dutch and for an Italian climate, we simulated combinations of different vegetation, soil characteristics, and groundwater levels and –salinities using a 1D model. Using step wise linear regression, we assessed the relative importance of all parameters on the fresh water availability and on the stress experienced by vegetation. Salt stress, oxygen stress and drought stress are quantified and put in perspective. Fresh water availability in winter and vegetation stress are quantified to assess the impact of the different input parameters on the system. Salinity stress is substantial, but small compared to stress caused by lack of oxygen and drought, which cause twice and four times larger reductions of transpiration, respectively. Soil type, weather and climate are shown to be the most important parameters for both fresh water availability in winter and vegetation stress. Salt stress is also dependent on groundwater level and rooting depth of the vegetation. This study suggests that water- and soil management are the main tools to guarantee sustainability of fresh water dependent vegetation in the future, for salt stress as well as stress caused by too dry or wet conditions. Only in particular cases an increased salt tolerance of vegetation could make a significant difference.

This chapter is based on: S. Eeman, P. Torfs, S.E.A.T.M van der Zee, A. Leijnse. First order assessment of the influence of saline groundwater on crop growth. In preparation.

6.1 Introduction

Deltaic areas throughout the world are densely inhabited, and economically of large importance. The consequences of climate change and sea level rise for the low lying areas have been investigated by many (e.g. Underwood, 1992; Oude Essink, 1996; Pauw et al., 2012 and Mollema et al. 2014). Also possible mitigation measures have been evaluated (e.g. Pauw et al., 2015; Scott et al., 2014). An issue that arises is salinization of ground-, soil- and surface water. When focusing on soil water, salinization in or near the root zone can have different causes. Salt originating from irrigation is the most common cause (e.g. Yeo et al. 1989), particularly in semi-arid areas. However, also in rain fed coastal areas, saline water in the root zone may invoke loss of agricultural production or changes in the ecological system during the dry season, where salts transport into the root zone in upward seeping groundwater. This saline groundwater is often present in the subsurface, either due to sea water intrusion or due to geological deposition of salt containing sediments (Post at al. 2004, Delsman et al.,2014a).

The surface of low-lying coastal zones is considerable, for example in the Netherlands (Van Huissteden et al. 2006), and currently growing due to sea level rise (Day et al., 1995; Lebbe et al, 2008). Several studies have investigated the consequences of sea level rise for low lying coastal zones. Zeidler (1997a), for example, indicates that in the Polish Gdansk area an increase of salinity is expected to decrease yields within the coming decades. Vietnam (Zeidler 1997b) and Bangladesh (Habibullah et al., 1999) will lose considerable amounts of agriculturally productive area due to the extension of saline zones. Osterkamp et al. (2001) studied the consequences of sea level rise for the Weser Estuary in Northern Germany, considering the ecological consequences of soil moisture patterns caused by sea level rise and changes in precipitation. They did not include possible associated changes in the salinity of the soil moisture, which could substantially aggravate crop damage and ecological consequences (De Jong van Lier et al., 2009).

The sensitivity of plants to salinity has received some attention (Yeo, 1998), and different assumptions to allow quantification were proposed (e.g. Feddes et al. 1988, De Jong van Lier et al. 2008). Although in practical situations, variations of sensitivity to saline water are often found, for example during different crop stages (Van Dam, 2007, Van Bakel et al. 2011), the current Dutch method to assess expected crop damage caused by salinity is based on fixed tables. These tables quantify the salinity beyond which crop damage occurs and a gradient for crop loss at salinities above this damage level. Differences between crop sensitivities are estimated in this way.

Research concerning salinity induced vegetation damage generally concerns the use of brackish irrigation water. In this CH+apter, we study the influence of saline seepage, reaching the root zone from the underlying groundwater. Saline seepage is not necessarily a threat for crops, as a superficial fresh water lens may counterbalance the saline groundwater sufficiently to allow plant growth. However, in dry periods the risk of capillary rise of saline water may be significant enough to influence vegetation development.

To study this possible negative influence, we statistically analyze a variety of numerically simulated agricultural field situations. The models are one dimensional and assess the interactions between soil, groundwater, plant and the atmosphere. Different values for characteristics of all four components have been simulated. Our aim is to understand the relative importance of climate, geohydrology and plant characteristics for the occurrence of salinity induced vegetation stress. To put the results in perspective, salinity stress is compared to the stress caused by drought and wetness (oxygen stress), and interactions between different factors are identified.

6.2 Theory and methods

We have used numerical modelling to produce a large variety of crop growth data for different climatic, geohydrologic and vegetation related conditions. These data were analysed using basic statistics to determine the importance of the different parameters for the different causes of vegetation stress; drought, lack of oxygen and salinity. All symbols and units are in the Nomenclature on p. vii and viii.

6.2.1 Numerical model

We used the package SWAP (Kroes et al., 2008) to model interactions between the climatic conditions, plant characteristics and the hydrogeological parameters. SWAP is a physically based, 1 dimensional eco-hydrological model, widely used to simulate the different processes and their interactions in the soil-water-atmosphere-plant system. SWAP solves the Richards equation (Eq. 6.1) to simulate partially-saturated water flow in the soil profile:

$$\frac{\partial \theta}{\partial t} = \frac{\partial}{\partial z}\left[k(h_p)\left(\frac{\partial h_p}{\partial z} + 1\right)\right] - S_a(h_p, \omega) \qquad (6.1)$$

The maximum possible root water uptake, S_p, over the rooting depth is equal to the potential transpiration T_p, which is governed by atmospheric conditions. Potential root water uptake at a certain depth $S_p(z)$ is determined by the root length density at this depth $l_r(z)$, as a fraction of integrated root length density

$$S_p(z) = \frac{l_r(z)}{\int_{-D_r}^{0} l_r(z)\mathrm{dz}} T_p \qquad (6.2)$$

The actual root water uptake is determined by reducing potential uptake for water stress r_d, (Feddes et al, 1978), salt stress r_s (Maas and Hoffman, 1977), oxygen stress r_w (Bartolomeus et al. 2008) and stress caused by frozen soil conditions (not further considered in this paper). The reduction factors are multiplied as proposed by Skaggs (2006)

$$S_a = r_d r_s r_w S_p \tag{6.3}$$

Integrating over the root zone then yields the actual transpiration. Splitting up the transpiration reduction into the individual contributions is performed, see Kroes et al., 2008.

Soil moisture retention and hydraulic conductivity are defined by the Mualem-van Genuchten (Van Genuchten, 1980) equations.

$$S_r = \frac{\theta-\theta_r}{\theta_s-\theta_r} = \left[\frac{1}{1+|\mathrm{ih}|^j}\right]^{1-1/j} \text{ and } \quad k = k_0 S_r^{\lambda}\left(1-\left[1-S_r^{j/(j-1)}\right]^{1-1/j}\right)^2 \tag{6.4 a,b}$$

Reference evaporation was included in the weather data. The potential transpiration T_p and evaporation $E_p$were separated using the leaf area index (LAI). In the SWAP manual (Kroes et al., 2008), this method is elaborated.

6.2.2 Boundary conditions

The model was setup such that the simulations resemble a polder situation with controlled, shallow groundwater levels with a given salinity (Table 6.1) and an upward flux of 0.5 mm/day. Drainage was at the given groundwater level, also capable of infiltration with a resistance of 100 days. The soil profile was homogeneous for a one dimensional column with a depth of 2.1 m. Discretization was 1 cm vertically for the upper 10 cm, then 5 cm up to 1 m depth, and 10 cm for the lower 1.1 m. Time steps are adjusted between $0.1 \cdot 10^{-6}$ and 0.2 days, based on default values for maximum changes within a time step for groundwater level, pressure head and a maximum allowed number of iterations (Kroes et al. 2008).

6.2.3 Input data

Hydraulic data for three typical top soils from the Dutch Staring series (Wösten et al. 2013) were used for the simulations (Table 1). For each soil type, we simulated two different saturated conductivities within the range proposed in the Staring series. Groundwater level (GWL) and salinity were varied for each soil type, based on realistic conditions in the Southwestern Netherlands (see Chapter 4).

Twenty years of daily weather data from the southwest of The Netherlands and from northern Italy were used (1987-2006), including temperature, precipitation and potential evaporation. These were chosen since both have large agricultural areas in

low-lying coastal zones, while differing considerably in climate. All data were analyzed per year and climate to detect the influence of different parameters on fresh water availability in the simulations. Then the driest and wettest year within the 20 simulated years were selected for both locations (Figure 6.1), using cumulative annual precipitation per climate. These were used to assess influence of soil and vegetation parameters on different forms of stress under relatively dry and wet conditions.

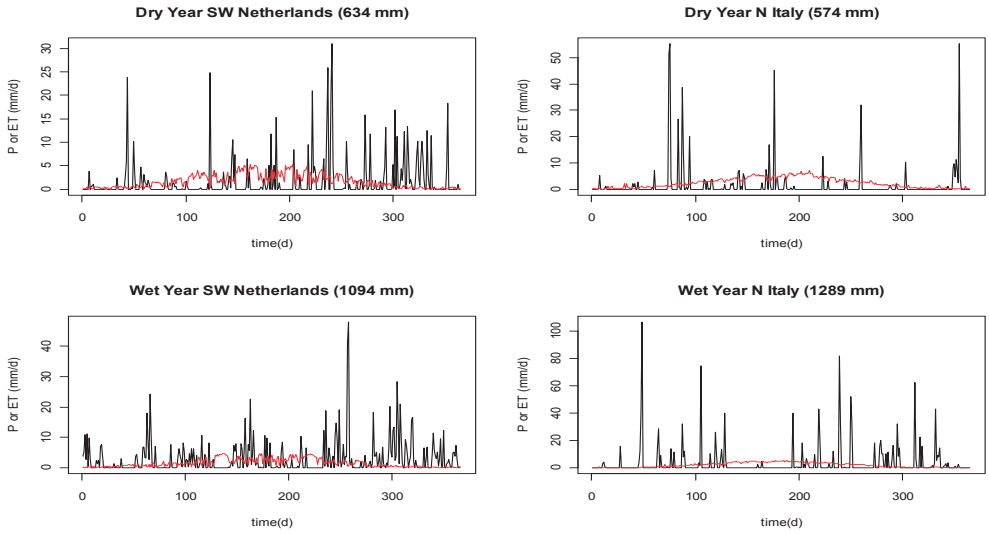

Figure 6.1: a dry (top) and a wet (middle) year for both The Netherlands (left) and Italy (Right). For The Netherlands 1996 was the driest year and 1998 was the wettest year. In Italy the years 2001 and 2000 were used respectively.

Vegetation was modeled using simple crop modules as available in SWAP, for three different crops: maize, potatoes and grass. They vary in rooting depth, but also in growth and associated evaporation throughout the season. Grass grows 365 days a year, and varies in leaf area index according to a mowing/grazing pattern. Maize and potatoes grow 168 days per year, and maize grows until it is ripening, whereas potatoes stop growing approximately 2 months earlier. For a more extensive description of crop growth, we refer to Kroes et al. (2008). Our basic interest is to test the effect of differences in salinity tolerance. Therefore we tested different salt sensitivity parameters within the standard crop models above. The realistic range of threshold values for soil water salinity to cause stress was based on salt tolerance guidelines after Maas (1990). Above the threshold, transpiration decreases according to a gradient, for which we chose 2 realistic values based on the same table. An overview of all parameters and their variation is shown in Table 6.1. When simulating vegetation growth, groundwater level is overruling maximum rooting depth, implying that roots do not grow below the groundwater level, which is adequate for most vegetation.

Table 6.1Model input parameter values

Input parameter			
Climate			
Location	Wilhelminadorp (NL)	Piacenza (IT)	
Associated average ET_p, (mm/y)	616	771	
Associated average P (mm/y)	821	855	
Soil			
Type (-)	Sand	Loam	Clay
Low Ksat associated with type (m/d)	10	1	1
High Ksat associated with type (m/d)	200	14	5
Groundwater			
Groundwater level (m)	0.7	1.1	1.5
Salinity of the groundwater (g/l)	10	25	
Vegetation			
Type (-)	Potatoes	Maize	Grass
Rooting depth associated to type (m)	0.5	1	0.3
Threshold salinity level (g/l)	1.5	3.5	7
Decrease in T per mg/l salt (%)	5	15	
Root Distribution (-)	Uniform	Linear	

6.2.4 Fresh water availability and salinity stress

There are two output variables of interest for this study. First the availability of fresh water in the column in January, and secondly the three stress factors that influence plant transpiration negatively.

The amount of fresh water available in the simulated soil column in January and December of the same calendar year were compared to assess whether systems have lost or gained fresh water in one year. This depends on the cumulative fluxes, but also on drainage depth and soil type, especially in the polder situation we modeled. It can be used as indicator for the sustainability on the longer term of freshwater dependent vegetation and is determined using the annual water and solute balance of the simulations:

$$\Delta F_r = \frac{-\Delta Sal}{C_s} \tag{6.5}$$

Where ΔFr indicates the change in fresh water present in the column in cm^3/cm^2. The unit was chosen for its clear physical meaning. ΔSal is the change in dissolved salts stored in the column and C_s is the concentration of the seepage water.

In this study, the relative transpiration is used as performance indicator to evaluate the impact of stress on crop transpiration (De Wit, 1958):

$$T_r = \frac{T_{act}}{T_{pot}} \quad (6.6)$$

This parameter can be attributed to by the possible causes for decreased transpiration in the growing season which are drought, oxygen- and salt stress. Potential transpiration is calculated by SWAP based on the growing stage of the vegetation and the temperature. Actual transpiration is maximized at the potential transpiration, but might be less because of lack of water or oxygen in the root zone, or difficulty in water take-up due to the presence of saline water in the root zone.

6.2.5 Statistical analysis

The outcomes of all simulations were analysed using the software package R, by making step wise linear regression models of factors created from the input parameters, listed in Table 6.2. Their relative impact on fresh water availability in winter and the different stress types (salt, drought and oxygen) leading to transpiration reduction was investigated. The setup and uncertainties concerning the crop data do not justify more extensive analyses.

Table 6.2 Factors used in regression analysis

Regression factors	Nr of classes	Class names
Climate	2	Wilhelminadorp and Piacenza
Soil type	6	Sand high, Sand low, Loam high, Loam low, Clay high, Clay low *
Groundwater level	3	0.7 m, 1.1 m, 1.5 m
Groundwater salinity	2	10 g/l, 25 g/l
Vegetationtype	3	grass, maize, potatoes
Rooting distribution	2	linear, uniform
Salt tolerance threshold	3	1.5 g/l, 3.5 g/l, 7 g/l
Decrease in T per mg/l salt	2	5%, 15%

*low and high have been specified in Table 6.1

6.3 Results

The results of the statistical analyses of the annual changes in availability of fresh water are presented first. Then an overview of the amount of transpiration decrease for different conditions followed by the two analyses of the relative effects of the different parameters.

6.3.1 Changes in fresh water availability in winter.

Only climate, weather and soil type have a significant influence on the amount of fresh water in winter. These factors are shown in Fig. 6.2. Absolute differences are very small, which can be attributed to the simulated control of the groundwater level. Figure 6.2 shows a vertical bar plot for the individual years per climate, sorted by the associated change in fresh water availability. Within each bar, the grey line gives the mean for that year and the colours show ranges for the different soil types. Weather

variations within a year explain the change in fresh water availability for 55% (measured in cm column height on January 1st according to Eq. 6.5). Climate also has a very significant influence: weather variation within a year + climate gives 80% explained variance. Differences in the variation of fresh water availability between the Dutch (temperate) and Italian (Mediterranean) climate are in the extremes and in the variation around the annual mean. These variations are smaller in the Dutch climate, in line with generally shorter dry and wet periods compared to the Italian climate. The different order of colours in every bar shows the importance of interaction between weather and soil. In general, sand, with a high conductivity, increases effects of both loss or increase of fresh water availability, whereas soils with a low conductivity damp this effect. There are some exceptions that may be attributed to the specific weather conditions within a certain year.

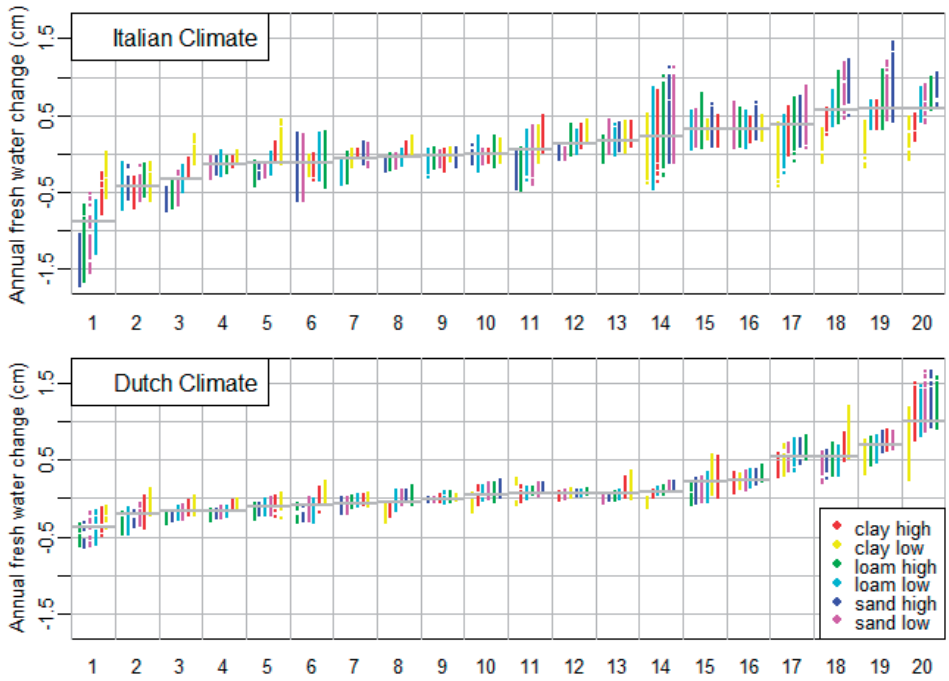

Figure 6.2: Results of linear regression for both climates show that changes in fresh water availability are mainly dependent on weather variability. The x-axis shows individual years sorted by their change in fresh water availability. Soil type is of significant influence as well, especially in the years where changes in fresh water availability are larger. The y-axis shows the changes in freshwater availability according to Eq. 6.5.

6.3.2 Transpiration reduction caused by different types of stress

For each simulation, actual and potential transpiration were compared. For the entire ensemble of simulations and for 20 years, the transpiration reduction was on average $\left[\left(T_p - T_a\right)/T_p\right] \cdot 100\% = 23\%$. If we specify this percentage per climate, the decrease is only 15% for the Dutch climate and 30% for the Italian. This situation is a little

different if we consider the wettest and driest year per climate. Dry years cause much more damage in the Italian than in the Dutch climate. Table 6.3 gives an overview of the average transpiration reduction overall and per climate. Figure 6.3 shows the relative importance of drought, oxygen- and salt stress for the wettest and the driest year. Salt stress is smaller compared to drought and oxygen stress. In dry circumstances, salt stress may cause 20% of the transpiration decrease for the Italian climate and 10% for the Dutch climate. For the Italian climate that is 6% transpiration decrease for such a year.

Table 6.3: Transpiraton reduction as fraction of potential transpiration (20-30 cm/y), caused by all types of stress.

Simulations	20 years average	20 years mean standard deviation	Wettest year average	Driest year average
All	0.23	0.10	0.19	0.22
Dutch climate	0.15	0.08	0.16	0.13
Italian climate	0.30	0.12	0.23	0.31

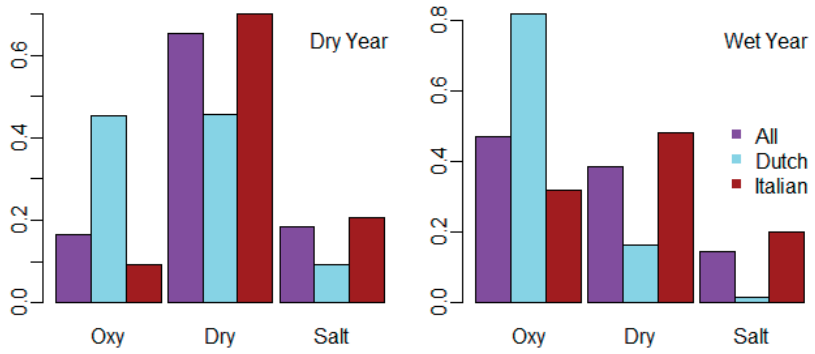

Figure 6.3: Barplot of the relative amounts of oxygen stress, drought and salt stress in dry and wet conditions for all simulations and per climate.

6.3.3 Salt-, drought-, and oxygen stress in very wet and very dry years

Figure 6.4 shows the relative influence of all factors (Table 6.4) that were varied according to Table 6.2 (horizontal), on different types of stress (vertical) in the wettest and the driest year for each climate. Colours show, according to the colour key, the extra variance that is explained by introducing the factor and this is also represented by the numbers. Variances are expressed as fraction of the total variance.

The Figure illustrates basically the strong effects of soil type and climate on drought and salt stress as well as the important effect of groundwater level on both salt- and oxygen stress. Vegetation type (and the implicitly associated rooting depth) is the second important impact factor for oxygen stress. Crop parameters that characterise salt sensitivity have very little influence compared to the geohydrological parameters.

Differences between dry and wet years are small; the same parameters are of importance, although to a different extent.

Dendrograms on both sides are a way to visualize cluster analysis (Davis, 1973), providing in this case information on the similarity of the impact of the different factors (dendrogram above the heat maps in Figure 6.4) and the connections between resulting stresses (dendrogram left of the heat map in Figure 6.4). They visualise the results of clustering. The first dendrogram (above the heat map), shows that the "main" factors, soil and climate are closely related, as are groundwater level and vegetation type, in line with their combined influence on drought and oxygen stress respectively. Above that, crop and groundwater are separated from soil and climate. The second dendrogram (left of the figure) shows a separation of stress caused by lack of oxygen, salinity and drought, confirming that dry or wet conditions do not significantly change the relative impact of the different factors.

Table 6.4: Desciption of labels in Figure 6.4 and 6.5

Horizontal:		**Vertical:**	
clim:	climate	Max:	year with most precipitation
soil:	soil type incl. Ksat	Min:	year with least precipitation
gwl:	groundwater level	Oxy:	stress by lack of oxygen
gwsal:	groundwater salinity	Dry:	stress by lack of water
vegtype:	vegetation type incl. rooting	Salt:	stress by too much salt
vegsaltr:	threshold salinity stress		
vegsalgr:	gradient vegetationloss above		
vegrdist:	vegetation root distribution		

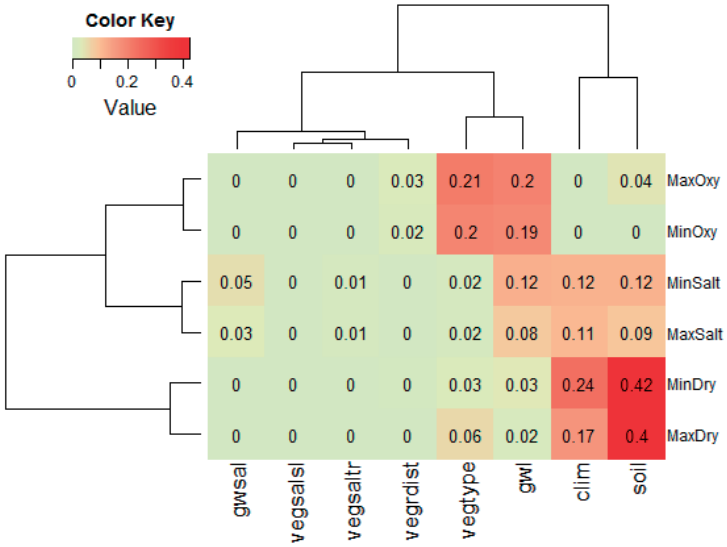

Figure 6.4: Classical heat map, showing the relative influence of the different parameters on vegetation stress caused by lack of oxygen, salt and drought in the year with highest (Max) and lowest (Min), precipitation, determined per climate. Numbers indicate the extra variance explained by introduction of the factor. The two dendrograms visualise correlations between the input factors and resulting stresses.

6.3.4 *Different severities of salt- drought- and oxygen stress.*

Figure 6.5 uses a more extended dataset. All simulated years are used instead of only the wettest and driest year. Secondly, salt-, oxygen and drought stress that occurred annually were divided into four severities: >2%, >5%, >10% and >20% transpiration reduction (cumulatively, implying that the >2% years also include all years with larger transpiration reduction). With this dataset we investigated whether different amounts of stress under a range of weather conditions change the relative effect of the input parameters. Again a heat map was used in Figure 6.5 to visualize the set of step wise linear regressions. The similarity with Figure 6.4 confirms the observation that wet or dry years do not lead to different factors that influence transpiration reduction. The figure indeed provides insight with respect to changing parameter influence for increasing transpiration reduction. For drought stress, the factor soil decreases with increasing transpiration reduction whereas the effect of climate increases. For oxygen stress, crop type becomes more important and groundwater level less important with increasing transpiration reduction and the effect of soil type sharply decreases. Salt stress shows a sudden increase in the influence of soil at 20% stress. The effect for climate is opposite and smoother and the influence of groundwater level is nearly stable.

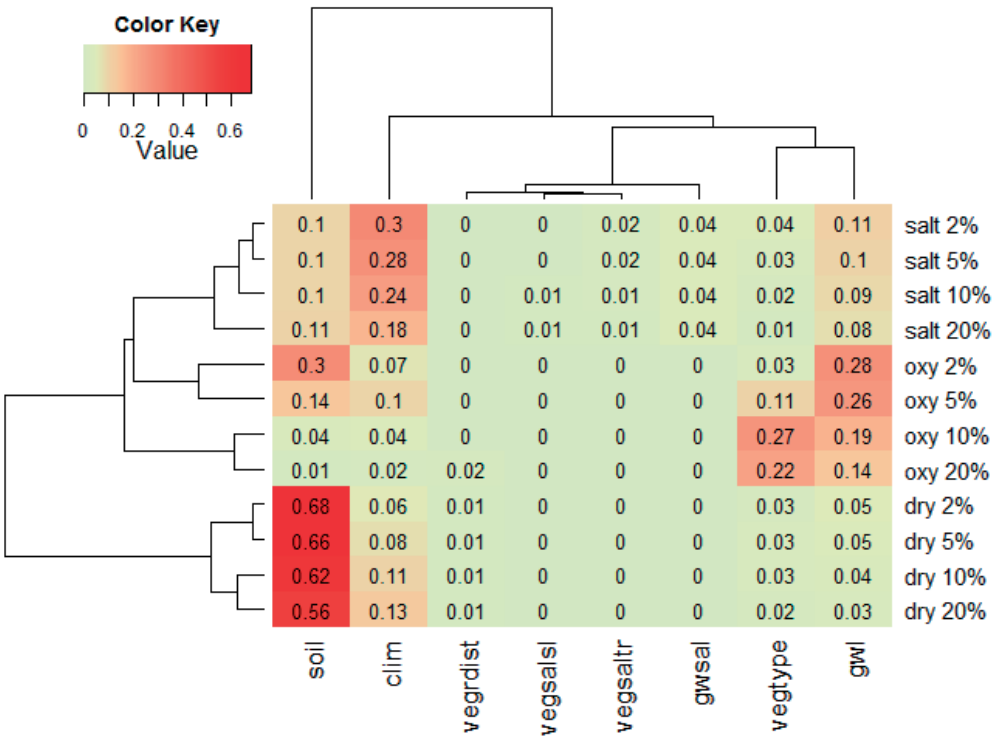

Figure 6.5: A classical heat map showing the dependence of the chance for decreased transpiration due to salt, oxygen or drought stress on the parameters in Table 6.4. The transpiration loss of >2, >5, >10 or >20% per stress type is calculated according to Eq. 6.5. The numbers in the map show the extra variance explained by introduction of a factor (x-axis).

The dendrograms are similar to those of Figure 6.4. Similarity between salt and oxygen stress are a little stronger in than in Figure 6.4 and the separation between soil and climate is slightly different.

6.4 Discussion and conclusions

The analyses of all the simulations give several suggestions concerning the more and the less important factors related to sustainability of agriculture and vegetation stress in areas with saline groundwater. In addition, we relate the outcomes to possible priorities in water management and suggestions for further research.

For winter conditions, there are small changes in freshwater availability between different years (see Figure 6.3) and this represents normal (polder) conditions well. The effects of climate and weather on the fresh water availability are larger than those of soil (K_{sat}). This suggests that water management (storage options) is the main tool to prevent a long term trend of decreasing fresh water availability.

The main cause of transpiration reduction over all simulations is drought, and oxygen stress is the second important. Salt stress is significant in dry years for the Italian climate (Figure 6.2). In view of the expected climate change, salinity stress is likely to increase, like drought stress. For the Italian climate, this may pose severe limitations to agricultural production, or at least large dependence on irrigation water.

The influence of the vegetation on salt stress seems limited to its rooting depth. This is suggested by Figures 6.4 and 6.5, where the parameter “vegetation type” includes rooting depth and shows significant effect, while the salt tolerance related vegetation parameters have a negligible effect. Shallow roots cause lower sensitivity for oxygen- and salt stress, which can be explained by the larger distance between the groundwater and the root zone. However, the effect of shallow roots on drought is opposite. These conflicting aspects of root zone thickness suggest that there is an optimum, depending on the pressures of drought, salinity, and anaerobicity, that deserves further study.

The possibility to increase sustainability of agriculture in coastal zones by increasing the salt tolerance of plants is not evident from this study, given the negligible impact of salt related vegetation parameters on transpiration reduction by salt stress. The setup of the study, with groundwater salinities representative for the South and West of The Netherlands, and crop salt tolerances in compliance with literature are a possible reason: maximum tolerance is still far below groundwater salinity. However, given the limited salt stress found in this study, lower groundwater salinities are unlikely to lead to substantial transpiration reduction caused by salt. Improving the simulation of plant response to saline water in hydrological models may lead to different outcomes.

Soil type has an important effect on both drought and salt stress (Figures 6.4 and 6.5). The way in which soil type influences the system depends on the actual situation, which complicates adequate management. We would expect that coarse soils with high saturated conductivity are more sensitive to drought. However, these soils also have low capillarity, thereby decreasing in dry periods the amount of salt that moves upward from the saline groundwater into the root zone. Therefore, it might be beneficial to identify whether conditions exist where the positive effects on salt stress outweigh the negative effects of drought.

Mitigation of climate effects and appropriate soil management are likely to be effective ways to guarantee future sustainability of agricultural production in areas with saline groundwater. Anticipating on the future water demand and availability can help to maintain the stable fresh water availability in winter. This may prevent a negative trend caused by successive dry summers, which are likely to occur more frequently according to predicted climate change (Bates et al. 2008) for both Italy and The Netherlands. Increasing organic matter content in the soil is another measure that increases sustainability of freshwater dependent vegetation in coastal zones by decreasing sensitivity to oxygen-, drought- and salt stress by storing more fresh water.

7 SYNTHESIS

7.1 Introduction

This chapter combines the findings of all previous chapters. I show how this thesis has contributed to the understanding of the dynamics of rainwater lenses in areas with upward seepage of saline water. This overview is followed by implications for sustainable use of thin rain water lenses and recommendations for future research.

7.2 Rainwater lenses on upward seeping groundwater

Several tools in Chapters 2 and 3 in the form of simple analytical relations assess the thickness of a thin rainwater lens on top of saline groundwater (Figure 7.1). Since assuming a sharp interface is inappropriate for such thin lenses (Chapter 1), this thickness comprises two components; the average thickness of the lens itself and the thickness of the mixing zone between the lens and the underlying saline groundwater. Numerically, thickness of lens and mixing zone are represented by the first and second spatial moment of the derivative of the salinity profile (Figure 2.1), which is appropriate when the derivative of the salinity profile is normally distributed. Near drains or ditches, or in cases where the upper groundwater is not completely fresh, it should be noted that spatial moments may cause deviations. In a field study, as presented in Chapter 4, measured salinities at different depths can be used to determine the depth of the center and bottom of the mixing zone from where thickness of lens and mixing zone can be derived.

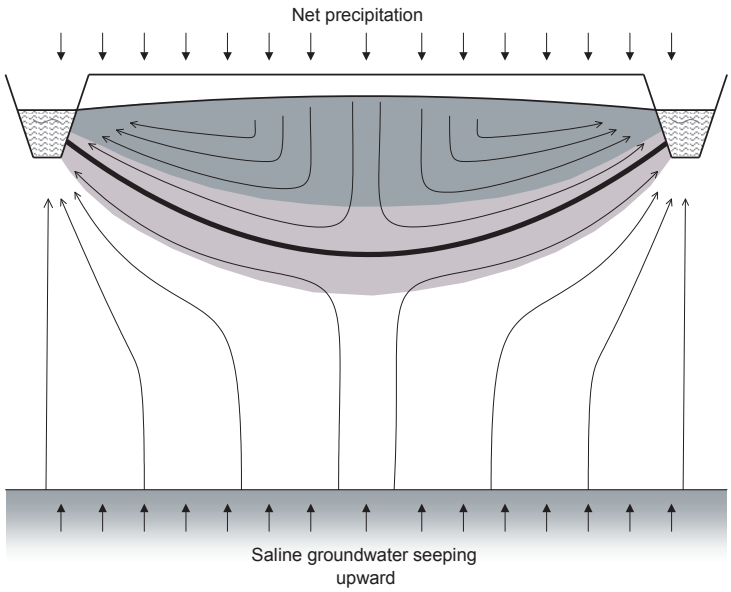

Figure 7.1: (also shown in chapter 2) System studied in this thesis. A rainwater lens (in grey) on top of saline upward flowing ground water (white) with arrows that illustrate flow lines. The mixing zone (light grey) lies in between. The thick black line indicates the "position of the interface".

The influence of geometry, soil hydrology, mixing parameters and fluxes are taken into account systematically using dimensionless groups to assess their relative influence on lens thickness. It is shown numerically that the average thickness and volume of a lens, after the influence of initial conditions has disappeared, can be determined adequately from an analytical approximation based on the distance between drains and the ratio between recharge and seepage water, including the effect of density difference. I compared this approach with observations at a study site in Zeeland, which are presented in Chapter 4. Box 7.1 illustrates that the analytical approximation for a steady state situation is within the range of observed thicknesses for a study site in Zeeland (Southwestern Netherlands).

Combined findings of Chapters 2 and 4: analytical formula vs field observations

Data field site B in Chapter 4

Seepage: 0,29 mm/d

Recharge: 1 mm/d

Density seepage water: 1014.8 kg/m³

Distance between drains: 10 m

Height of system: 1.7 m

(limited by low conductivity clay layer)

Analytical approach Chapter 2

Rayleigh number: 91.6

Lens thickness according to Maas (sharp interface):0.51 m

After correction of 10% according to G=0.34: ***0.56m***

G= H/L, where H= height modelled domain, L is half field width

Observation Chapter 4

Lens thickness from GWL until center of mixing zone, Chapter 4: ***0.5-0.75 m.***

Box 7.1: Synthesis of approximated average lens thickness and field observations.

The thickness of the mixing zone is strongly related to the recharge and seepage fluxes on one hand, and to dispersion and diffusion on the other hand. For a steady state lens, vertical mixing and the associated dominance of mechanical dispersion, becomes negligible after initial conditions have lost influence. This leads to a relatively narrow mixing zone, dominated by diffusion. Towards drains or ditches, convergence of stream lines is illustrated by numerical models (Chapter 2). In case of drains, the small outlet requires such a pattern, also visible in figures like for example 5.1. The observations of mixing zones near and in between drains, studied in Chapter 4, confirm this pattern. For ditches, mixing zones do not necessarily become much narrower, since a larger area is available for the outflow of groundwater. However, as I now compare field observations from both study sites in Zeeland near ditches, the convergence found numerically in Chapter 2 is also well visible and shown in Box 7.2. Apparently, the theoretical finding concerning the dominance of converging streamlines over increased transversal dispersion caused by increasing flow velocity is valid for field sites.

Combined findings of Chapters 2 (left) and 4 (right): convergence near a ditch

Simulated narrowing mixing zone towards a ditch

Two observed profiles at a distance of 1 resp. 5 m from a ditch

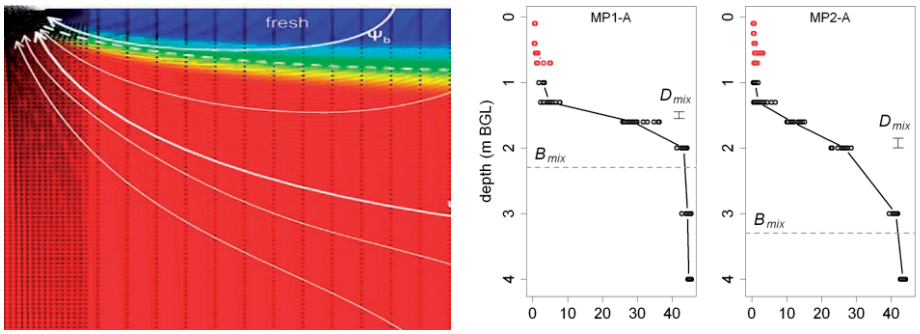

Box 7.2: Convergence of stream lines towards a ditch, simulated and observed.

The system response to long term changes of the average of system parameters, like climate change and sea level rise can be considered as relatively static processes. The change described in Chapter 3 is a change in basic system parameters, e.g. seepage flux. Then the response of both the average lens and mixing zone thickness on changes in constant recharge can be predicted using convolution theory. Although this change as such has not been studied in the field, the good agreement between the steady state approximations and field observations gives confidence in these predictions.

Estimating the mixing zone thickness, which is mainly dependent on mass flux ratio, transverse dispersion and diffusion, is possible for steady lenses. In reality, steady state does not occur, but can be seen as a time averaged situation. Whereas the average lens thickness for steady state conditions provides a useful estimate of the available fresh water on an annual basis, the mixing zone thickness in the field is dominated by variations in flux, the latter obviously disregarded in a steady state approach.

7.3 Dynamic relations

Using the same study site in Zeeland as presented in Chapter 4, we can compare simulated and observed findings for variations in thickness of lens and mixing zone. Precipitation and evaporation data used are the same in Chapters 3 and 4. Movements of the centre of the mixing zone are more profound in the models of Chapter 3 than observed in the field. This is not likely due to minor differences between quantifying lens and mixing zone thicknesses in simulations and in field observations (disregard of unsaturated zone, Box 7.3).

Comparing mixing zone dynamics theoretically and in the field, the differences are on first sight striking. Even after correction for a thinner average lens simulated in Chapter 4 compared to Chapter 3, differences are evident, illustrated in Box 7.3. These differences on one hand show limitations of the theoretical model of Chapter 3. An important difference between these models is the soil layering, which has not been applied in the theoretical model established in Chapter 3. The low permeability layer in the field, starting at a depth of 1.7 m below surface, limits free downward movement of the mixing zone effectively. Whereas this layer did not influence the average lens thickness that much (Box 7.1), its effect cannot be neglected in assessment of the mixing zone thickness and its dynamics.

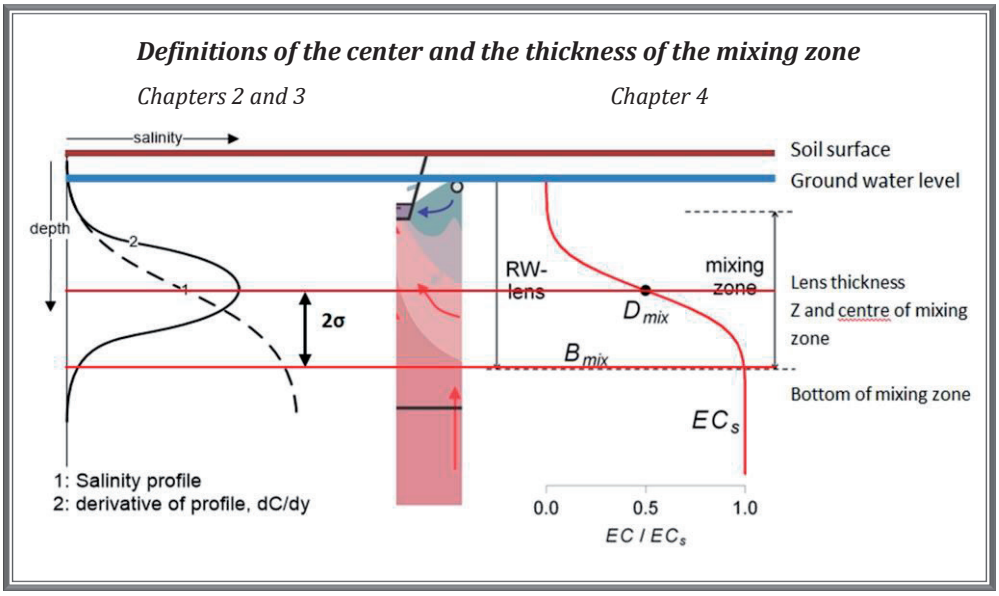

Box 7.3: Illustrating the very similar definitions of thickness of both the lens and the mixing zone in different Chapters. The left part shows spatial moments used in Chapter 2 and 3. The right part shows the measurement-based approach in Chapter 4.

The effect of soil layering should be taken into account when applying the results of Chapter 3 to a field situation. The water level dynamics observed in the field however, are well comparable to the dynamics found in the simulated mixing zone thickness, when defining the upper half of the mixing zone as two standard deviations above the mean (Box 7.3). Since the mixing zone center is relatively stable, dynamics of the upper half of the mixing zone are close to the water level fluctuations. Their similarity to numerical outcomes of variations in thickness of the mixing zone increases my confidence that soil layering is the main disturbing factor in predicting the mixing zone dynamics.

The modelled dynamics of the rainwater lens based on field data (Chapter 4) have been used to get an appreciation of how this would affect profiles of interaction of exchanging cations in lenses. The very low velocity of this process, nearly stagnant

towards the bottom of the mixing zone, in line with the observations in Chapter 4, is qualitatively reflected in the soil samples that were analysed. Deeper samples show a smaller change since the saline conditions were replaced by the vertical oscillating pattern of fresh and saline water. The combination of physical and chemical processes leads to an exchange pattern of the main ions that is complex. However, I show that it can be explained and understood from basic exchange theory, combined with mixing caused by the vertically oscillating flow direction. Though still reduced in complexity, the gained understanding may support the interpretation of a more complex set of chemical data to analyze for example also redox reactions, availability of nutrients and quality effects on surface water that drains from a field.

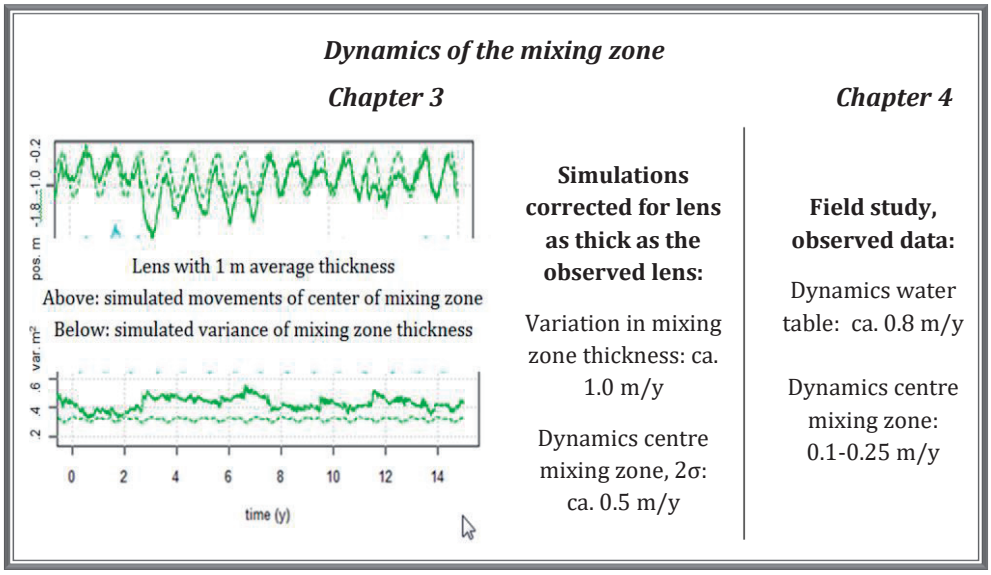

Box 7.4: Simulated and observed variations in mixing zone position and thickness caused by natural recharge variation.

Given the negligible effect of seasonal variation on the slow exchange processes, a steady state approximation of the current average lens thickness, may well be used to estimate the exchange pattern in a lens. Much more important than the short term variation, is some knowledge on the long term drainage history, which can help in estimating the exchange development since the lens has developed. Another more important feature is the actual quality of the seepage water at a specific site, since we showed its influence on the exchange also on the longer term (i.e. centuries). When long-term predictions of system changes are needed, the convolution based system change (Chapter 3) can be applied, for the physical response. For exchange this is not the case for two reasons: (1) this exchange is strongly nonlinear and (2) time scales are at least a factor 10 larger.

Concerning drain water quality, a first assessment is provided in the cation exchange study of Chapter 5. It shows that flow rates from the groundwater and atmosphere

reach a relatively stable situation within a few years, leading to drainage water variations that can be attributed to weather variations. This variation on the short term is rather large, as shown in the field (Chapter 4). However, this is a consequence of mixing with more/less recharge water with the more constant seepage flux. The cation exchange development shows that exchange processes are not expected to cause large or sudden changes in water quality, both in the root zone and in the drains. Redox and nutrient related processes may, of course, influence this result.

The relation between saline groundwater and salt stress depends for a large part on climate and soil type. Dryer, warmer climates cause more salt stress to occur. For groundwater salinities as found in the sites in Zeeland, both weather and soil type significantly influence salt stress, however, this stress is minor compared to that caused by drought and wet conditions. The importance of soil again raises the question concerning the influence on soil layering, which was not taken into account in this study. Vegetation tolerance does not play a role, which can be attributed to large gap between plant tolerance and the salinity of the groundwater (the latter is approximately three times higher). The actual stress caused by saline water is small in this study, which was aimed at discriminating between less and more influencial parameters rather than calculating the actual crop loss. This small stress however suggests that for lower groundwater salinities, like for example in the north of The Netherlands, large negative effects of salt stress are not likely to occur.

7.4 Implications for water management

The findings in Chapter 2 and 3 can be used in various ways to assess local development of rainwater lenses, and the best water management options to increase sustainability. Water management often takes place on a regional rather than a field scale, as the latter is often small compared to water management units. Upscaling of local lens systems behaviour to a regional water system, based on the physical relations found has been brought a step closer, and some of this upscaling was already investigated by Pauw et al. (2015) and Stofberg et al. (2016).

This research shows that agriculture of fresh water dependent natural vegetation will most likely be sustainable for a long time. Risks will increase, however, especially in case of long dry (hot) spells. In Mediterranean climates, salt damage may go hand in hand with drought stress. Then, besides water availability, also the persistence of a lens (i.e. fresh water) is crucial. This thesis allows both assessment of the variation of the lens thickness and of mixing zone thickness due to varying atmospheric forcing. This gives a first indication of situations in which damage, due to disappearing (non-persistent) lenses can be expected. We also show the relative effect of hydrogeologic, atmospheric and plant related parameters on salinity damage to vegetation. Together, these can be used to identify areas where measures to prevent salinity induced

vegetation stress need to be taken and which type of measures (i.e. influencing water, soil or vegetation) may be most effective.

In Chapter 6, the influence of soil type on vegetation damage in case of saline groundwater, does open a door towards different types of measures that could increase sustainability of agricultural areas. Ways to improve water storage in the soil and enhance infiltration of rainwater, for example by improving soil structure through changes in tillage and increasing organic matter in the soil. Such measures can help in decreasing salinity induced damage, thereby increasing their cost efficiency. Concerning vegetation characteristics, a shallow root system could be a solution in case of shallow saline groundwater. This requires the possibility to irrigate with fresh water though, since drought stress will become more severe. Increasing salt tolerance of crops is only useful where the groundwater has a salinity that is close to realistic tolerance levels. For example in the western and northern coastal zones of the Netherlands, geology and historical flooding have led to subsoil groundwater levels which are less saline then were studied.

7.5 Outlook

Although it was shown that the volume of rainwater lenses can be anticipated upon with relatively simple means, this is the case for homogeneous soil profiles. When assessing the variations in thickness, most noticeable in the mixing zone, the effect of hydrogeology, mainly variations in soil hydraulic conductivities, requires more attention. Variations in mixing zone thickness may affect the quality of water available for vegetation during dry spells, and we found that the effect of weather is suppressed by layers of low conductivity. Quantifying this, and finding for example correction factors for thickness variation of the mixing zone based on position and conductivity of low permeability layers would enable extension of a quick analysis to seasonal variations in water quantity and quality (with respect to salinity). It would allow estimation of minimum lens thickness on a local scale, now and in the future, based on easily accessible data. Especially layers that are too shallow or too thin to completely impede infiltration need to be investigated for their actual influence as a function of their position, thickness and conductivity.

The influence of organic matter on the soil chemistry may be of significant importance in areas where peat layers in the shallow subsoil are found within the mixing zone. This may influence the outcomes of the hydrogeochemical study presented in this thesis, affecting e.g. carbonate equilibria, redox potential and pH: gross factors in soil chemistry. We could show for the study site, containing very little peat, that precipitation of calcium as affected by carbonate equilibria, was not to be expected. As organic matter influences redox reactions, this balance could shift and precipitation of calcium could have impact on cation exchange as well.

Many stake holders are well aware of the big knowledge gap concerning the sensitivity of plants to salinity and their potential to survive and grow on brackish water. We are approaching a point where predicting the salinity of groundwater and its effects on root zone salinity are not the main unknowns, and focus will have to shift to the effects on crops and vegetation of different types and in different stages of development. This is apparent from the current debate on crop and botanic species and their salinity tolerances. Both fundamental understanding on how to combine salt and drought stress (Vermue et al., 2013), how to deal with their variability as a function of depth (Kuhlmann et al. 2007) and sensitivity of botanic species to begin with (Stofberg et al., 2015) is poor. Not surprisingly, this resulted in a re-assessment of how to deal with the impact of salinity on primary production in the Netherlands. (STW/Ministry I&M funded WaterNexus). Chapter 6 is a small pilot compared to the research needed to appropriately quantify the influence of saline (ground)water on vegetation.

BIBLIOGRAPHY

Abarca, E., J. Carrera, X. Sánchez-Vila, M. Dentz. 2007. Anisotropic dispersive Henry problem. Advances in Water Resources 30(4): 913-826.

Acharya, R.C., S.E.A.T.M. van der Zee, A. Leijnse. 2005. Transport modeling of nonlinearly sorbing solutes in physically heterogeneous pore networks. Water Resources Research 41(2). doi: 10.1029/2004WR003500.

Alvarez M.D.P., C.E. Dapeña. 2015. The role of evapotranspiration in the groundwater hydrochemistry of an arid coastal wetland (Península Valdés, Argentina). Science of the Total Environment Journal 506: 299-307.

Andersen, P.F., J.W. Mercer, H.O. White jr. 1988. Numerical modeling of salt water intrusion at Hallandale, Florida. Ground Water 26: 619-630.

Antonellini, M., P.N. Mollema. 2009. Impact of groundwater salinity on vegetation species richness in the coastal pine forests and wetlands of Ravenna, Italy. Ecological Engineering 36: 1201–1211.

Appelo C.A.J., D. Postma. 2005. Geochemistry, Groundwater and Pollution. Balkema Publishers, Leiden, 649 p.

Archie, G.E. 1942. The electrical resistivity log as an aid in determining some reservoir characteristics. Petroleum Transactions of AIME 146: 54–62.

Badon Ghyben, W. 1688. Nota in verband met de voorgenomen putboring nabij Amsterdam. Tijdschrift Van Koninklijk Instituut Van Ingenieurs 5: 8–22. (in Dutch)

Bakker, M. 2000. The size of the freshwater zone below an elongated island with infiltration. Water Resources Research 36: 109-117.

Bartholomeus, R.P., J.P.M. Witte, P.M. van Bodegom, J.C. van Dam, R. Aerts. 2008. Critical soil conditions for oxygen stress to plant roots: Substituting the Feddes-function by a process-based model. Journal of Hydrology 360(1): 147-165.

Bates, B.C., Z.W. Kundzewicz, S. Wu, J.P. Palutikof. 2008. Eds. IPCC Technical Paper VI, Climate change and water. IPCC Secretariat, Geneva, 210 p.

Bear, J. 1972. Dynamics of fluids in porous media. American Elsevier, New York, 764 p.

Benini L., M. Antonellini, M. Laghi, P.N. Mollema. 2015. Assessment of water resources availability and groundwater salinization in future climate and land use change scenarios: a case study from a coastal drainage basin in Italy. Water Resources Management 30(2): 731-745.

BMNED. 2011. Geotechnical research for CLIWAT pilot area B (climate change and water). Report 0100685/ 071032292, rev. B. (in Dutch)

Boekelman, R.H. 2001. Development of freshwater lenses, Proc. 16th Salt Water Intrusion Meeting, Miedzyzdroje, Wolin Island, Poland, 5–9.

Bolt, G.H., M.G.M. Bruggenwert. 1976. Soil chemistry, A. Basic Elements. Elsevier, Amsterdam, 271p.

Bolt, G.H. 1982. Movement of solutes in soil: Principles of adsorption/exchange chromatography. In: Soil Chemistry, B. Physico-Chemical Models, Bolt, G.H. (Ed.), Elsevier, Amsterdam, The Netherlands, 285–348, 538 p.

Bruggeman, G.A. 1999. Analytical solutions of geohydrological problems. Elsevier, Amsterdam, 956 p.

Cartwright, N., L. Li, P. Nielsen. 2004. Response of the salt–freshwater interface in a coastal aquifer to a wave-induced groundwater pulse: field observations and modeling. Advances in Water Resources 27: 297-303.

Childs, E.C. 1969. An introduction to the physical basis of soil water phenomena. Wiley, London, 493 p.

Cirkel, D.G., S.E.A.T.M. van der Zee, J.C.L. Meeussen. 2014. Front spreading with nonlinear sorption for oscillating flow. Water Resources Research 51: 2986–2993.

Cirkel, D.G., C.G.E.M. Van Beek, J.P.M. Witte, S.E.A.T.M. van der Zee. 2014. Sulphate reduction and calcite precipitation in relation to internal eutrophication of groundwater fed alkaline fens. Biogeochemistry 117: 375-393.

Colombani N., M. Mastrocicco, B.M.S. Giambastiani. 2014. Predicting salinization trends in a lowland coastal aquifer: Comacchio (Italy). Water Resources Management 29: 603–618.

Collins, W.H., D.H. Easley. 1999. Fresh-water lens formation in an unconfined barrier-island aquifer. Journal of the American Water Resources Association 35: 1-22.

Custodio, E., G.A. Bruggeman. 1987. Groundwater Problems in Coastal Areas. Studies and Reports in Hydrology, UNESCO, International Hydrological Programme, Paris. 596 p.

Dagan, G. 1989. Flow and transport in porous formations. Springer Verlag, Heidelberg, 465 p.

Davis, J.C. 1973. Statistics and data analysis in Geology. Wiley & Sons, New York, 550 p.

Day, J.W., D. Pont, P.F. Hensel, C. Ibañez. 1995. Impacts of Sea-Level Rise on Deltas in the Gulf of Mexico and the Mediterranean: The Importance of Pulsing Events to Sustainability. Estuaries 18: 636-647.

De Jong van Lier, Q., J.C. van Dam, K. Metselaar. 2008. Root water extraction under combined water and osmotic stress. Soil Science Society of America Journal 73(3): 862-875.

De Josselin de Jong, G., C.J. Van Duyn. 1986. Transverse dispersion from an originally sharp fresh-salt interface caused by shear flow. Journal of Hydrology 84: 55-79.

De Louw, P.G.B., G.H.P. Oude Essink, P.J. Stuyfzand, S.E.A.T.M. van der Zee. 2010. Upward groundwater flow in boils as the dominant mechanism of salinization in deep polders, The Netherlands. Journal of Hydrology 394: 494-506.

De Louw, P.G.B., S. Eeman, B. Siemon, B.R. Voortman, J. Gunnink, E.S. Van Baaren, G.H.P. Oude Essink. 2011. Shallow rainwater lenses in deltaic areas with saline seepage. Hydrology and Earth Systems Sciences 15: 3659–3678.

De Louw, P.G.B., Y. van der Velde, S.E.A.T.M. van der Zee. 2011. Quantifying water and salt fluxes in a lowland polder catchment dominated by boil seepage: a probabilistic end-member mixing approach. Hydrology and Earth Systems Sciences 15: 2101–2117.

De Louw P.G.B., S. Eeman, G.H.P. Oude Essink, E. Vermue, V.E.A. Post. 2013. Rainwater lens dynamics and mixing between infiltrating rainwater and upward saline

groundwater seepage beneath a tile-drained agricultural field. Journal of Hydrology 501: 133–145.

De Louw, P.G.B. 2013. Saline seepage in deltaic areas. Preferential groundwater discharge through boils and interactions between thin rainwater lenses and upward saline seepage. PhD Thesis. Free University of Amsterdam. 202 p.

Delsman, J.R., K.R.M. Hu-a-ng, P.C. Vos, P.G.B. de Louw, G.H.P Oude Essink, P.J. Stuyfzand, M.F.P. Bierkens. 2014a. Paleomodelling of coastal saltwater intrusion during the Holocene: an application to the Netherlands. Hydrology and Earth Systems Sciences 18: 3891-3905.

Delsman, J.R., M.J. Waterloo, M. Groen, P. Stuyfzand. 2014b. Investigating summer flow paths in a Dutch agricultural field using high frequency direct measurements. Journal of Hydrology 519: 3069-3085.

Delsman, J.R. 2015. Saline groundwater-surface water interaction in coastal lowlands. PhD Thesis. Free University of Amsterdam. 194 p.

De Wit, C.T. 1958. Transpiration and Crop yields. Agricultural Research Reports 64.6, Pudoc, Wageningen, 88 p.

Eeman, S., A. Leijnse, P.A.C. Raats, S.E.A.T.M. van der Zee. 2011. Analysis of the thickness of a fresh water lens and of the transition zone between this lens and upwelling saline water. Advances in Water Resources 34: 291–302.

Eeman, S., S.E.A.T.M. van der Zee, A. Leijnse, P.G.B. de Louw, C. Maas. 2012. Response to recharge variation of thin rainwater lenses and their mixing zone with underlying saline groundwater. Hydrology and Earth System Sciences 16: 3535-3549.

Eeman, S., P.G.B. de Louw and S.E.A.T.M. van der Zee. 2016. Cation exchange in a temporally fluctuating thin fresh water lens on top of saline groundwater. Hydrogeology Journal. doi:10.1007/s10040-016-1475-y.

Ernst, L.F. 1962. Grondwaterstromingen in de verzadigde zone en hun berekening bij aanwezigheid van horizontale evenwijdige open leidingen. Verslagen van Landbouwkundige Onderzoekingen 67(15) Pudoc, Wageningen. 185 p. (in Dutch)

Feddes, R., P. Kabat, P.J.T. van Bakel, J.J.B. Bronswijk, J. Halbertsma. 1988. Modelling soil water dynamics in the unsaturated zone - state of the art. Journal of Hydrology 100: 69-104.

Feseker T. 2007. Numerical studies on saltwater intrusion in a coastal aquifer in northwestern Germany. Hydrogeology Journal 15: 267–279.

Fetter, C.W. 1972. Position of the saline water interface beneath oceanic islands. Water Resources Research 8: 1307-1314.

Fiori, A., G. Dagan. 2000. Concentration fluctuations in aquifer transport: a rigorous first-order solution and applications. Journal of Contaminant Hydrology 45: 139–163.

Flowers, T.J. 2004. Improving crop salt tolerance. Journal of Experimental Botany 55: 307–319.

Foppen, J.W., J. Griffioen. 1995. Contribution of groundwater outflow to the phosphate balance of ditch water in a Dutch polder. In: Proceedings of a Boulder Symposium,

Man 's Influence on Freshwater Ecosystems and Water Use, IAHS Publication no. 230.

Friedman, P.S. 2005. Soil properties influencing apparent electrical conductivity: a review. Computers and Electronics in Agriculture 46: 45–70.

Gelhar, L.W., C. Welty, K.R. Rehfeldt. 1992. A critical review of data on field-scale dispersion in aquifers. Water Resources Research 28: 1955-1974.

Giambastiani, B.M.S., M. Antonellini, G.H.P. Oude Essink, R.J. Stuurman. 2007. Saltwater intrusion and water management in the unconfined coastal aquifer of Ravenna (Italy): a numerical model. Journal of Hydrology 340: 91–104.

Gillman, G.P. 1979. A proposed method for the measurement of exchange properties of highly weathered soils. Australian Journal of Soil Research 17: 129-139.

Goes, B.J.M., G.H.P. Oude Essink, R.W. Vernes, F. Sergi. 2009. Estimating the depth of fresh and brackish groundwater in a predominantly saline region using geophysical and hydrological methods, Zeeland, The Netherlands. Near Surface Geophysics 7: 401–412.

GO-FRESH. visited in May 2016. https://publicwiki.deltares.nl/display/ZOETZOUT/GO-FRESH+-Valorisatie+kansrijke+ oplossingen+robuuste+zoetwatervoorziening.

Govindaraju, R.S., B.S. Das. 2007. Moment analysis for subsurface hydrologic applications. Water science and technology library Volume 61, Springer, Dordrecht. 296 p.

Habibullah, M., A.U. Ahmed, Z. Karim. 1999. Assessment of food grain production loss due to climate induced enhanced soil salinity. In: Decision criteria and optimal inventory processes, B. Liu, A.O. Esogbue (Eds.). Kluwer Academic Publishers, Dordrecht, The Netherlands. 55-70, 210 p.

Hantush, M.S. 1968. Unsteady movement of fresh water in thick unconfined saline aquifers. Hydrological Sciences Journal 13(2): 40-60.

Harbough, A.W., E.R. Banta, M.C. Hill, M.G. McDonald. 2000. MODFLOW-2000, the U.S. Geological Survey modular ground-water model- User guide to modularization concepts and the groundwater flow process. U.S. Geological Survey Open-File Report 00-92, 121 p.

Henry, H.R. 1964. Effects of dispersion on salt encroachment in coastal aquifers. US Geological Survey Water Supply Paper 1613-C, 71-84.

Herzberg, A. 1901. Die Wasserversorgung einiger Nordseebäder. Journal Gasbeleucht. Wasserversorg. 44: 815–819. (In German)

Hooghoudt, S.B. 1937. Bijdragen tot de kennis van eenige natuurkundige grootheden van de grond 6. Verslagen van Landbouwkundige Onderzoekingen 43: 461–676. (in Dutch)

Janssen, G.M.C.M., O.A. Cirpka, S.E.A.T.M. van der Zee. 2006. Stochastic analysis of non-linear biodegradation in regimes controlled by both chromatographic and dispersive mixing. Water resources Research 42: W01417.

Jelgersma, S. 1996. Land subsidence in coastal lowlands. In: Sea level rise and coastal subsidence, Causes, consequences and strategies. Milliman, J.D., Haq, B.U. (Eds.). Kluwer academic publishers, Dordrecht. 370 p.

Jolly, I.D., K.L. McEwan, K.L. Holland. 2008. A review of groundwater-surface water interactions in arid/semi-arid wetlands and the consequences of salinity for wetland ecology. Ecohydrology 1: 43–58, 2008.

Kacimov, A.R. 2008. On the Maas problem of seawater intrusion combated by infiltration. Journal of Hydrology 358: 354-358.

Kaleris, V., G. Lagas, S. Marczinek, J.A. Piotrowski. 2002. Modelling submarine groundwater discharge: an example from the western Baltic Sea. Journal of Hydrology 265: 76–99.

Kaleris, V. 2006. Submarine groundwater discharge: Effects of hydrogeology and of near shore surface water bodies. Journal of Hydrology 325: 96–117.

Katerji, N., J.W. van Hoorn, A. Hamdy, M. Mastrorilli. 2003. Salinity effect on crop development and yield, analysis of salt tolerance according to several classification methods. Agricultural Water Management 62: 37–66.

Keary, P., M. Brooks. 1991. An Introduction to Geophysical Exploration, 2nd edition, Blackwell Science, London, 254 p.

Kiro, Y., Y. Yechieli, V. Lyakhovsky, E. Shalev, A. Starinsky. 2008. Time response of the water table and saltwater transition zone to a base level drop. Water Resources Research 44: W12442.

KNMI: https://data.knmi.nl/datasets. Visited several times between 2010-2016.

Kroes, J.G., J.C. van Dam, P. Groenendijk, R.F.A. Hendriks, C.M.J. Jacobs. 2008. SWAP version 3.2. Theory description and user manual. Alterra Report1649. 262 p.

Kuhlmann, A., I. Neuweiler, S.E.A.T.M. van der Zee, R. Helmig. 2012. Influence of soil structure and root water uptake strategy on unsaturated flow in heterogeneous media. Water Resources Research 48: W02534.

Landman, A.J., R.J. Schotting. 2007. Heat and brine transport in porous media: the Oberbeck Boussinesq approximation revisited. Transport in Porous Media 70: 355-373.

Langevin, C.D., W.B. Shoemaker, W. Guo. 2003. MODFLOW-2000, the U.S. Geological Survey modular ground-water model–documentation of the SEAWAT-2000 Version with the Variable-Density Flow Process (VDF) and the integrated MT3DMS transport process (IMT). U.S. Geological Survey Open-File Report 03-426, 43 p.

Langevin, C.D., M. Zygnerski. 2013. Effect of sea-level rise on salt water intrusion near a coastal well field in southeastern Florida. Ground Water 51:781–803.

Lebbe, L. 1999. Parameter identification in fresh-saltwater flow based on borehole resistivities and freshwater head data. Advances in Water Resources 22: 791–806.

Lebbe, L., N. Van Meir, P. Viaene. 2008. Potential implications of sea-level rise for Belgium. Journal of Coastal Research 24: 358–366.

Maas, C. 2007. Influence of climate change and sea level rise on a Ghijben Herzberg lens. Journal of Hydrology 347: 223-228.

Maas, E.V., G.J. Hoffman. 1977. Crop salt tolerance – current assessment. ASCE Journal of Irrigation Drainage Division 103, 115–134.

Maas, E.V. 1990. Crop salt tolerance. In 'Agricultural salinity assessment and management', K.K. Tanji (Ed.). ASCE Manuals and Reports on Engineering practice 71, New York.

Makkink, G.F. 1957. Testing the Penman formula by means of lysimeters. Journal of the Institution of Water Engineers 11: 277-288.

Marconi V., M. Antonellini, E. Balugani, E. Dinelli. 2011. Hydrogeochemical characterization of small coastal wetlands and forests in the Southern Po plain (Northern Italy). Ecohydrology 4(4): 597-607.

McNeill, J.D. 1980. Electromagnetic terrain conductivity at low induction numbers. Geonics Ltd. Technical Note TN-6, Geonics Ltd., Mississauga, Ontario.

Meinardi, C.R. 1983. Fresh and brackish groundwater under coastal areas and islands. GeoJournal 7(5): 413–425.

Meisler, H., P.P. Leahy, L.L. Knobel. 1984. Effect of eustatic sea level changes on saltwater-freshwater relations in the Northern Atlantic coastal plain. U.S. Geological Survey Water-Supply Paper 2255.

Mollema P.N., M. Antonellini, E. Dinelli, G. Gabbianelli, N. Greggio, P.J. Stuyfzand. 2013. Hydrochemical and physical processes influencing salinization and freshening in Mediterranean low-lying coastal environments. Applied Geochemistry 34: 207-221.

Navoy, A.S. 1991. Aquifer-estuary interaction and vulnerability of groundwater supplies to sea level rise-driven saltwater intrusion. PhD Thesis. Pennsylvania State University.

NIST Chemistry WebBook. 2015. NIST Standard Reference Database Number 69. United States of America.

Olver, F.W., D.W. Lozier, R.F. Boisvert, C.W. Clark. 2010. NIST handbook of mathematical functions. Cambridge University Press, New York, 951 p.

Olsthoorn, T N. 2008. Do a bit more with convolution. Ground Water 46: 13-22.

Osterkamp, S., D. Kraft, M. Schirmer. 2001. Climate change and the ecology of the Weser estuary region: assessing the impact of an abrupt change in climate. Climate Research 18: 97-104.

Oude Essink, G.H.P. 1996. Impact of sea level rise on groundwater flow regimes, a sensitivity analysis for the Netherlands. PhD Thesis. Technical University Delft.

Oude Essink, G.H.P. 1998. MOC3D adapted to simulate 3D density-dependent groundwater flow. MODFLOW ’98, Golden, Colorado,vol. I: 291-303.

Oude Essink, G.H.P. 2000. Density dependent groundwater at the Island of Texel, The Netherlands. 16th Salt Water Intrusion Meeting, Miedzyzdroje, Poland.

Oude Essink, G.H.P. 2001. Salt water intrusion in a three-dimensional groundwater system in the Netherlands: a numerical study. Transport in Porous Media 43: 137-158.

Oude Essink, G.H.P., E.S. van Baaren, P.G.B. de Louw. 2010. Effects of climate change on coastal groundwater systems: A modeling study in the Netherlands. Water Resources Research 46: W00F04.

Parker, J.C., A.J. Vallocchie. 1986. Constraints on the validity of equilibrium and first-order kinetic transport models in structured soils. Water Resources Research 22: 399-407.

Parkhurst, D.L., C.A.J. Appelo. 1999. User's guide to PHREEQC (version 2)—a computer program for speciation, batch-reaction, one-dimensional transport and inverse chemical calculations. Water Resources Investigations Report 99-4259.

Paster, A., G. Dagan. 2007. Mixing at the interface between two fluids in porous media: a boundary layer solution. Journal Fluid Mechanics 584: 455–472.

Paster, A., G. Dagan. 2008. Mixing at the interface between fresh and salt waters in 3D steady flow with application to a pumping well in a coastal aquifer. Advances in Water Resources 31: 1565–1577.

Pauw, P.S., S.E.A.T.M. van der Zee, A. Leijnse, J.R. Delsman, P.G.B. de Louw, W.J. de Lange, G.H.P. Oude Essink. 2014. Low-resolution modeling of dense drainage networks in confining layers. Groundwater 53(5): 771-781.

Pauw, P.S. 2015. Field and model investigations of fresh water lenses in coastal aquifers. PhD Thesis. Wageningen University.

Pauw, P.S., E.S. van Baaren, M. Visser, P.G.B. de Louw, G.H.P. Oude Essink. 2015a. Increasing a fresh water lens below a creek ridge using a controlled artificial recharge and drainage system: a case study in the Netherlands. Hydrogeology Journal 23 (7): 1415-1430.

Pauw, P.S., A. Leijnse, S.E.A.T.M. van der Zee, G.H.P. Oude Essink. 2015b. Salt water upconing due to cyclic pumping by finite horizontal wells in freshwater lenses. Groundwater. doi: 10.1111/gwat.12382.

Post, V.E.A. 2004. Groundwater salinization processes in the coastal area of The Netherlands due to transgressions during the Holocene. PhD Thesis. Free University of Amsterdam.

Post V.E.A., H. Kooi. 2003. Rates of salinization by free convection in high-permeability sediments: Insights from numerical modelling and application to the Dutch coastal area. Hydrogeology Journal 11: 549-559.

Post V.E.A., H. Kooi, C.T. Simmons. 2007. Using hydraulic head measurements in variable-density ground water flow analyses. Ground Water 45: 664-671.

Post, V.E.A., E. Abarca. 2010. Saltwater and freshwater interactions in coastal aquifers. Hydrogeology Journal 18: 1–4.

Prommer H., V.E.A. Post. 2010. A reactive multicomponent transport model for saturated porous media. User's Manual v2.10.

Raats, P.A.C. 2015. Salinity management in the coastal region of the Netherlands: A historical perspective. Agricultural Water Management 157: 12-30.

Robinson, C., L. Li, D.A. Barry. 2007. Effect of tidal forcing on a subterranean estuary. Advances in Water Resources 30: 851-865.

Röper T., K.F. Kröger, H. Meyer, J. Sültenfuss, J. Greskowiak, G. Massmann. 2012. Groundwater ages, recharge conditions, and hydrochemical evolution of a barrier island freshwater lens (Spiekeroog, Northern Germany). Journal of Hydrology 454-455: 173-186.

Rozema, J., T. Flowers. 2008. Crops for a salinized world. Science 322: 1578–1582.

Ruppel, C., G. Schultz, S. Kruse. 2000. Anomalous fresh water lens morphology on a strip barrier island, Ground Water 38: 872-881.

Sakr, S.A. 1999. Validity of a sharp-interface model in a confined coastal aquifer. Hydrogeology Journal 7: 155-160.

Schot, P.P., S.C. Dekker, A. Poot. 2004. The dynamic form of rainwater lenses in drained fens. Journal of Hydrology 293: 74–84.

Scott, C.A., S. Vicuña, I. Blanco Gutiérrez, F. Meza, C. Varela Ortega. 2014. Irrigation efficiency and water-policy implications for river-basin resilience. Hydrology and Earth System Sciences 18(4): 1339-1348.

Siemon, B., A.V. Christiansen, E. Auken. 2009. A review of helicopter-borne electromagnetic methods for groundwater exploration. Near Surface Geophysics 7: 629–646.

Siemon, B., A. Ullmann, I. Mitreiter, M. Ibs-von Seht, W. Voß, J. Pielawa. 2011. Airborne geophysical investigation of CLIWAT pilot areas, survey area Schouwen, The Netherlands. Technical Report.

Sikkema, P.C., J.C. van Dam. 1982. Analytical formulae for the shape of the interface in a semi-confined aquifer. Journal of Hydrology 56: 201–220.

Simmons, C.T. 2005. Variable density groundwater flow: From current challenges to future possibilities. Hydrogeoly Journal 13: 116–119.

Skaggs, T.H., M.T. van Genuchten, P.J. Shouse, J.A. Poss. 2006. Macroscopic approaches to root water uptake as a function of water and salinity stress. Agricultural Water Management 86(1): 140-149.

Stafleu, J., D.M. Maljers, J.L. Gunnink, A. Menkovic, F.S. Busschers. 2011. 3-D modelling of the shallow subsurface of Zeeland, the Netherlands. Netherlands Journal of Geosciences 90 (4): 293-310.

Stephens B.D., K.C. Hsu, M.A. Prieksat, M.D. Ankeny, N. Blandford, T.L. Roth, J.A. Kelsey, J.R. Whitworth. 1998. A comparison of estimated and calculated effective porosity. Hydrogeology Journal 6: 156–165.

Steppuhn, H., M.T. van Genuchten, C.M. Grieve. 2005. Root-zone salinity. I. Selecting a product-yield index and response function for crop tolerance. Crop Science 45: 209–220.

Stofberg, S.F., G.H.P. Oude Essink, P.S. Pauw, P.G.B. de Louw, A. Leijnse, S.E.A.T.M. van der Zee. 2016. Fresh water lens persistence and root zone salinization hazard under temperate climate. Water Resources Management. doi: 10.1007/s11269-016-1315-9

Stuyfzand, P.J. 1993. Hydrochemistry and hydrology of the coastal dune area of the western Netherlands. PhD Thesis. Free University Amsterdam.

Stuyfzand, P.J., R.J. Stuurman. 1994. Recognition and genesis of various brackish to hypersaline groundwaters in The Netherlands. In: Proc. 13th Salt Water Intrusion Meeting, Barrocu, G. (Ed.), University of Cagliari, Sardinia, 125–136, 377 p.

Tan K. 1996. Soil sampling, preparation and analysis. Marcel Dekker Inc, New York, 408 p.

Technical Report. 2011. Interreg IVB Project: CLIWAT – Adaptive and sustainable water management and protection of society and nature in an extreme climate. BGR Archives-No. 0129932, Hannover.

Tiemeyer, B., R. Moussa, B. Lennartz, M. Voltz. 2007. MHYDASDRAIN: A spatially distributed model for small, artificially drained lowland catchments. Ecological Modeling 209: 2–20.

Underwood, M.R., F.L. Peterson, C.I. Voss. 1992. Groundwater lens dynamics of atoll islands. Water Resources Research 28(11): 2889-2902.

Vaeret, L. 2008. Responses to global change and management actions in coastal groundwater resources, Maputaland, Southeast Africa. PhD Thesis. Norwegian University of Life Sciences.

Vaeret, L., A. Leijnse, F. Cuamba, S. Haldorsen. 2012. Holocene dynamics of the salt-fresh groundwater interface under a sand island, Inhaca, Mozambique. Quaternary International 257: 74-82.

Van Baaren, E.S., G.H.P. Oude Essink, G.M.C.M. Janssen, P.G.B. de Louw, R. Heerdink, B. Goes. 2011. Freshening/ salinization of phreatic groundwater in the province of Zeeland: Results of a 3-D-density dependent groundwater model. Deltares Report. (in Dutch)

Van Dam, J.C., P.C. Sikkema. 1982. Approximate solution of the problem of the shape of the interface in a semi-confined aquifer. Journal of Hydrology 56: 221–237.

Vandenbohede, A., K. Luyten, L. Lebbe. 2008. Effects of global change on heterogeneous coastal aquifers: a case study in Belgium. Journal of Coastal Research 24: 160-170.

Vandenbohede, A., L. Lebbe. 2007. Effects of tides on a sloping shore: Groundwater dynamics and propagation of the tidal wave. Hydrogeology Journal 15: 645–658.

Van den Hurk, B., A. Klein Tank, G. Lenderink, A. van Ulden, G.J. van Oldenborgh, C. Katsman, H. van den Brink, F. Keller, J. Bessembinder, G. Burgers, G. Komen, W. Hazeleger, S. Drijfhout. 2006. KNMI Climate Change Scenarios 2006 for the Netherlands. KNMI, De Bilt, Scientific Report WR 2006-01.

Van den Eertwegh, G.A.P.H., J.L. Nieber, P.G.B. de Louw, H.A. van Hardeveld, R. Bakkum. 2006. Impacts of drainage activities for clay soils on hydrology and solute loads to surface water. Irrigation and Drainage 55: 235–245.

Van de Plassche, O. 1982. Sea-level change and water-level movements in the Netherlands during the Holocene. Mededelingen Rijks Geologische Dienst 36: 1–93.

Van der Meij, J.L., B. Minnema. 1999. Modelling of the effect of a sea-level rise and land subsidence on the evolution of the groundwater density in the subsoil of the northern part of the Netherlands. Journal of Hydrology 226: 152–166.

Van der Veer, P. 1977. Analytical solution for steady interface flow in a coastal aquifer involving a phreatic surface with precipitation. Journal of Hydrology 34: 1-11.

Van der Velde, Y., G.H. de Rooij, P. Torfs. 2009. Catchment-scale non-linear groundwater-surface water interactions in densely drained lowland catchments. Hydrology and Earth Systems Sciences 13: 1867–1885.

Van de Ven, G.P. (Ed.). 2003. Man-made lowlands, history of water management and land reclamation in The Netherlands, Matrijs, Utrecht. 336 p.

Van Dijke, M.IJ., S.E.A.T.M van der Zee. 1998a. Analysis of oil lens removal by extraction through a seepage face. Computational Geoscience 2: 47-72.

Van Dijke, M.IJ. ,S.E.A.T.M van der Zee. 1998b. Modeling of Air Sparging in a Layered Soil: Numerical and Analytical Approximations. Water Resources Research 34: 341–353.

Van Duijn, C.J., R.J. Schotting. 1998. Brine transport in porous media: On the use of Von Mises and similarity transformations, Computational Geoscience 2: 125-149.

Van Genuchten, M.Th. 1980. A closed form equation for predicting the hydraulic conductivity of unsaturated soils. Soil Science Society of America Journal 44: 892-898.

Van Genuchten, M.Th., F.M. Dalton. 1986. Models for simulating salt movement in aggregated field soils, Geoderma 38: 165-183.

Van Meir, N. 2001. Density-dependent groundwater flow: Design of a parameter identification test and 3-D-simulation of sea-level rise. PhD Thesis. Ghent University, Ghent.

Van Rees Vellinga, E., C.G. Toussaint, K.E. Wit. 1981. Water quality and hydrology in a coastal region of The Netherlands. Journal of Hydrology 50: 105–127.

Van Wirdum, G. 1991. Vegetation and hydrology of floating rich fens. PhD Thesis. University of Amsterdam.

Vermue, E., K. Metselaar, S.E.A.T.M. van der Zee. 2013. Modelling of soil salinity and halophyte crop production. Environmental and Experimental Botany 92: 186–196.

Vernes, R.W., T.H.M. van Doorn. 2005. REGIS II, Hydrogeological model of The Netherlands. From guide layer to Hydrogeological Unit. Explanation of the construction of the data set. TNO report NITG 05-038-B. (in Dutch)

Vos, P. and Zeiler, F. 2008. Holocene transgressions of southwestern Netherlands, interaction between natural and antrophogenic processes. Grondboor & Hamer, 3–4. (in Dutch)

Voss, C.I., W.R. Souza. 1987. Variable density flow and solute transport simulation of regional aquifers containing a narrow freshwater-saltwater transition zone. Water Resources research 23: 1851-1866.

Voss, C.I., A.M. Provost. 2008. SUTRA, a model for saturated-unsaturated variable-density groundwater flow with solute or energy transport. Manual, US Geological Survey, Reston, Virginia.

Weast, R.C. 1982. Handbook of chemistry and physics. 63rd ed., CRC Press, Boca Raton.

Weert, F., J. van der Gun, J. Reckman. 2009. Global Overview of saline groundwater occurrence and genesis. Report no. GP 2009-1, IGRAC.

Worland, S.C., G.M. Hornberger, S.L. Goodbred. 2015. Source, transport, and evolution of saline groundwater in a shallow Holocene aquifer on the tidal deltaplain of southwest Bangladesh. Water Resources Research 51(7): 5791-5805.

Wösten, H., F. de Vries, T. Hoogland, H., Massop, A. Veldhuizen, H. Vroon, J. Wesseling, J. Heijkers, A. Bolman. 2013. BOFEK2012, de nieuwe, bodemfysische schematisatie van Nederland. Alterra-rapport 2387 Wageningen UR, Wageningen. (in Dutch)

Zeidler, R.B. 1997. Continental shorelines: climate change and integrated coastal management. Ocean & Coastal Management 37(1): 41-62.

Zheng C., P.P. Wang. 1999. MT3DMS: A modular three-dimensional multispecies transport model for simulation of advection, dispersion, and chemical reactions of contaminants in groundwater systems. Documentation and user's guide. Report SERDP-99-1 University of Alabama, 221 p.

APPENDIX I

Mixing

Particularly if the thickness of the mixing zone between fresh and salt water is of concern, the choice of the dispersivities is important. In Chapter 1 we used dispersivities of 0.25 (longitudinal) and 0.05 (transversal), which comply with reported macro dispersivities for aquifers (Gelhar, 1992; Kaleris, 2006; Kaleris, 2002). The value of the dispersivities that follows from Fiori and Dagan (2000) would easily be one (or more) order(s) of magnitude smaller. The macroscopic values represent pore scale mixing, but also larger scale spatial variability of soil that does not necessarily lead to true mixing. Mostly, those values are derived for two scales of variability (pore scale and scale of variability of hydraulic conductivity in porous formations). Due to exchange of solute between stream tubes with different velocities, stream tube interfaces enhance true mixing (Janssen et al., 2006), similar as mobile/immobile exchange (Van Genuchten and Dalton, 1986; Parker and Vallocchi, 1986; Bolt, 1982).

Larger dispersivities, even after considering their reliability (Gelhar et al., 1992), may be caused by model (including dimensionality), fitting, and experimental bias. For instance, the mixing may well occur in the extraction wells: if wells have a relatively large screen, water from different strata is mixed. Non-invasive techniques, as used for the data of Figure 1b, may lead to apparent mixing by averaging through a limited spatial support of the technique. For instance, in Figure AI.1, we compare simulated and measured mixing zones for two sites at Schouwen-Duiveland (southwestern Netherlands) that we monitored for the past two years (De Louw et al. 2011). Figure AI.1 a illustrates that a dispersivity α_l of 0.25 m (for a moving interface) reflects the observed mixing zone thickness of 1 to 2 m better than the smaller α_l of 0.05 m. However, these larger dispersivities are obtained by fitting a homogeneous 2D model that disregards the actual layering at the sites.

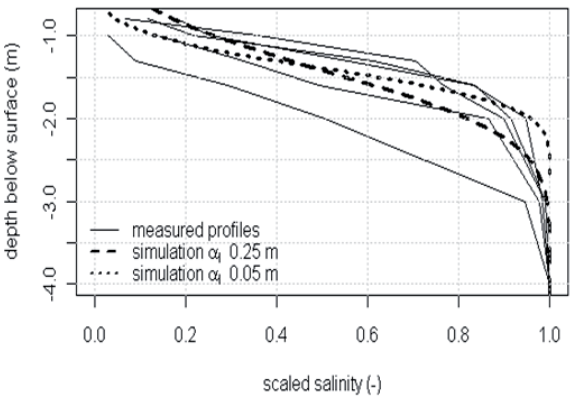

Fig. AI.1: Profiles of salinity as a function of depth for thin lenses. Numerical simulations with different dispersivities are compared to several representative soil profiles measured on two field sites on the island of Schouwen-Duiveland, The Netherlands.

A relatively large effective dispersivity could be caused by different processes. For non-uniform media, the presence of mobile and immobile water regions affects mixing. This leads to a larger effective dispersion coefficient of the form (Parker and Valocchi,1986)

$$\boldsymbol{D}_{eff} = \boldsymbol{D}\phi_m + \frac{(1-\phi_m) r_{agg}^2 v^2}{15\, D_{agg}} \qquad \text{(AI.1)}$$

where the first term on the right side presents the hydrodynamic pore scale dispersion in the mobile phase and the second term gives the extra dispersion caused by the exchange between the mobile and immobile phases. The pore water velocity has a large influence, and is related with the mobile water fraction according to

$$v = \frac{P_s}{n\phi_m} \qquad \text{(AI.2)}$$

The relative magnitude of this exchange process compared to the mobile phase dispersion is shown in Figure AI.2 for r_{agg} from 0.05 to 0.25 m (with $D_{agg} = 10^{-10}$ m^2s^{-1}) and D_{agg} from $5x10^{-11}$ to $5x10^{-10}$ m^2s^{-1} (with $r_{agg} = 0.1$ m). We show, for illustration, parameter combinations that lead to $\alpha_{eff} = D_{eff}/v = 0.1$ m. Average recharge $\langle P \rangle$ is in the order of 0.3-3 mm d^{-1}. The combinations of parameters leading to $\alpha_{eff} = 0.1$ m give plausible values for aggregate size r_{agg}, aggregate diffusivity D_{agg} and mobile phase fraction ϕ_m, whereas $\alpha_{eff} = 0.25$ leads to more extreme values . In view of all above, we use a longitudinal dispersivity of 0.1 m, and a transversal dispersivity of 0.01 m.

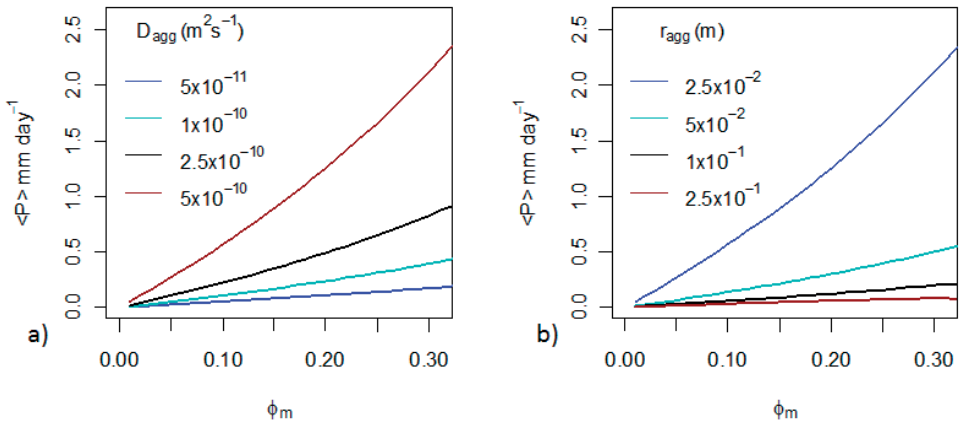

Fig. AI.2: Relations based on Eq. (AII1) between the mobile fraction (ϕ_m), average net precipitation $\langle P \rangle$ and aggregate diffusivity D_{agg} for a given aggregate radius (r_{agg}) of 10-2 m (a) and with aggregate radius (r_{agg}) for a given aggregate diffusivity (D_{agg}) of 10-9 m2s-1 (b), leading to an effective dispersivity (α_{eff}) of 0.1 m.

APPENDIX II

Derivation of the amplitude and delay using convolution theory

The response of the small fresh water lens is assumed to be given by the convolution integral (equation (11)):

$$\bar{z}(t) - \bar{z}(0) = \int_0^t 2P_s(t-\tau)I(\tau)d\tau \qquad \text{(AII.1)}$$

Where the Impulse response function is given by (Eq. 3.4)

$$I(t) = \Delta\, a\, e^{-at} \qquad \text{(AII.2)}$$

The recharge is taken as sinusoidal:

$$P_s = A\sin(2\pi f t) \qquad \text{(AII.3)}$$

Combining AII.1, AII.2 and AII.3 then gives for the reaction of the lens:

$$\bar{z}(t) - \bar{z}(0) = 2Aa\Delta z \int_0^t \sin\{2\pi f(t-\tau)\}\, e^{-a\tau}(\tau)d\tau =$$

$$2Aa\Delta z \int_0^t \{\sin(2\pi f t)\cos(2\pi f\tau) - \cos(2\pi f t)\sin(2\pi f\tau)\}e^{-a\tau}(\tau)d\tau =$$

$$2Aa\Delta z\sin(2\pi f t)\int_0^t \cos(2\pi f\tau)\, e^{-a\tau}(\tau)d\tau - 2Aa\Delta\cos(2\pi f t)\int_0^t \sin(2\pi f\tau)\, e^{-a\tau}(\tau)d\tau \qquad \text{(AII.4)}$$

The following expressions for the integrals are taken from NIST handbook of mathematical functions (page 122, 4.26.7 and 4.26.8)

$$\int_0^t \cos(2\pi f\tau)\, e^{-a\tau}(\tau)d\tau = \left(\frac{e^{-a\tau}}{(2\pi f)^2 + a^2}\{-a\cos(2\pi f\tau) + 2\pi f\sin(2\pi f\tau)\}\right)\Big|_0^t$$
$$= \left(\frac{e^{-at}}{(2\pi f)^2 + a^2}\{-a\cos(2\pi f t) + 2\pi f\sin(2\pi f t)\} + \frac{a}{(2\pi f)^2 + a^2}\right)$$

$$\int_0^t \sin(2\pi f\tau)\, e^{-a\tau}(\tau)d\tau = \left(\frac{e^{-a\tau}}{(2\pi f)^2 + a^2}\{-a\sin(2\pi f\tau) - 2\pi f\cos(2\pi f\tau)\}\right)\Big|_0^t$$
$$= \left(\frac{e^{-at}}{(2\pi f)^2 + a^2}\{-a\sin(2\pi f t) - 2\pi f\cos(2\pi f t)\} + \frac{2\pi f}{(2\pi f)^2 + a^2}\right)$$

For larger values of t, if $at >> 1$, the terms with e^{-at} will become negligible, leading to:

$$\bar{z}(t) - \bar{z}(0) = 2Aa\Delta z \sin(2\pi ft)\frac{a}{(2\pi f)^2 + a^2} - 2Aa\Delta \cos(2\pi ft)\frac{2\pi f}{(2\pi f)^2 + a^2} =$$

$$= \frac{2}{\sqrt{(2\pi f)^2 + a^2}} Aa\Delta z \sin(2\pi ft)\frac{a}{\sqrt{(2\pi f)^2 + a^2}}$$

$$- \frac{2}{\sqrt{(2\pi f)^2 + a^2}} Aa\Delta z \cos(2\pi ft)\frac{2\pi f}{\sqrt{(2\pi f)^2 + a^2}}$$

Defining $\varepsilon = \arctan\frac{2\pi f}{a}$ which gives:

$$\sin(\varepsilon) = \frac{2\pi f}{\sqrt{(2\pi f)^2 + a^2}} \text{ and } \cos(\varepsilon) = \frac{a}{\sqrt{(2\pi f)^2 + a^2}} \qquad \text{(AII.5)}$$

we arrive at the following expression for the lens response to sinusoidal recharge:

$$\bar{z}(t) - \bar{z}(0) = \frac{2}{\sqrt{(2\pi f)^2 + a^2}} Aa\Delta z \sin(2\pi ft)\cos\varepsilon$$

$$- \frac{2}{\sqrt{(2\pi f)^2 + a^2}} Aa\Delta z \cos(2\pi ft)\sin\varepsilon =$$

$$\frac{2Aa\Delta z}{\sqrt{(2\pi f)^2 + a^2}} \sin(2\pi ft - \epsilon) = \frac{2Aa\Delta z}{\sqrt{(2\pi f)^2 + a^2}} \sin\left(2\pi ft - \arctan\frac{2\pi f}{a}\right) =$$

$$\frac{2Aa\Delta z}{\sqrt{(2\pi f)^2 + a^2}} \sin\left(2\pi ft - \arctan\frac{2\pi f}{a}\right) =$$

$$\frac{2Aa\Delta z}{\sqrt{(2\pi f)^2 + a^2}} \sin\left\{2\pi f\left(t - \frac{1}{2\pi f}\arctan\frac{2\pi f}{a}\right)\right\} =$$

$$Q\sin\{2\pi f(t - T)\}$$

Where $Q = \frac{2Aa\Delta z}{\sqrt{(2\pi f)^2 + a^2}}$ and $T = \frac{1}{2\pi f}\arctan\frac{2\pi f}{a}$ (AII.6 or 3.7a, b)

are respectively the amplitude and the delay of the lens response to a sinusoidal recharge pattern.

SUMMARY

Fresh water is generally a limited resource in coastal areas which are often densely populated. In low-lying areas (at or below sea level), groundwater is mostly saline and agriculture and freshwater nature depend on a thin lens of rainwater that is formed by precipitation surplus on top of the saline, upward seeping groundwater. Understanding the dynamics of such lenses is vital for sustainable food production and development of natural vegetation and biodiversity under changing conditions like sea level rise and climate change. The thickness of the mixing zone between the fresh and saline water is substantial, meaning that a sharp interface cannot be assumed, and characteristics of this mixing zone need to be taken into account when studying these lenses. In this thesis we have studied the behaviour of these thin rainwater lenses and their mixing zone.

To study the most basic relations of such a system, we considered in Chapter 2 the development of a rainwater lens, starting from initially saline conditions. To effectively link parameters, dimensionless groups are introduced that show the behaviour of different aspects of the lens. The group that represents the ratio of net precipitation and seepage and the group that shows the effect of density differences both have a significant impact on the thickness of the lens as well as of the mixing zone. The geometry of the flow domain also influences both, although to a lesser extent. Of course the thickness of the mixing zone is also significantly influenced by dispersion (largely determining the thickness as the lens grows) and diffusion (dominant for a steady state lens).

If there is significant seepage, the thickness of a lens can be estimated based on an analytical solution (Maas, 2007) including only drain distance, net precipitation and seepage flux and salinity. As seepage becomes negligible, the implicit assumption of stagnant salt water in cases of zero seepage, causes significant deviations from a numerical solution. Thickness of the mixing zone also depends on the distance from a drain; towards a drain, convergence causes narrowing of this zone, despite the higher velocities that create more dispersion.

In Chapter 4, field observations show that geological layering also plays a major role in the formation of a lens. Generally, a layer with low hydraulic conductivity will impede rainwater to infiltrate deeper, even if this would be expected based on the precipitation/seepage ratio and differences in density. The density difference is also overruled by the differences in hydraulic head, and therefore need not necessarily be taken into account when modelling a field situation.

Chapter 3 described the amplitude and frequency of events that would influence a certain system. The average lens thickness is hardly influenced by variations in thickness caused by weather fluctuations. Minimum and maximum lens thickness can

therefore be simply related to the average thickness based on the average net precipitation and the amplitude and frequency of net precipitation. For the mixing zone, the thickness can be derived from the so-called “travelled distance” of the middle of the zone. The more this zone moves up and down, due to alternating precipitation and evaporation, the more mixing occurs between rainwater and seepage, leading to a wider mixing zone. Changes in mixing zone thickness can be calculated analytically, however, one dataset or numerical model is needed to determine the actual thickness. Based on numerical simulations, short term precipitation events influence the mixing zone thickness due to the effect above, even though they hardly influence the thickness of the lens itself. However, in the field, as described in Chapter 4, the dynamics of the lens are concentrated in the top of the lens. This seems contradictory, but since the mixing zone for this site starts very near the ground water table, it is indeed the mixing zone thickness that is influenced by precipitation events.

Convolution theory was used to determine the impulse-response function for a thin lens, based on parameter groups described in Chapter 2. Using this function, the delay and amplitude of a lens reaction on a change in climate, the average net flux, was derived. Such values can easily be calculated for many different systems.

The temporal dynamics of thin lenses were observed and modelled for two years at two tile-drained agricultural fields in the south-western part of the Netherlands as described in Chapter 4. Monthly measurements of salinity profiles at different distances from the ditch and drain combined with daily precipitation and water table data showed large difference in dynamics between the top and the base of the mixing zone. Whereas the highly dynamic top part of the lens is dominated by the direct influence of precipitation and evaporation, the lower part of the mixing zone is showing slow and small oscillations, caused by the damped, delayed effect of alternating flow at the top combined with the constant upward flow of seepage water. These small movements control the mixing of seepage and precipitation water. The dynamics of the salt concentration in the upper part of the lens are small compared to the dynamics of the groundwater level. The damping of salt dynamics in the top part is caused by re-mixing of saline soil water that remains in the unsaturated zone as the water level declines. Soil water mixes again with relatively small amounts of rainwater, causing a salinity of the upper groundwater that is similar to the soil water salinity.

The soil water salinity is shown to be influenced by dual porosity as well. Capillary seepage of relatively saline water in dry periods is not immediately flushed out by the next precipitation event, since the rain water largely flows down through the macro pores that are formed by cracking of the clayey and loamy soils. Upper groundwater is therefore less saline then soil water in the capillary fringe after a dry spell has finished, which may well influence vegetation growth.

Preferential flow of rainwater in cracked soil also explains the fast decrease in salinity of drain water caused by individual precipitation events. Groundwater of variable salinity, originating from different parts of the lens, as well as infiltrated rainwater, contribute to the drain tile discharge in proportions that vary on a timescale of hours to days, and this causes dynamic behaviour of drain water salinity. This latter effect is important for the sustainability of small rainwater lenses. Rapid removal of fresh water is a threat for their persistence since it inhibits sufficient growth of a lens during wet periods (winter) to compensate for the loss during dry (summer) periods.

The cation exchange process occurring in rainwater lenses that are situated on upward seeping saline water start as a lens develops from initially saline conditions. On the short term, this process is characterized by the salt-shock caused by the large difference in concentration between rainwater and seepage water (Chapter 5). The pore water quality changes quickly from saline to relatively fresh and from sodium and magnesium dominated to calcium dominated. The latter effect is strengthened by the presence of shells in the unsaturated zone, leading to enrichment in calcium of the precipitation water before this reaches the groundwater.

The changes of the soil complex are much slower, because the amount of cations in the fresh solution is very small compared to the amount of cations adsorbed to the soil. Initially, both calcium and magnesium in the sorption complex increase due to the relative preference of divalent cations for soil adsorption sites as the pore water freshens. In the long term, magnesium is outcompeted by calcium on the complex. The time involved in this process is in the order of centuries for the shallow systems studied Zeeland. The net flux downward, i.e. net precipitation, has a much larger effect on the mixing process than short-term variations, which do not visibly influence the soil complex. The influence of tile drainage turns out to be rather minor as well. Only very close to the drains, mixing is limited and the complex hardly develops towards equilibrium with fresh water below the drain itself. Only one to two m away from the drain, the mixing zone is nearly horizontal. This implies that the horizontal flow component towards the drain has little effect on the mixing between fresh and saline water. Although it is the main flow component, the water quality is not changing in this direction, because the small vertical flow component is dominant for the composition of the soil adsorption complex. Comparison of the numerical model with field data from both study sites in Zeeland confirm the expected increase of calcium, decrease of sodium, and the mixing zone has progressed significantly towards equilibrium with rain water, although equilibrium has not yet been reached. Also, differences in the chemical composition of the seepage water between the two sites are still visible on the complex, although the freshening for both sites has started centuries ago. The influence of tile drains which could be analysed for one site is hardly visible on the complex after the approximately four decades that they have functioned so far.

Influence of saline groundwater on vegetation development has been assessed in Chapter 6. We simulated combinations of different vegetation types, soil characteristics and groundwater levels and –salinities for two different climates. This enabled us to assess the relative importance of all parameters on the fresh water availability and stress experienced by vegetation. We are primarily interested in salinity stress, but this is put in perspective of stress due to drought and lack of oxygen (very wet conditions). Soil type and climate are shown to be the most important parameters for both fresh water availability and vegetation stress. Salinity stress is substantial, but still small compared to stress caused by lack of oxygen and drought. Based on the statistics, the salt tolerance of the vegetation is of minor influence, which can be attributed to the fact that groundwater in the research setup is always more saline than the highest vegetation tolerance. For areas with less saline groundwater, salt tolerance may be a parameter that can be used to improve sustainability of agriculture. Where groundwater is very saline, adequate management of the soil and to a lesser extent control of the groundwater level, are likely to have more effect.

SAMENVATTING

Zoet water is in het algemeen schaars in vaak dichtbevolte kustgebieden. Grondwater is veelal zout, waardoor landbouw en zoetwater natuur in laaggelegen gebieden (op of onder de zeespiegel) afhankelijk zijn van een dunne zoetwaterlens die zich als gevolg van een neerslagoverschot vormt op het zoute kwelwater. Het begrijpen van de dynamiek van dergelijke lenzen is essentieel in het licht van duurzame ontwikkeling van voedselproductie en natuur onder veranderende omstandigheden zoals zeespiegelstijging en klimaatverandering. De mengzone tussen een dergelijke lens en het zoute grondwater is substantieel, waardoor aanname van een scherp grensvlak niet realistisch is en het gedrag van de mengzone ook van belang is. In dit proefschrift hebben we het gedrag van deze dunne lenzen en bijbehorende mengzone beschreven.

Om de basisrelaties van een regenwaterlens te onderzoeken, hebben we in Hoofdstuk 2 de ontwikkeling van een lens beschouwd die zich vormt vanuit een beginsituatie met alleen zout grondwater. Om het effect van alle parameters die de dikte van de lens en de mengzone beïnvloeden te kunnen onderzoeken, zijn dimensieloze groepen geformuleerd die de verschillende aspecten van het gedrag van de lens laten zien. De groepen die respectievelijk de neerslag-kwel ratio en de invoed van dichtheidsverschillen beschrijven hebben een substantieel effect op de dikte van zowel de lens als de mengzone. De geometrie van het gemodelleerde domein beïnvloedt ook de lens en de mengzone, zij het in geringere mate. Zoals te verwachten, wordt de dikte van de mengzone sterk beïnvloed door dispersie, dominant zolang de lens zich aan het ontwikkelen is, en diffusie, bepalend in een stabiele lens.

Als de hoeveelheid kwel substantieel is, kan de lensdikte geschat worden met behulp van een analytische oplossing (Maas, 2007) die alleen netto neerslag, hoeveelheid en zoutgehalte van het kwelwater en de afstand tussen drainagemiddelen beschouwt. Wanneer de kwelflux erg klein wordt, gaat deze benadering afwijken van numerieke oplossingen door de impliciete aanname dat zout water stil staat wanneer er geen kwelflux is. De dikte van de mengzone is mede afhankelijk van de afstand van een drain of waterloop. Het dunner worden van de mengzone richting de drainbuis of sloot komt door convergentie van stroomlijnen. Dit effect blijkt sterker dan de hogere mechanische dispersie die optreedt bij de hogere snelheden in de buurt vaneen drainbuis of sloot.

In Hoofdstuk 4 laten we met behulp van veldwaarnemingen zien dat bodemgelaagdheid een grote rol speelt in de vorming van regenwaterlenzen. In het algemeen zal een slecht doorlatende laag verhinderen dat regenwater dieper infiltreert, zelfs als dat te verwachen is op basis van de neerslag-kwel ratio en de dichtheidsverschillen. Ook blijkt het effect van dichtheidsverschil kleiner dan het effect van verschil in stijghoogte tussen de onderliggende laag van waaruit het kwelwater omhoog stroomt en de laag waarin de grondwaterspiegel zich bevindt.

Daarom is het niet noodzakelijk dichtheidsverschillen mee te nemen in het modelleren van een veldsituatie.

In Hoofdstuk 3 wordt onderzocht welke amplitudes en frequenties van netto neerslag een lens systeem noemenswaardig beïnvloeden. De gemiddelde lensdikte hangt nauwelijks af van de variaties die door het weer worden veroorzaakt. De minimale en maximale dikte van de lens zijn daarom eenvoudig te relateren aan de gemiddelde lensdikte en de frequentie en amplitude van netto neerslag. De dikte van de mengzone is af te leiden uit de weg die het centrum van die zone heeft afgelegd. Hoe meer het midden van de mengzone op en neer beweegt, als gevolg van afwisselend neerslag en verdamping, hoe beter neerslag en kwel water worden gemengd en dus hoe breder de mengzone zal zijn. Veranderingen van deze dikte zijn analytisch te bepalen. Er is echter wel een numeriek model of een dataset nodig als referentie om werkelijke diktes te kunnen berekenen. Op basis van numerieke simulaties kan worden gesteld dat korte, heftige buien invloed hebben op de dikte van de mengzone hoewel ze de dikte van de lens zelf nauwelijks beïnvloeden. Volgens de veldwaarnemingen, in Hoofdstuk 4, is de dynamiek van de lens alleen te vinden in het bovenste gedeelte van de lens, bij de grondwaterspiegel. Dit lijkt in tegenspraak met de bevinding dat individuele buien vooral de mengzone beïnvloeden. Aangezien de top van de mengzone en de grondwaterspiegel op de studielocatie zeer dicht bij elkaar liggen, klopt echter ook in dit geval de conclusie dat het de mengzone is die wordt beïnvloed door individuele buien.

We hebben convolutietheorie gebruikt om de impuls-respons functie voor een dunne regenwaterlens te bepalen, gebaseerd op de dimensieloze groepen uit Hoofdstuk 2. Met deze functie kunnen demping en vertraging van de reactie van en lens op klimaatverandering (oftewel de gemiddelde netto flux) worden afgeleid. Deze waarden kunnen eenvoudig voor uiteenlopende lenssystemen worden berekend.

De temporele variatie van dunne lenzen is gemeten en gemodelleerd voor een periode van twee jaar op twee gedraineerde landbouwpercelen in Zuidwest Nederland, zoals beschreven in Hoofdstuk 4. Maandelijkse metingen van zoutprofielen op verschillende afstanden van drains en sloten, gecombineerd met dagelijkse gegevens voor weer en grondwater, laten zien dat de dynamiek erg afhankelijk is van de diepte. Terwijl het zeer dynamische bovenste gedeelte van de lens wordt gedomineerd door de directe invloed van neerslag en verdamping, zijn in het onderste deel van de lens alleen kleine, trage oscillaties zichtbaar. Deze worden veroorzaakt door het gedempte, vertraagde effect van oscillerende stroomrichting bovenin de lens en de constante opwaartse kwelflux. Het zijn deze kleine bewegingen die de mate van mengen van neerslag en kwelwater bepalen. Schommelingen in zoutgehalte in het bovenste deel van de lens zijn klein in vergelijking met de grondwaterstandsvariatie. Dit gedempte effect wordt veroorzaakt door het uitspoelen naar de lens van zout water dat achterblijft in de onverzadigde zone op het moment dat de grondwaterstand zakt. Dit water mengt met

relatief kleine hoeveelheden neerslagwater, waardoor het zoutgehalte van het bovenste grondwater vergelijkbaar is met dat van het bodemwater.

Duale porositeit is aantoonbaar van invloed op het zoutgehalte van het bodemwater. Capillaire opstijging van relatief zout water in droge perioden spoelt niet direct uit tijdens de eerstvolgende bui, omdat het regenwater grotendeels naar beneden stroomt via macroporiën zoals scheuren in klei- of leemhoudende bodems. Daardoor is het bovenste grondwater net nadat een droge periode is geëindigd zoeter dan de volcapillaire zone op dat moment. Dit zou effect kunnen hebben op de kwaliteit van het water in de wortelzone en daarmee op de ontwikkeling van vegetatie.

Preferente stroming in scheurvormende bodems verklaart ook de snelle afname van het zoutgehalte in drainwater die veroorzaakt wordt door individuele buien. Zowel grondwater met een zoutgehalte dat afhangt van de precieze plaats in de lens waar het water vandaan komt, als het infiltrerende regenwater, dragen bij aan de samenstelling van het drainwater. Dit zorgt voor een zeer dynamische drainwater kwaliteit op een tijdschaal van uren tot dagen. Dit effect is ook van belang voor de duurzaamheid van dunne lenzen. Snelle afvoer van zoetwater is een bedreiging voor het intact blijven van dunne lenzen, omdat de lens hierdoor niet maximaal aangroeit in natte perioden.

Het proces van kationen-uitwisseling in regenwaterlenzen op zoute kwel begint bij de ontwikkeling van een lens vanuit zoute omstandigheden. Op de korte termijn wordt dit proces gekarakteriseerd door de zoutschok, veroorzaakt door het grote concentratieverschil tussen regenwater en kwelwater. De kwaliteit van het poriewater verandert snel van zout naar relatief zoet en van natrium en magnesium gedomineerd naar calcium gedomineerd. Dit laatste effect wordt versterkt wanneer schelpen in de onverzadigde zone het regenwater verrijken met calcium voordat dit het grondwater bereikt.

Veranderingen in het bodemcomplex verlopen veel trager, omdat het aantal kationen in het regenwater heel klein is in vergelijking met het aantal dat aan de bodem geadsorbeerd is. Initieel nemen zowel calcium als magnesium toe aan het complex door de grotere aantrekkingskracht van tweewaardige ionen in zoeter water. Op de lange termijn, wordt magnesium weer van het complex gestoten door calcium. Het tijdsbestek van deze processen is in de orde van honderden jaren voor de ondiepe systemen die in Zeeland zijn onderzocht. De jaarlijkse netto neerslag heeft hierbij een veel groter effect op het mengproces dan weersveranderingen, die het bodemcomplex niet zichtbaar beinvloeden. Ook de invloed van drains blijkt relatief beperkt. Alleen heel dicht rond de drains vindt minder menging plaats en recht onder de drain vindt nauwelijks uitwiseling plaats. Op slechts 1 tot 2 meter afstand van de drain is de mengzone praktisch horizontaal. Daardoor heeft de horizontale waterstroming richting de drain nauwelijks effect op het mengen van zoet en zout water. Hoewel dit duidelijk de dominante stromingscomponent is, is het de kleine verticale component

die de verandering van het bodemcomplex veroorzaakt. Vergelijking van het numerieke model met beide locaties in Zeeland bevestigen de verwacht toename van calcium, de afname van natrium, en de tijdelijke toename van magnesium aan het complex. Beide locaties laten zien dat het bodemcomplex in het bovenste gedeelte van de lens richting evenwicht met aangerijkt regenwater gaat, alhoewel dit evenwicht nog niet is bereikt. Daarnaast zijn verschillen in kwelwaterkwaliteit tussen de locaties nog steeds zichtbaar in het bodemcomplex, hoewel de verzoeting in beide gevallen al eeuwen geleden is begonnen. De invloed van veertig jaar drainage daarentegen, die voor een van de locaties goed bekeken kon worden, is nauwelijks zichtbaar in het complex.

In Hoofdstuk 6 is gekeken naar de invloed van zout grondwater op de ontwikkeling van planten. Deze ontwikkeling werd voor twee soorten klimaat gesimuleerd met verschillende combinaties van vegetatietype, bodemsoort en zoutgehalte en de stand van het grondwater. De relatieve invloed van deze factoren op de zoetwaterbeschikbaarheid en het effect op de plantengroei kon zo worden bepaald. Hoewel het ons voornamelijk gaat om het bepalen van effecten van zout op planten, hebben we deze effecten vergeleken met effecten van droogte en zuurstoftekort (onder te natte omstandigheden) om een totaalbeeld te krijgen. Bodemsoort en klimaat blijken de belangrijkste factoren. Het effect van zout is weliswaar substantieel, maar klein in vergelijking met de effecten van droogte of zuurstofgebrek. Statistisch gezien is de zouttolerantie van de planten nauwelijks van invloed op de groei. Dit is verklaarbaar doordat binnen dit onderzoek het grondwater altijd zouter was dan de meest zouttolerante gewassen kunnen verdragen. In gebieden waar grondwater minder zout is, zou het vergroten van de zouttolerantie van gewassen wellicht kunnen leiden tot verduurzaming van de landbouw. In gebieden met erg zout grondwater, lijken adequaat bodembeheer en in mindere mate grondwaterbeheer hiervoor belangrijkere instrumenten.

DANKWOORD

Na 11 jaar wil ik heel veel mensen bedanken! Het waren intensieve jaren waarvan dit “project” samen met veel andere mensen en gebeurtenissen deel uitmaakte, waardoor het langer geduurd heeft dan ooit de bedoeling was. Toch kan ik nu aan het eind zeggen dat ik geen spijt heb en dat ik op veel vlakken een boel heb bijgeleerd. Over zoet en zout water, over lesgeven en begeleiden, over moeder zijn, enz. enz. En het is af. Ik ben er niet trots op dat het zo veel tijd heeft gekost, maar ik ben wel trots dat ik het uiteindelijk heb kunnen afronden. Dankzij velen:

Sjoerd, dank voor je geduld, wat ik op verschillende manier op de proef heb gesteld, en het vertrouwen wat je me toch steeds weer gaf. Dat vond ik zeker de laatste jaren niet vanzelfsprekend, maar jij wel. Toon, voor de altijd bemoedigende toon, die ik regelmatig hard nodig heb gehad. Ook inhoudelijk natuurlijk, jullie allebei: dank voor al het mee- en overdenken, voor het mij laten zien van de mogelijkheden, methodes, technieken die hydrologie en aanverwante vakgebieden te bieden hebben.

Perry, fijn om samen veldwerk te doen in Zeeland, waarin je me om te beginnen praktisch hebt bijgespijkerd, maar ook jouw “fysisch geografische blik” op systemen heeft me vaak geholpen. Ik vond de lange dagen behoorlijk zwaar nu en dan, zeker in de winter, maar tijdens de autoritten was er altijd genoeg gepsreksstof.

Pieter Raats, Cees Maas en Paul Torfs, dank voor jullie hulp en inspiratie, die in verschillende hoofdstukken voor een flinke bijdrage aan de wiskundige en statistische inhoud heeft gezorgd. Vincent, bedankt voor je hulp bij het chemische werk en vooral het gebruik van de bijbehorende software.

Esther, Claudia, Dieuwke, Willemijn, Marieke, Sija, Tineke, Ryan, Hidde, Bram, Joris, Bart, Anne, Marjolein en alle toenmalige aio’s van SEG en HWM in Atlas en Aqua: het wandelen en koffiedrinken was gezellig, vaak interessant en gaf weer een fris hoofd om verder te gaan. Soms ook bij dat koffiedrinken, maar ook voor allerhande inhoudelijke en minder inhoudelijke vragen: bedankt Klaas, Jos, Harm en George en de andere collega’s van SEG en HWM.

Ad, Angelique, Anouk, Bert, Bertus, Dan, Dennis, Dick, Erwin, Freddy, Freek, Harrie, Harry, Gertjan, Gert Jan, Jack, Hans, Jos, Karen, Lubbert, Mia, Maartje, Michel, Michiel, Peter, Sylvia, Sieger, Thijs, Walter, Willy: het is hard werken bij LWM, maar jullie aanmoediging en waardering afgelopen jaren hebben mij wel kracht gegeven om uiteindelijk naast al dat werk toch dit “project” te kunnen afronden.

Atsje, Andre, Marjolein, Pablo, Carolina, Ard, Rens, Nathalie, Sanne, Jeroen, Jordy, Anneke, Loes, Sander, Vivienne, Pascal, Harm, Dori: veel fijne en ook een aantal verdrietige momenten gedeeld. Het blijven vragen naar mijn proefschrift was een stimulans. Zo nu en dan confronterend, maar nodig. Hartelijk dank voor alle steun!

Selina en Erik: behalve fijne vrienden gaf en geeft het hebben van een veilige fijne plek voor de kinderen veel rust. Bedankt!

Salle, inmiddels een jaar of 15 terug heb jij me al aangemoedigd mijn eigen weg te kiezen en me daar actief in ondersteund. Dat heeft me geholpen om de keuzes te maken die bij mij passen.

Els, Bart en Mark: dank voor jullie steun, samen lekker eten, naar musea in Leiden en natuurlijk zwemmen aan het Banjaardstrand in de zomer en fijne logeerpartijen voor de jongens.

Anna, Tijf, Maya: heel fijn dat we altijd op elkaar kunnen rekenen en samen lol kunnen hebben. Evi, bedankt voor je perfecte afleiding van al het gedenk. Jij bent gewoon wie je bent!

Wiljo dank voor alle liefde, steun, tijd en begrip die ik nog steeds van je krijg, net als de jongens. In veel opzichten ben je nog steeds een voorbeeld voor mij (geduld, openheid). Rob, hoewel je er al weer 8 jaar niet meer bent, haal ik nog steeds, en ik denk zelfs weer steeds meer, steun uit de liefde, veiligheid en structuur die je me hebt meegegeven.

Stan en Tobias: mijn prachtjongens! Allereerst natuurlijk dank voor de voorkant en verdere versiering! Voor mij is dit boekje daar veel mooier van geworden. Stan, fijn dat je met een stralende nieuwsgierige blik naar de wereld kijkt en je verwondering met ons deelt. Tobias, heerlijk om met jou samen in de tuin te werken of lekkere dingen te maken. Samen lekker bezig zijn, ik hoop dat we daar nog heel lang mee doorgaan.

Michiel, zonder jouw onvoorwaardelijke liefde, steun en incasserinsvermogen voor al mijn frustraties, was ik niet waar ik nu ben en waren wij niet waar we nu zijn. Ook in tijden dat ik niet erg in een goede afloop geloofde heb je me gesteund en de ruimte gegeven zonder het op te geven. Tot ik zelf uiteindelijk ook weer verder kon. Ik hou en leer nog steeds meer van je.

CV

Sara Eeman werd op 17 april 1979 geboren in Dreumel. Ze groeide op in Nijmegen, waar ze in 1997 haar diploma behaalde aan het Stedelijk Gymnasium. Na een tussenjaar in Australie begon zij in 1998 aan de studie Technische Aardwetenschappen aan de TU in Delft, die zij afrondde in 2004 met geotechniek als specialisatie. Haar afstudeeronderzoek werd uitgevoerd bij Alterra en ging over het modelleren van grondwater in de heuvels van het tropische eiland Viti Levu, Fiji.

Daarna woonde zij met haar partner Michiel de Vries 3 jaar in Senegal. Toen begon het idee een promotieonderzoek te gaan doen vorm te krijgen. In 2006 startte dat onderzoek en tot 2012 was zij als promovenda aan Wageningen Universiteit verbonden. Daarna is ze als docent hydrologie gaan werken bij Van Hall Larenstein in Velp bij de opleiding Land- en Watermanagement.

Sara is getrouwd en heeft 2 zoons.

Netherlands Research School for the
Socio-Economic and Natural Sciences of the Environment

D I P L O M A

For specialised PhD training

The Netherlands Research School for the
Socio-Economic and Natural Sciences of the Environment
(SENSE) declares that

Sara Eeman

born on 17 April 1979 in Dreumel, The Netherlands

has successfully fulfilled all requirements of the
Educational Programme of SENSE.

Wageningen, 25 January 2017

the Chairman of the SENSE board	the SENSE Director of Education
Prof. dr. Huub Rijnaarts	Dr. Ad van Dommelen

The SENSE Research School has been accredited by the Royal Netherlands Academy of Arts and Sciences (KNAW)

KONINKLIJKE NEDERLANDSE
AKADEMIE VAN WETENSCHAPPEN

The SENSE Research School declares that **Ms Sara Eeman** has successfully fulfilled all requirements of the Educational PhD Programme of SENSE with a work load of 51.5 EC, including the following activities:

SENSE PhD Courses

- Advanced soil physics (2008)
- Environmental research in context (2008)
- Research in context activity: 'Co-organizing SENSE Symposium on Land-Water-Atmosphere Interactions (Wageningen, 9 March 2010)'

Other PhD and Advanced MSc Courses

- Upscaling and modelling of coupled transport in the subsurface, Utrecht University (2006)
- Competence assessment, Wageningen University (2006)
- Scientific writing, Wageningen University (2007)
- Project- and time management, Wageningen University (2007)
- Academic consultancy training mentor procedure course, Wageningen University (2009)
- Guide to scientific artwork, Wageningen University, (2009)
- Career perspectives, Wageningen University (2010)

Management and Didactic Skills Training

- Supervising two MSc students with thesis entitled 'Hydrochemical processes at a shallow fresh-/saltwater interface in Schouwen-Duiveland' (2009) and 'Assessing the influence of saline seepage water on soil and pore water chemistry C/S: Dutch polder landscape of Schouwen-Duiveland' (2011)
- Co-organising the PhD meeting for the annual Boussinesq meeting, Amsterdam, The Netherlands (2009)
- Supervising in the MSc course 'Academic Consultancy Training', Wageningen University (2009-2011)
- Annotation for didactics, Hogeschool van Arnhem en Nijmegen (2013)
- Co-developing the minor 'Sustainable river engineering', Van Hal Larenstein Velp (2015)
- Organising excursion days for students in Environmental Sciences of Wageningen University and Van Hal Larenstein (2010-2016)
- Coordinating the BSc program 'Infrastructure and Hydraulic engineering for land and water managment', Van Hal Larenstein Velp (2013 -2016)

Selection of Oral Presentations

- *Upward seepage of salt water in low lying areas under changing conditions.* Non-linearities and upscaling in porous media (NUPUS) symposium, 7-9 April 2008, Zeist, The Netherlands
- *Dispersive behaviour of the mixing zone between a shallow freshwater lens and upward seeping saline groundwater,* Salt Water Intrusion Meeting (SWIM), 23-27 June 2008, Florida, US
- *Mixing zone between a shallow freshwater lens and upward seeping saline groundwater,* European Geosciences Union (EGU) General Assembly, 19-24 April 2009, Vienna, Austria

SENSE Coordinator PhD Education

Dr. ing. Monique Gulickx

Cover Design: Sara Eeman
Cover Art Work: Stan and Tobias de Vries